

THE DETERMINATION OF TEMPERATURE-DEPENDENT CPA DIFFUSION  
PROPERTIES IN FELINE TESTICULAR TISSUE

by

Kaitlyn Kirkland

A dissertation submitted to the faculty of  
The University of North Carolina at Charlotte  
in partial fulfillment of the requirements  
for the degree of Doctor of Philosophy in  
Mechanical Engineering

Charlotte

2022

Approved by:

---

Dr. Gloria Elliott

---

Dr. Harish Cherukuri

---

Dr. Edward Morse

---

Dr. Ahmed El-Ghannam

---

Dr. Russell Keanini

---

Dr. Didier Dréau

©2022

Kaitlyn Kirkland

ALL RIGHTS RESERVED

## ABSTRACT

KAITLYN KIRKLAND. The Determination of Temperature-dependent CPA Diffusion Properties in Feline Testicular Tissue. (Under the direction of DR. GLORIA ELLIOTT)

Fertility preservation would benefit young males who must undergo treatments that can result in sterilization, such as radiation treatments for cancer. This can be achieved by removing some testicular tissue before treatment and putting it into frozen storage, a process known as cryopreservation. Cryopreservation has been successfully performed for many types of mammalian testicular tissue, but with only limited success for human tissue [1-4]. In general, immature spermatozoa are more vulnerable to toxicity damage caused by cryo-protective agents, or CPAs, which are necessary to prevent freezing damage [5]. To determine the optimal concentrations of CPAs to use during preservation procedures while minimizing the risk of damage due to CPA toxicity, toxicity cost models have been used to predict the CPA diffusion time into tissues, with the goal of avoiding overexposure [6-8]. The accuracy of these predictions is limited in part by the lack of tissue property data such as CPA diffusion coefficients. The goal of the current work is to determine the effective diffusion coefficient for DMSO in testicular tissue at 22°C and 4°C, to support the planning of CPA loading protocols that minimize toxicity damage during preservation procedures.

Testicular tissue consists of Leydig and myoid cells and seminiferous tubules containing various other cell types [9]. The arrangement of cells within tissues can vary spatially and from testis to testis. Sectioning, even within the same sample, can thus yield different values of the same property, which complicates the identification of sources of error in diffusion testing. The creation of a reference standard is pursued in this work, to support the identification of experimental errors

in the development of diffusion testing methodology and to provide a means of standardizing measurements between different labs and investigators. Sodium alginate cross-linked with gelatin and low melting point agarose were evaluated for their potential as reference standards.

Sample thickness, which is an essential input when estimating diffusivity, was determined before and after sample placement using ATOS Scanbox 4105 employing the triple scan principle.

A Frontier (PerkinElmer, MA, USA) Fourier transform infrared spectroscopy (FTIR) with a Gladi-ATR attachment (Pike Technologies, WI, USA) was used to obtain absorbance values as DMSO diffused into SA-gels (n=4), agarose (n=9), or testicular tissue (n=9) at room temperature. These absorbance values were fit to a model developed by Barbari and Fieldson (1993) to determine diffusion coefficients for each sample [10, 11]. A 2-parameter estimation program was created in Excel to allow simultaneous estimation of the effective diffusivity,  $D_{\text{eff}}$ , values and the equilibrium absorbance,  $A_{\infty}$ , values. For samples that equilibrated within a 2-hour period, the absorbance values were normalized to the final equilibrium values and fit using a 1-parameter estimation Excel program for only the diffusion coefficient. The pooled average  $D_{\text{eff}}$  values were determined to be  $4.3 \pm 0.3 \times 10^{-6} \text{ cm}^2/\text{s}$ ,  $9.2 \pm 0.2 \times 10^{-6} \text{ cm}^2/\text{s}$ , and  $10 \pm 4 \times 10^{-6} \text{ cm}^2/\text{s}$  for SA-gels, agarose, and testes, respectively. The variation in effective diffusion coefficients between batches and between replicates within the same batch for agarose was much lower than for alginate-gelatin. It was also easier to slice into prescribed thicknesses and thus was the preferred reference material for diffusion studies utilizing FTIR. The good repeatability of diffusion coefficient estimates in agarose established the validity of the set-up and methodology. The variability in the diffusion coefficients determined for testicular tissue could thus be attributed to inherent differences between tissue samples.

A thermal control system was assembled which held temperatures within a range of  $4^{\circ}\text{C} \pm 4^{\circ}\text{C}$ . The pooled average  $D_{\text{eff}}$  values at  $4^{\circ}\text{C}$  were determined to be  $5.6 \pm 0.2 \times 10^{-6} \text{ cm}^2/\text{s}$  and  $7 \pm 5 \times 10^{-6} \text{ cm}^2/\text{s}$  for agarose and testicular tissue, respectively. As expected, the diffusion coefficients decreased with temperature. The standard deviation between testis samples increased compared to room temperature samples. Programming of CPA loading procedures will need to consider the variability that is inherent in testicular tissue.

## ACKNOWLEDGEMENTS

I would like to express my utmost gratitude to my advisor Dr. Gloria Elliott, for her outstanding mentorship. I appreciate you for working with me through extenuating circumstances and difficult times. Your advice throughout my academic and research career has been invaluable.

I would also like to express my appreciation to my committee members, Dr. Harish Cherukuri, Dr. Edward Morse, Dr. Ahmed El-Ghannam, Dr. Russell Keanini, and Dr. Didier Dreau for their guidance and feedback on my work.

I would also like to thank the wonderful staff at the Cabarrus Spay and Neuter Clinic for providing resources for experiments and the Hirsch Foundation for financially supporting my work. Thank you to my colleagues in the Biostability Lab. Finally, I want to express my extreme gratitude to my parents, my grandparents, my family, and my husband for always encouraging and supporting me unconditionally. I dedicate this dissertation to them.

## TABLE OF CONTENTS

CHAPTER 1 SIGNIFICANCE: MASS DIFFUSIVITY IN THE CONTEXT OF CRYOPRESERVATION .....	1
1.1 Cryopreservation of sperm and testicular tissue .....	1
1.2 The role of cryoprotectants and their limitations .....	1
1.2.1 Current work on CPA loading optimization .....	2
1.3 Diffusivity and the diffusion coefficient .....	3
1.3.1 CPA diffusion coefficients in tissue .....	3
1.3.2 Modeling diffusion kinetics to estimate diffusion coefficient .....	9
1.4 Challenges of working with soft tissue and the need for a reference standard .....	12
1.5 Desirable reference standard characteristics .....	13
CHAPTER 2 OVERVIEW OF EXPERIMENTAL DESIGN .....	16
2.1 Rationale .....	16
2.2 Goals and outcomes .....	17
2.3 Specific aims .....	17
CHAPTER 3 GENERAL MATERIALS AND METHODOLOGY .....	20
3.1 Density measurements .....	20
3.2 Estimation thickness from mass and density measurements .....	21
3.3 Estimation of sample thicknesses .....	21
3.4 FTIR testing .....	24
3.5 Diffusion coefficients estimation program .....	33
CHAPTER 4 DEVELOPMENT OF A REFERENCE STANDARD FOR CPA DIFFUSION IN SOFT TISSUES .....	35
4.1 Alginate-gelatin reference material .....	35
4.1.1 Rationale .....	35
4.1.2 Casting materials and methods .....	36
4.1.3 Estimating the thickness of alginate-gelatin .....	37
4.1.4 Estimated diffusion coefficients in alginate-gelatin .....	41
4.2 Agarose .....	44
4.2.1 Rationale .....	44

4.2.2	Materials and methods .....	44
4.2.3	Estimating thickness of agarose.....	46
4.2.4	Estimated diffusion coefficients in agarose at 22°C .....	49
CHAPTER 5 DETERMINATION OF EFFECTIVE DIFFUSIVITY FOR TESTICULAR TISSUES USING FTIR .....		60
5.1	Rationale .....	60
5.2	Slicing materials and methods .....	60
5.3	Estimating thickness of testicular tissue inside sample holder .....	61
5.3.1	Estimated diffusion coefficients in testicular tissue at 22°C .....	64
CHAPTER 6 DESIGN OF AN APPARATUS FOR TEMPERATURE-CONTROLLED CPA EXPOSURE FOR TISSUE.....		74
6.1	Rationale .....	74
6.2	Development of a custom sample holder for 1-D CPA diffusion studies .....	74
6.3	Thermal control design and evaluating temperature profile .....	76
6.4	Diffusivity measurements using temperature control .....	80
6.4.1	Estimating temperature dependent effective diffusion coefficient of agarose.....	80
6.4.2	Estimating temperature dependent effective diffusion coefficient of testicular tissue	91
6.4.3	Refinement of thermal monitoring system to support improvements in temperature control	100
CHAPTER 7 OVERALL ASSESSMENT OF RESEARCH OUTCOMES .....		103
7.1	Choice of reference standard for diffusion studies .....	103
7.2	Development of temperature-controlled CPA delivery system.....	106
7.3	Determination of the temperature-dependent diffusion coefficient for testicular tissue ..	109
7.3.1	Understanding the relationship between temperature and diffusion of DMSO in testicular tissue.....	112
CHAPTER 8 FUTURE WORK .....		116
8.1	Further development and application of reference material for diffusion studies .....	116
8.2	Refinement of sample holder and thermal control system .....	116
8.3	Expansion of known temperature-dependent CPA properties of testicular tissue.....	117
APPENDIX.....		125

LIST OF TABLES

Table 1 Diffusion coefficients in tissues obtained using NMR imaging<sup>1</sup>, simulation compared against a priori NMR data<sup>2</sup>, FTIR methods<sup>3</sup>, osmolality methods<sup>4</sup>, or Raman spectroscopy<sup>5</sup> ..... 8

Table 2 Estimated thickness of alginate-gelatin (n=12) in mm, determined at various points on the top surface, measured directly after trimming, before placement into the sample holder. The center point of each SA-gel is highlighted in green..... 38

Table 3 Diffusion Coefficients and Equilibrium Absorbances for Alginate-gelatin ..... 44

Table 4 Estimated thickness of agarose (n=12) in mm, determined at various points on the top surface, measured directly after slicing and punching, before placement into the sample holder. The center point of each agarose is highlighted in green..... 46

Table 5 Estimated thickness of agarose (n=12) in mm, determined at various points on the top surface, measured after placement into the sample holder. The center point of each agarose is highlighted in green. .... 48

Table 6 Diffusion Coefficients [ $\times 10^{-6} \text{ cm}^2/\text{s}$ ] for Agarose Obtained at Room Temperature ..... 52

Table 7 Comparison between average effective diffusion coefficients from individual batches and fits with other agarose absorbance data for validation of agarose effective diffusion coefficients at 22°C..... 54

Table 8 Comparison between average effective diffusion coefficients from individual samples and fits with other agarose absorbance data for validation of effective diffusion coefficients at 22°C ..... 57

Table 9 Estimated thickness of testicular tissue (n=8) in mm, determined at various points on the top surface, measured directly after slicing and punching, before placement into the sample holder. The center point of each testicular tissue is highlighted in green..... 61

Table 10 Estimated thickness of testicular tissue (n=8) in mm, determined at various points on the top surface, measured after placement into the sample holder. The center point of each testicular tissue is highlighted in green..... 63

Table 11 Diffusion coefficients [ $\times 10^{-6} \text{ cm}^2/\text{s}$ ] for fresh testicular tissue obtained at room temperature for three separate days ..... 68

Table 12 Comparison between average effective diffusion coefficients from individual collection days and fits with other testicular tissue absorbance data for validation of effective diffusion coefficients at 22°C..... 69

Table 13 Estimated required time to reach equilibrium for testicular tissue at 22°C ..... 73

Table 14 Diffusion coefficients for agarose obtained at 4°C..... 84

Table 15 Comparison between average effective diffusion coefficients from individual batches and fits with other agarose absorbance data for validation of agarose effective diffusion coefficients at 4°C..... 85

Table 16 Comparison between average effective diffusion coefficients from individual samples and fits with other agarose absorbance data for validation of agarose effective diffusion coefficients at 4°C.....	88
Table 17 Diffusion coefficients for testicular tissue obtained at 4°C for three separate days .....	93
Table 18 Comparison between average effective diffusion coefficients from individual collection days and fits with other testicular tissue absorbance data for validation of effective diffusion coefficients at 4°C.....	96
Table 19 Estimated required time to reach equilibrium for testicular tissue at 4°C.....	100
Table 20 Thickness and effective diffusion coefficient and equilibrium absorbance values for sodium alginate-gelatin and agarose 22°C and 4°C.....	104
Table 21 Thickness and effective diffusion coefficient and equilibrium absorbance values for testicular tissue at 22°C and 4°C.....	110
Table 22 Effective diffusion coefficient, equilibrium absorbance value, sum of squares error, and mean square error for agarose samples obtained at room temperature.....	125
Table 23 Effective diffusion coefficient, equilibrium absorbance value, sum of squares error, and mean square error for agarose samples obtained at 4°C .....	125
Table 24 Effective diffusion coefficient, equilibrium absorbance value, sum of squares error, and mean square error for testicular tissue samples obtained at room temperature .....	126
Table 25 Effective diffusion coefficient, equilibrium absorbance value, sum of squares error, and mean square error for testicular tissue samples obtained at 4°C .....	126

## LIST OF FIGURES

Figure 1 Effective diffusion coefficients for DMSO (blue), glycerol (orange), sucrose (gray), propylene glycol (yellow), and ethylene glycol (green) into ovarian tissues, articular cartilage, and arterial valve tissue at five temperatures. Values determined at 4°C, 17°C, 22°C, 27°C, and 37°C are represented by squares, X marks, circles, diamonds, and triangles, respectively. The bordered values were determined in for single values in mixtures.....	9
Figure 2 Reference points were used to register the top surface of the alginate-gelatin using the ATOS Scanbox (left). The thickness was estimated as the distance between the surface below the alginate-gelatin and the reference points (right). The thickness of the reference points was removed to define the thickness of the alginate-gelatin alone at each point. ....	22
Figure 3 A small piece of paper was used to register the top surface after packing (left). A point at the center of the surface defined the thickness of the alginate-gelatin after packing (right). The thickness of the paper slip was removed to define the thickness of the alginate-gelatin only. ....	23
Figure 4 Agarose (left) and testicular tissue (right) were compacted into rings inside the sample holder with inner diameters of 7.4mm and 6mm, respectively.....	24
Figure 5 Full-scale spectral response from 4000 $\text{cm}^{-1}$ to 900 $\text{cm}^{-1}$ for alginate-gelatin. Bands unique to alginate exist from 1400 to 1490 $\text{cm}^{-1}$ , associated with C-N stretching, and from 1000 to 1080 $\text{cm}^{-1}$ , associated with C-H stretching [74]. ....	26
Figure 6 Full-scale spectral response from 4000 $\text{cm}^{-1}$ to 900 $\text{cm}^{-1}$ for agarose. The band from 1015 to 1080 $\text{cm}^{-1}$ is associated with C-H stretching. ....	26
Figure 7 Full-scale spectral response from 4000 $\text{cm}^{-1}$ to 900 $\text{cm}^{-1}$ for testicular tissue. Only the water peaks can be observed for feline testicular tissue. ....	27
Figure 8 Full-scale spectral response from 4000 $\text{cm}^{-1}$ to 900 $\text{cm}^{-1}$ for 3.1M DMSO. Peaks from 1310 to 1380 $\text{cm}^{-1}$ and from 1395 to 1440 $\text{cm}^{-1}$ indicate O-H bending. A S=O stretching peak can be observed from 980 to 1070 $\text{cm}^{-1}$ , and the unique DMSO peak from 930 to 970 $\text{cm}^{-1}$ is used to quantify absorbance for DMSO during diffusion studies [75]. ....	27
Figure 9 Fingerprint region spectral response from 1500 $\text{cm}^{-1}$ to 900 $\text{cm}^{-1}$ for alginate-gelatin..	28
Figure 10 Fingerprint region spectral response from 1500 $\text{cm}^{-1}$ to 900 $\text{cm}^{-1}$ for agarose. ....	28
Figure 11 Fingerprint region spectral response from 1500 $\text{cm}^{-1}$ to 900 $\text{cm}^{-1}$ for testicular tissue.	29
Figure 12 Fingerprint region spectral response from 1500 $\text{cm}^{-1}$ to 900 $\text{cm}^{-1}$ for 3.1M DMSO....	29
Figure 13 Diffusion study ATR-FTIR setup.....	32
Figure 14 Casting procedures for ~1.8mm thick alginate-gelatin samples for diffusion studies .	37
Figure 15 A comparison of the theoretical and experimental thicknesses before (left) and after (right) packing in sample holder for alginate-gelatin. A solid orange line represents the theoretical thicknesses before and after packing. Experimental thicknesses are shown as blue diamonds. The correlation line for the experimental thicknesses after packing in the sample	

holder is represented by a blue dashed line, equation: thickness = 4.97*mass in grams + 1.03 mm (R <sup>2</sup> = 0.0389).....	41
Figure 16 Absorbance as a function of time for different samples of alginate-gelatin from the same preparation batch, exposed to DMSO. Sample 1 (blue circles), 2 (orange squares), 3 (gray diamonds), and 4 (yellow triangles) were processed in time exposure. ....	42
Figure 17 Diffusion coefficient estimation fits for alginate-gelatin sample 1 (top left), 2 (top right), 3 (bottom left), and 4 (bottom right). The experimental values are indicated by orange circles, the predicted values are represented by the blue line. ....	43
Figure 18 Casting procedures for ~1mm thick agarose samples for diffusion studies .....	46
Figure 19 A comparison of the theoretical and average experimental thicknesses of agarose before (left) and after (right) packing in sample holder. A solid orange line represents the theoretical thicknesses before and after packing. Experimental thicknesses are shown as blue diamonds. The correlation line for the experimental thicknesses after packing in the sample holder is represented by a blue dashed line, thickness = 3.46*weight in grams + 0.94 mm (R <sup>2</sup> = 0.005). ....	49
Figure 20 Absorbance as a function of time for agarose exposed to DMSO obtained at 22°C. The data represents three individual samples (blue circles, orange squares, and gray diamonds) from a single preparation batch. ....	50
Figure 21 Absorbance data fit to determine D <sub>eff</sub> for agarose batch 1 sample 1 at 22°C. Experimental absorbances are indicated by gray circles, and predicted values are represented by the blue line.....	51
Figure 22 Residual plots for absorbance value fits obtained for three agarose samples across three batches at 22°C. Each row is a different batch, and each column is a different sample within each batch. ....	52
Figure 23 Residual plots for validation of the average effective diffusion coefficient for batch 1 of agarose obtained at 22°C using batches 2 (top row) and 3 (bottom row) absorbance time series. Each column is a different sample in each batch.....	55
Figure 24 Residual plots for validation of the average effective diffusion coefficient for batch 2 of agarose obtained at 22°C using batches 1 (top row) and 3 (bottom row) absorbance time series. Each column is a different sample in each batch.....	55
Figure 25 Residual plots for validation of the average effective diffusion coefficient for batch 2 of agarose obtained at 22°C using batches 1 (top row) and 2 (bottom row) absorbance time series. Each column is a different sample in each batch.....	56
Figure 26 Residual plots for validation of the average effective diffusion coefficient for sample 1 across all batches of agarose obtained at 22°C using the absorbance time series for samples 2 (top row) and 3 (bottom row) across all batches. Each column represents a different batch. ....	58
Figure 27 Residual plots for validation of the average effective diffusion coefficient for sample 2 across all batches of agarose obtained at 22°C using the absorbance time series for samples 1 (top row) and 3 (bottom row) across all batches. Each column represents a different batch. ....	58

Figure 28 Residual plots for validation of the average effective diffusion coefficient for sample 3 across all batches of agarose obtained at 22°C using the absorbance time series for samples 1 (top row) and 2 (bottom row) across all batches. Each column represents a different batch. .... 59

Figure 29 A comparison of the theoretical and average experimental thicknesses before (left) and after (right) packing in sample holder for testicular tissue. A solid orange line represents the theoretical thicknesses before packing. Experimental thicknesses are shown as blue diamonds. The correlation line for the experimental thicknesses after packing in the sample holder is represented by a blue dashed line, equation: thickness = 14.7\*weight in grams + 0.75 mm ( $R^2 = 0.3323$ ). ..... 64

Figure 30 Absorbance as a function of time obtained at 22°C for different samples of testicular tissue across three collection days 1 (left), 2 (middle), and 3 (right). For each day, samples 1, 2, and 3 are represented by blue circles, orange squares, and gray diamonds, respectively. .... 65

Figure 31 Absorbance data fit to determine  $D_{eff}$  for testicular tissue collection day 1 samples 1 (left), 2 (middle), and 3 (right). Experimental absorbance values are indicated by pink circles and predicted absorbance values are represented by the blue line. .... 66

Figure 32 Residual plots for normalized absorbance value generated during estimation of the diffusion coefficient for DMSO in testicular tissue at 22°C. Each row is a different collection day and each column is a different sample for each collection day. .... 67

Figure 33 Absorbance as a function of time for testicular tissue collection day 2 samples 1 (left), 2 (middle), and 3 (right) fit using the average effective diffusion coefficient from collection day 1. Experimental values are indicated by pink circles, and predicted absorbance is represented by the blue line. .... 70

Figure 34 Residual plots for validation of the average effective diffusion coefficient for collection day 1 of testicular tissue obtained at 22°C using collection days 2 (top row) and 3 (bottom row) absorbance time series. Each column corresponds to a different sample on each collection day. .... 71

Figure 35 Residual plots for validation of the average effective diffusion coefficient for collection day 2 of testicular tissue obtained at 22°C using collection days 1 (top row) and 3 (bottom row) absorbance time series. Each column corresponds to a different sample on each collection day. .... 71

Figure 36 Residual plots for validation of the average effective diffusion coefficient for collection day 3 of testicular tissue obtained at 22°C using collection days 1 (top row) and 2 (bottom row) absorbance time series. Each column corresponds to a different sample on each collection day. .... 72

Figure 37 Design and dimensions for sample holder for CPA diffusion studies. Only the ring designed for alginate-gelatin is shown here. Two more rings with inner diameters of 6mm and 7.4mm were also machined from acetal for use with testicular tissue and agarose..... 75

Figure 38 System diagram of scaling comparison for pressure introduced by DMSO on top of sample inside the holder..... 76

Figure 39 Thermal control design setup for diffusion studies with thermocouple placement (left) and PCM bag placement (right)..... 78

Figure 40 Average thermal profile of DMSO inside sample holder (left) the surface of FTIR (right) of three parallel thermal controlled diffusion studies. In the left figure, the experimental and target temperature values for the DMSO inside the sample holder are presented as orange circles and a green line, respectively. In the right figure, the temperatures for the front surface of the FTIR and the surface of the ring around the sensing window plate are represented by dark blue circles and light blue squares, respectively. .... 80

Figure 41 Absorbance as a function of time obtained at 4°C for different agarose samples from the same preparation batch. Batch 1 samples 1 (left), 2 (middle), and 3 (right). The first, second, and third samples in each batch are represented by blue circles, orange squares, and gray diamonds, respectively..... 81

Figure 42 Diffusion coefficient estimation fits obtained at 4°C for agarose batch 1 samples 1 (left), 2 (middle), and 3 (right). Experimental absorbance values are indicated by gray circles, and predicted values are represented by the blue line..... 82

Figure 43 Residual plots for normalized absorbance value generated during estimation of the diffusion coefficient for DMSO in agarose at 4°C. Each row is a different batch, and each column is a different sample within each batch. .... 83

Figure 44 Residual plots for validation of the average effective diffusion coefficient for batch 1 of agarose obtained at 4°C using batches 2 (top row) and 3 (bottom row) absorbance time series. Each column corresponds to a different sample in each batch. .... 86

Figure 45 Residual plots for validation of the average effective diffusion coefficient for batch 2 of agarose obtained at 4°C using batches 1 (top row) and 3 (bottom row) absorbance time series. Each column corresponds to a different sample in each batch. .... 87

Figure 46 Residual plots for validation of the average effective diffusion coefficient for batch 3 of agarose obtained at 4°C using batches 1 (top row) and 2 (bottom row) absorbance time series. Each column corresponds to a different sample in each batch. .... 87

Figure 47 Residual plots for validation of the average effective diffusion coefficient for sample 1 across all batches of agarose obtained at 4°C using the absorbance time series for sample 2 (top row) and 3 (bottom row) across all batches. Each column represents a different batch..... 89

Figure 48 Residual plots for validation of the average effective diffusion coefficient for sample 2 across all batches of agarose obtained at 4°C using the absorbance time series for samples 1 (top row) and 3 (bottom row) across all batches. Each column represents a different batch..... 90

Figure 49 Residual plots for validation of the average effective diffusion coefficient for sample 3 across all batches of agarose obtained at 4°C using the absorbance time series for samples 1 (top row) and 2 (bottom row) across all batches. Each column represents a different batch..... 90

Figure 50 Absorbance as a function of time obtained at 4°C for testicular tissue days 1 (left), 2 (middle), and 3 (right). The first, second, and third sample each day are represented by blue circles, orange squares, and gray diamonds, respectively. .... 92

Figure 51 Diffusion coefficient estimation fits obtained at 4°C for testicular tissue collection day 1 samples 1 (left), 2 (middle), and 3 (right). Experimental absorbance values are indicated by pink circles, and predicted values are represented by the blue line. .... 93

Figure 52 Residual plots for normalized absorbance value generated during estimation of the diffusion coefficient for DMSO in testicular tissue at 4°C. Each row is a different collection day, and each column is a different sample for each collection day. .... 95

Figure 53 Absorbance data for testicular tissue collection day 2 samples 1 (left), 2 (middle), and 3 (right) fit using the average effective diffusion coefficient from collection day 1. Experimental values are indicated by pink circles and predicted values are represented by the blue line. .... 97

Figure 54 Residual plots for validation of the average effective diffusion coefficient for collection day 1 of testicular tissue obtained at 4°C using batches 2 (top row) and 3 (bottom row) absorbance time series. Each column corresponds to a different sample on each collection day. 98

Figure 55 Residual plots for validation of the average effective diffusion coefficient for collection day 2 of testicular tissue obtained at 4°C using batches 1 (top row) and 3 (bottom row) absorbance time series. Each column corresponds to a different sample on each collection day. 98

Figure 56 Residual plots for validation of the average effective diffusion coefficient for collection day 3 of testicular tissue obtained at 4°C using batches 1 (top row) and 2 (bottom row) absorbance time series. Each column corresponds to a different sample on each collection day. 99

Figure 57 Thermal control design setup modification for diffusion studies with revised thermocouple placement. The original thermocouple placement (left) was modified for the refined monitoring system (right) to minimize the contribution of the PCM bags to the temperature registered by the thermocouple compared to the surface of the FTIR..... 101

Figure 58 Thermal profile for DMSO inside the sample holder (left) and the contact point between the sample and the FTIR surface (right) obtained using T-type thermocouples for three parallel temperature-controlled diffusion studies and corresponding average profiles. The values for the first, second, and third studies are presented as blue circles, and orange squares, gray diamonds, respectively. The average values are represented by purple stars and the target temperatures for the sample and DMSO are represented by a green line..... 102

Figure 59 Effective diffusion coefficients for glucose or DMSO in different diffusion mediums. Values in alginate beads and agar membranes were determined for glucose at 30°C (diamond) and 37°C (triangle). Values in alginate-gelatin and agarose were determined for DMSO at 22°C (circle) and 4°C (square). .... 105

Figure 60 Sample holder ring and cover and sample holder lid machined from acetal and aluminum, respectively. .... 107

Figure 61 Average thermal profile of DMSO inside sample holder and contact point between sample and sensing window (left), and average thermal profile of the surface of FTIR (right) of three parallel thermal controlled diffusion studies. In the left figure, the experimental temperature values for the DMSO inside the sample holder and the contact point between the sample and the sensing window are presented as orange circles and purple diamonds, respectively. The target temperature for the DMSO and the sample is represented by a green line. In the right figure, the

temperatures for the front surface of the FTIR and the surface of the ring around the sensing window plate are represented by dark blue circles and light blue squares, respectively..... 108

Figure 62 Effective diffusion coefficients reported for DMSO into various tissues together with diffusion coefficient for DMSO in alginate-gelatin, agarose, and testicular tissue, as established in this work. Values determined at 4°C, 17°C, 22°C, 27°C, and 37°C are represented by squares, X marks, circles, diamonds, and triangles, respectively..... 111

Figure 63 Arrhenius plot of the activation energy for diffusion of DMSO in agarose. The average values are indicated by a solid gray line. The values considering increasing by 1 standard deviation and decreasing by 1 standard deviation are represented by a dot-dashed blue line and a dashed orange line, respectively. .... 113

Figure 64 Arrhenius plot of the activation energy for diffusion of DMSO in testicular tissue. The average values are indicated by a solid pink line. The values considering increasing by 1 standard deviation and decreasing by 1 standard deviation are represented by a dot-dashed blue line and a dashed orange line, respectively. .... 114

## LIST OF ABBREVIATIONS

NIST	national institute of standards and technology
CPA	cryoprotective agent
DMSO	dimethyl sulfoxide
EG	ethylene glycol
PG	propylene glycol
SA-gels	sodium alginate-gelatin
TT	testicular tissue
FTIR	Fourier-transform infrared
ATR	attenuated total reflection
IR	infrared
DOE	design of experiments
PCM	phase change material

## **CHAPTER 1 SIGNIFICANCE: MASS DIFFUSIVITY IN THE CONTEXT OF CRYOPRESERVATION**

### **1.1 Cryopreservation of sperm and testicular tissue**

Cryopreservation of sperm cells has allowed advancements in animal agriculture, protection of endangered species, and human reproductive medicine but utilizes mature spermatozoa. Spermatozoa have been preserved using mixtures of cryoprotective agents (CPAs) such as glycerol, ethylene glycol, and DMSO, with glycerol acting as the standard protectant for spermatozoa [4]. However, immature spermatozoa have been shown to be more susceptible to toxicity damage from cryo-protective agents, or CPAs [1]. Several lifesaving treatments, such as those for cancer, as well as diseases can result in sterilization in pre-pubertal males [4, 12], thus cryopreservation strategies have been sought to preserve fertility in these patients. Thus far, attempts to cryopreserve testicular tissues have been successful in mammalian testicular tissue, but recovery rates for spermatogonia preserved using slow-freezing methods were lower than for vitrification methods [1, 2, 4, 12, 13]. While vitrification of immature human testicular tissue has shown potential for increasing fertility preservation, optimization of the vitrification procedures is still required to increase recovery rates after grafting from less than 10% [2].

### **1.2 The role of cryoprotectants and their limitations**

Cryoprotective agents (CPAs) are used to protect cells during preservation procedures. Penetrating CPAs prevent the formation of intracellular ice experienced at rapid cooling rates by increasing the concentration of solutes inside the cells and lowering the freezing point [14]. Non-penetrating CPAs are used to reduce damage from extracellular ice formation during freezing and warming procedures [4, 14-16]. While cryopreservation of cells has been studied extensively and has been highly successful, application of these processes to tissues is more challenging. The rate of loading and the distribution pattern of CPAs in tissues is dependent on factors including geometry, cellular

make-up of the tissue, density, and environmental temperature. Long CPA loading times are necessary to reach equilibrium throughout the tissue. While this reduces the risk of damage from extracellular ice formation within the tissue, it increases the risk of damage due to toxicity [17]. Similarly, vitrification typically requires high concentrations of CPAs, which further increases the risk of chemical toxicity damage [4, 15]. Successful vitrification of cells with reduced toxicity damage has been demonstrated using mixtures of common CPAs [18-20]. However, the loading times and behavior during loading of these mixtures has not been comprehensively investigated in testicular tissues thus far. The determination of CPA diffusion properties in testicular tissue will allow application of diffusion and toxicity models [6-8] to determine optimal CPA compositions for quick loading and unloading to facilitate successful preservation of testicular tissues.

### **1.2.1 Current work on CPA loading optimization**

Currently, design of cryopreservation procedures, including the temperature and time for loading and the concentration of CPA loaded, is done through rudimentary trial-and-error techniques. To maximize the success of cryopreservation processing, CPA diffusion and toxicity models have recently been developed [6-8]. These models enable prediction of viability outcomes, given appropriate transport and toxicity data, and can be used to run simulations of the effects of different loading conditions. However, the models rely on good input data, including mass diffusion coefficients, and indicators of toxicity. Diffusion parameters of DMSO and a few common vitrification solutions have been identified for ovarian tissues [21], pulmonary arterial valve tissue [22], and articular cartilage [23, 24] but comprehensive diffusion data is lacking. Furthermore, because of the lack of available data, the toxicity cost function developed by Davidson et al. (2015), while yielding important process improvements, considers the use of a single component rather than the mixtures of CPAs that have become more common [7]. Benson et al. (2018)

modified this toxicity cost function for use with thin tissues, but additional diffusion data is necessary to allow application to thicker tissues [8]. Furthermore, the diffusion coefficients for common CPAs, such as DMSO, in testicular tissue are unknown. Thus, in the current work, a diffusion model was applied to determine the effective diffusion coefficient for DMSO in feline testis samples.

### **1.3 Diffusivity and the diffusion coefficient**

Diffusion of CPAs is often modeled using Fick's second law of diffusion which considers effective motion of an infinite number of particles through a medium [25]. Fick's second law, shown in Equation 1, considers diffusivity of a material or species into a particular medium.

$$\frac{\partial C}{\partial t} = D \frac{\partial^2 C}{\partial x^2} \quad (\text{Eqn 1})$$

In this equation,  $C$  is the concentration of a diffusing species,  $x$  is the position in the medium,  $t$  represents time,  $D$  represents diffusivity. Diffusivity is defined as “a measure of the capability of a substance or energy to be diffused or to allow something to pass by diffusion” [26]. When diffusivity in a porous medium is being studied, an effective diffusion coefficient,  $D_{\text{eff}}$ , replaces  $D$  in Equation 1 and represents diffusion through the porous space as a whole. The effective diffusion coefficient is used as an input for models used to explore optimization of CPA loading into tissues.

#### **1.3.1 CPA diffusion coefficients in tissue**

Diffusion coefficients have been determined for several common CPAs, such as DMSO and glycerol, in various tissue types such as articular cartilage, pulmonary arterial valve tissue, and rat kidney and liver tissue [22, 24, 27-32]. For example, Sharma et al. (2007) determined the effective diffusion coefficient of DMSO and propylene glycol (PG) in porcine articular cartilage dowels at

4, 22, and 37°C using osmolality measurements [30, 32]. The porcine articular cartilage was submerged in a volume of 4mL of the chosen CPA, DMSO or PG for defined exposure times. The porcine articular cartilage was then moved to a 4mL volume of 1X PBS buffer solution and placed in sealed storage. After 24 hours, the osmolality of the CPA in the PBS and of the PBS itself is measured with an osmometer, and the difference of these two values is the concentration of CPA in the PBS surrounding the articular cartilage. The average concentration of the CPA in the porcine articular cartilage ( $C_{c,ave}$ ) can then be calculated using Equation 2.

$$C_{c,ave} = C_s \cdot V_s / V_c \quad (\text{Eqn 2})$$

In which,  $C_s$  is the concentration of CPA in the PBS from the articular cartilage,  $V_s$  is the volume of the solution, and  $V_c$  is the volume of PBS-like solution within native porcine articular cartilage.  $V_c$  can be estimated by determining the water volume at the same conditions. To do so, several pre-weighed, non-uniform sections of porcine articular cartilage were stored in a vacuum desiccator for one week. The mass difference was credited to the water in the articular cartilage and used to calculate the water volume,  $V_c$ . Fick's second law can be applied using existing analytical solutions, such as those presented by Crank (1975), which most often present concentration as functions of time, initial concentration of the CPA introduced, geometry of a specimen, and the diffusion coefficient [33]. The diffusion coefficient is determined by fitting an analytical solution against experimental CPA concentrations assuming a specific geometry (e.g. a thin disc) for the specimen,  $C_s$  as the concentration at infinity, and the exposure time as inputs. Sharma et al. (2007) determined that the effective diffusion coefficients in 5-10mm thick porcine articular cartilage for DMSO were  $2.0 \pm 1.9$ ,  $3.5 \pm 2.0$ , and  $3.5 \pm 2.2 \times 10^{-6}$  cm<sup>2</sup>/s for 4, 22, and

37°C, respectively. The  $D_{\text{eff}}$  for PG in porcine articular cartilage was determined to be  $1.0 \pm 0.6$ ,  $2.0 \pm 1.2$ , and  $2.5 \pm 1.6 \times 10^{-6} \text{ cm}^2/\text{s}$  at 4, 22, and 37°C, respectively.

Using thinner sections of porcine articular cartilage, Jomha et al. (2009) found the  $D_{\text{eff}}$  values for DMSO and PG at 4, 22, and 37°C, to be  $2.6$ ,  $3.1$ , and  $6.2 \times 10^{-6} \text{ cm}^2/\text{s}$  and  $0.8$ ,  $1.6$ ,  $2.7 \times 10^{-6} \text{ cm}^2/\text{s}$ , respectively [30]. The effective diffusion coefficients for ethylene glycol (EG) were determined to be  $2$ ,  $2.7$ , and  $4.2 \times 10^{-6} \text{ cm}^2/\text{s}$  for 4, 22, and 37°C. The effective diffusion coefficients for glycerol (GLY) were determined to be  $0.8$ ,  $1.8$ , and  $2.3 \times 10^{-6} \text{ cm}^2/\text{s}$  for 4, 22, and 37°C. While three samples were used to obtain average diffusion coefficients at all temperatures for each CPA, no indicators of variation were reported. This method has also been used to ascertain  $D_{\text{eff}}$  values of  $5.14$ ,  $1.04$ , and  $1.6 \times 10^{-6} \text{ cm}^2/\text{s}$  for DMSO, sucrose, and a DMSO-sucrose mixture, respectively, in pulmonary arterial valve tissue [22]. These diffusion coefficients were determined using three samples for each case with standard deviations of approximately 3%, 19%, and 6%, respectively.

Isbell et al. (1997) used nuclear magnetic resonance (NMR) imaging to determine diffusion coefficients for DMSO in rat kidney and liver slices. In this method, a magnetic field is used to perturb nuclei in the tissue sample and the resulting resonant signal can be related to physical, chemical, electronic, and structural information about molecules in the tissue. Isbell et al. (1997) suspended rat liver or rat kidney slices in NMR tubes with 5-8mL of cooled CPA solutions, and images were taken of the slices. An image processing software was used to define paths in the image from the surrounding fluid to the center of the tissue. The pixel intensities were determined, normalized to the highest intensity, and converted using the software to a concentration curve which can be used to estimate the diffusion coefficient and a “virtual velocity” of the CPA by fitting to the analytic solution for Fick’s second law, shown in Equation 3.

$$\frac{C}{C_0}(x, t) = \frac{2}{\sqrt{\pi}} \int_{\xi/2\sqrt{D_e t}}^{\infty} \exp(-\omega^2) d\omega \quad (\text{Eqn 3})$$

In this equation,  $C$  is the concentration and  $C_0$  is the concentration at the boundary  $x = 0$ ,  $x$  is the position in the diffusion medium,  $t$  represents time,  $D_e$  is the effective diffusion coefficient,  $\omega$  is a constant of integration, and  $\xi = x - Ut$  (where  $U$  is a virtual velocity of fluid convection). The effective diffusion coefficients were determined to be 55 and 180 x 10<sup>-6</sup> cm<sup>2</sup>/s for DMSO in rat kidney slices at 8 and 23°C, respectively. The effective diffusion coefficient was determined to be 35 and 50 x 10<sup>-6</sup> cm<sup>2</sup>/s for DMSO in rat liver slices at 10 and 25°C, respectively. Each diffusion coefficient was determined as an average of three to five images. While exact indicators of variation are not reported, Isbell et al. (1997) notes errors of 30% or more in many cases.

Devireddy (2005) modified an existing model which had been used to analyze net solute movements in biological systems to create an analytical model for determining effective diffusion coefficients for simulated human ovarian tissue units consisting of multiple cylindrical sections, referred to as Krogh cylinders [28]. The model was used to predict normalized CPA concentration values based on permeability parameters, such as the cell membrane permeability, and the mass diffusion coefficients of common CPAs diffusing into ovarian tissue sections. A priori concentration data obtained by Newton et al (1998) [34] for DMSO, PG, EG, and GLY in human ovarian tissue using NMR imaging was fit to the model and a least squares curve fitting technique was used to predict the prescribed parameters. The diffusion coefficient was predicted for DMSO (11, 14, and 12 x 10<sup>-6</sup> cm<sup>2</sup>/s), PG (9.2, 17, and 10 x 10<sup>-6</sup> cm<sup>2</sup>/s), EG (13.1, 20.8, and 18.5 x 10<sup>-6</sup> cm<sup>2</sup>/s), and GLY (8.5, 13.8, 13.5 x 10<sup>-6</sup> cm<sup>2</sup>/s) at 4°C, 27°C, and for a combined best fit of the values at the two temperatures. No indicators of variation were reported.

The effective diffusion coefficients obtained for DMSO in tissues using osmolality measurements, simulation, or NMR imaging outlined in this section are summarized in Table 1. The effective diffusion coefficients for DMSO, glycerol, sucrose, propylene glycol, and ethylene glycol into ovarian tissues, articular cartilage, arterial valve tissue at different temperatures are represented in Figure 1.

Table 1 Diffusion coefficients in tissues obtained using NMR imaging<sup>1</sup>, simulation compared against a priori NMR data<sup>2</sup>, FTIR methods<sup>3</sup>, osmolality methods<sup>4</sup>, or Raman spectroscopy<sup>5</sup>

Diffusion Medium	Temperature, °C	D <sub>eff</sub> [x 10 <sup>-6</sup> cm <sup>2</sup> /s]	Reference		
Rat Liver <sup>1</sup>	8	55	[29]		
	23	180			
Rat Kidney <sup>1</sup>	10	35			
	25	50			
Human Ovarian Tissue <sup>2</sup>	4	11	[28]		
	27	14			
Porcine Ovarian Tissue <sup>3</sup>	22	15.7	[21]		
Human Articular Cartilage <sup>1</sup>	100%	4	3.1	[27]	
		17	6.2		
		27	6.8		
		37	7.2		
	10%	4	6.1		
		17	10.7		
		27	14.4		
		37	17.9		
Porcine Articular Cartilage <sup>4</sup>	Bone Attached	4	2	[32]	
		22	3.5		
		37	3.5		
	No Bone Attached	4	2.5		[30]
		22	3.5		
	Not Specified	4	2.6		
		22	3.1		
	Pulmonary Arterial Valve Tissue <sup>4</sup>	DMSO alone	22	5.14	[22]
DMSO with Sucrose			22	1.6	
Pulmonary Arterial Valve Tissue <sup>3</sup>	DMSO alone	22	3.02	[22]	
		DMSO with Sucrose	22		3.35
		DMSO in VS83	22		6.51
		DMSO in VS55	22		4.63
Bovine Articular Cartilage <sup>1</sup>	DMSO	22	3.59	[24]	
	DMSO in VS55	22	4.63		
Fresh Porcine Skin Tissue <sup>5</sup>	50um depth	22	0.112	[31]	
	150um depth	22	0.112		
	250um depth	22	0.231		
	350um depth	22	0.328		
		22			

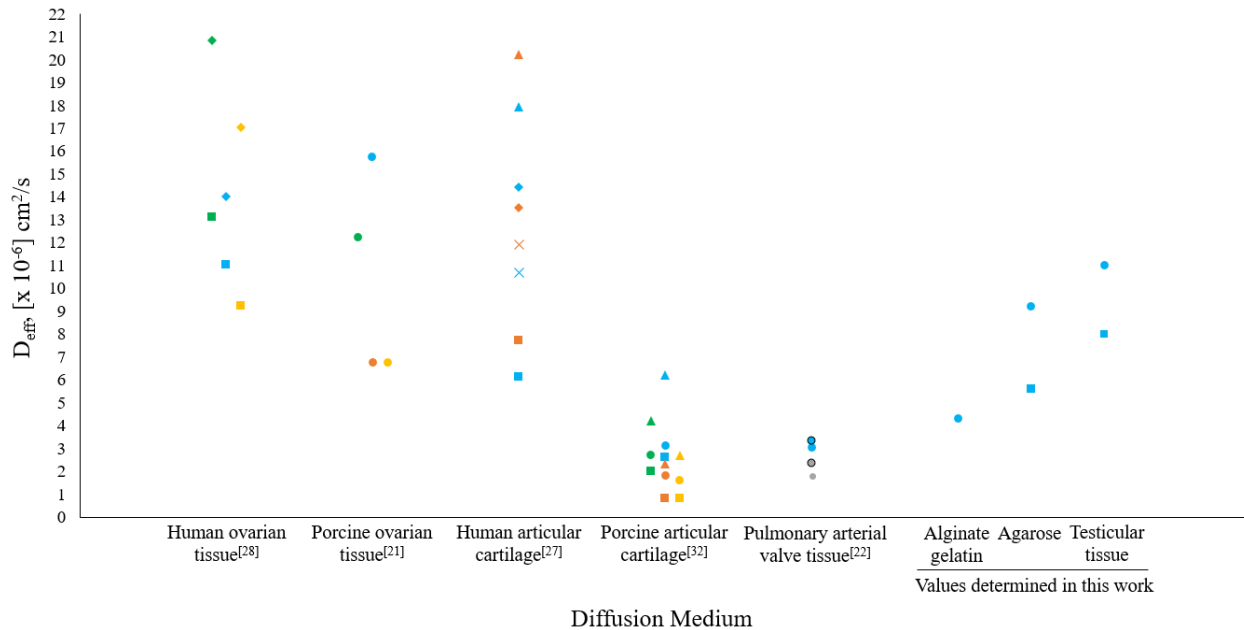


Figure 1 Effective diffusion coefficients for DMSO (blue), glycerol (orange), sucrose (gray), propylene glycol (yellow), and ethylene glycol (green) into ovarian tissues, articular cartilage, and arterial valve tissue at five temperatures. Values determined at 4°C, 17°C, 22°C, 27°C, and 37°C are represented by squares, X marks, circles, diamonds, and triangles, respectively. The bordered values were determined in for single values in mixtures.

### 1.3.2 Modeling diffusion kinetics to estimate diffusion coefficient

More recent work in estimating diffusion coefficients for CPA diffusion into tissues has utilized an equation relating Fourier transform infrared spectroscopy (FTIR) absorbance values to 1-dimensional diffusion of a species into a thin sample, a relationship developed by Barbari and Fieldson (1995) [10, 11]. This method is based on the assumption of bulk 1-D diffusion of a penetrant into a film, which assumes a constant pressure and that the diameter of the sample is much larger than the thickness. Strictly speaking, Fickian mass diffusion within heterogeneous media/tissue should be modeled using a (possibly space-dependent) diffusion matrix. However, given the impracticality of experimentally determining a diffusion matrix for heterogeneous testicular tissue, the present study assumes that in-tissue diffusion is homogeneous, and is thus describable by a single effective diffusion coefficient. The effective diffusion coefficient is a lumped parameter which accounts for physical factors, including porosity [35]. While porosity

affects the diffusion coefficient value, it is difficult to measure for tissues. It is not possible identify all pores in a tissue sample using only one method. In addition, the established methods for determining porosity have mostly been applied to “stiff” materials such as metal, ceramic, or polymer foams not soft tissues such as testicular tissue [36]. Thus, the use of an effective diffusion coefficient is necessary for efficiency and practicality of tissue preservation.

To develop a model for determining the effective diffusion coefficient, Fieldson and Barbari combined Fick’s law with the continuity equation to yield the following equation:

$$\frac{\partial C}{\partial t} = D_{eff} \frac{\partial^2 C}{\partial z^2}$$

In which  $C$  is the concentration of penetrating species,  $D_{eff}$  is the diffusion coefficient,  $t$  represents time, and  $z$  is the position in the medium. A concentration profile can be developed by solving this equation subject to the following boundary conditions.

$$C = 0 \text{ for } t < 0, 0 \leq z \leq L$$

$$C = C_L \text{ for } t \geq 0, z = L$$

$$\frac{\partial C}{\partial z} = 0 \text{ for } t \geq 0, z = 0$$

The variable  $L$  is the thickness of the film. The resulting normalized concentration profile solution is then defined as

$$\frac{C}{C_L} = 1 - \frac{4}{\pi} \sum_{n=0}^{\infty} \frac{(-1)^n}{2n+1} \exp \left[ \frac{-D(2n+1)^2 \pi^2 t}{4L^2} \right] \cos \left[ \frac{(2n+1)\pi z}{2L} \right]$$

The concentration profile can be substituted into the general absorbance expression for weak absorbers using FTIR, defined as

$$A = \int_0^L \epsilon^* C e^{-2\gamma z} dz$$

In which  $\epsilon^*$  is a constant including the refractive indices, the molar extinction coefficient, the number of reflections, and the cross-sectional area of the beam; and  $\gamma$  is the evanescent field decay coefficient. Substituting the concentration profile in the general absorbance expression and integrating produces an equation for the ratio of absorbance,  $A$ , at a given time point to the absorbance at equilibrium,  $A_\infty$ , shown below.

$$\frac{A}{A_\infty} = 1 - \frac{8\gamma}{\pi(1 - \exp(-2\gamma L))} \sum_{n=0}^{\infty} \frac{\exp\left(\frac{-D(2n+1)^2\pi^2 t}{4L^2}\right) \left[(-1)^n 2\gamma + \frac{(2n+1)\pi}{2L} \exp(-2\gamma L)\right]}{(2n+1) \left[4\gamma^2 + \left(\frac{(2n+1)\pi}{2L}\right)^2\right]}$$

Where  $\gamma$  is defined as

$$\gamma = \frac{2n_2\pi \sqrt{\theta - \frac{n_1^2}{n_2^2}}}{\lambda}$$

In this equation  $n_1$  is the refractive index of the sample,  $n_2$  is the refractive index of the ATR crystal (2.43),  $\theta$  is the angle of incidence ( $45^\circ$ ), and  $\lambda$  is the inverse of the characteristic wavenumber for the diffusing species. A refractive index of 1.3345 [37] was assumed for alginate-gelatin and agarose, while 1.4 was used for tissue [22, 38, 39]. The characteristic wavenumber, or the wavenumber corresponding to the maximum absorbance, for DMSO is  $950 \text{ cm}^{-1}$ .

Previously, Wang et al. (2014) used FTIR and a fitting algorithm for this model to determine diffusion coefficients for glycerol into leaflet tissue, artery tissue, and muscle tissue from decellularized heart valves as  $2.59$ ,  $5.08$ , and  $6.25 \times 10^{-6} \text{ cm}^2/\text{s}$  with approximate standard deviations of 25%, 23%, and 44%, respectively [38]. Han et al. (2019) also used this method to

determine diffusion coefficients in porcine ovarian tissue for DMSO ( $15.7 \pm 5.9 \times 10^{-6} \text{ cm}^2/\text{s}$ ), ethylene glycol ( $12.2 \pm 3.4 \times 10^{-6} \text{ cm}^2/\text{s}$ ), glycerol ( $6.73 \pm 2.1 \times 10^{-6} \text{ cm}^2/\text{s}$ ), and propylene glycol ( $6.76 \pm 0.6 \times 10^{-6} \text{ cm}^2/\text{s}$ ) [21]. Similarly, Vásquez-Rivera (2018) applied this method to determine the diffusion coefficients of DMSO and sucrose when they were used as individual CPAs as well as when they were used in combination in pulmonary arterial valve tissue using three samples in each case. The resulting average  $D_{\text{eff}}$  values were  $3.02 \times 10^{-6} \text{ cm}^2/\text{s}$  for DMSO alone,  $1.79 \times 10^{-6} \text{ cm}^2/\text{s}$  for sucrose alone, and  $3.35 \times 10^{-6} \text{ cm}^2/\text{s}$  for DMSO and  $2.31 \times 10^{-6} \text{ cm}^2/\text{s}$  for sucrose in the mixture [22]. The corresponding standard deviations were approximately 2.5%, 5.6%, 2.2%, and 4.3%, respectively. Wang et al. (2015) determined the effective diffusion coefficient of sucrose into decellularized heart valves as  $3.5 \pm 0.3$  and  $4.6 \pm 0.7 \times 10^{-6} \text{ cm}^2/\text{s}$  at 22 and 37°C (n=3 for each temperature), respectively. The  $D_{\text{eff}}$  of glucose into decellularized heart valves was determined to be  $5.0 \pm 1.1 \times 10^{-6} \text{ cm}^2/\text{s}$  at 22°C [38, 39]. The diffusion coefficients obtained using FTIR methods are also summarized in Table 1.

For this work, two software programs were developed using Excel (Microsoft, WA, USA). Absorbance as a function of time data for samples that reached equilibrium were fitted using the program for 1-variable estimation of the effective diffusion coefficient. Absorbance time series for non-equilibrated samples were fitted using the second program allowing 2-variable estimation of the effective diffusion coefficient and equilibrium absorbance value. At least 50 terms in the summation were assumed in both programs.

#### **1.4 Challenges of working with soft tissue and the need for a reference standard**

Optimization of CPA loading and unloading times can be achieved using models such as those developed by Benson and Higgins (2012, 2018), which rely on accurate diffusion coefficient estimations for CPAs such as DMSO in soft tissues such as testicular tissue as inputs. However,

determination of effective diffusion coefficient values using diffusion data, are generally dependent on well-defined geometries and boundary conditions, as described in Section 1.3.1. Thus, sectioning of tissues to known geometries and/or measuring dimensions accurately is a critical aspect of methodology development. Hard tissues have been studied more frequently, and they tend to retain their form during slicing and can be prepared in prescribed geometries that can be easily modelled [21, 23, 24, 28, 40-42]. Standard methodology to create toleranced sections of soft tissues has not been established. While paraffin wax can be used to facilitate sectioning, this requires dehydration of the tissues which can affect the diffusion behavior. Furthermore, specimens such as testes can vary widely in size with age and even between donors of the same age, which can impact cutting [43, 44]. Smaller specimens are often hard to section using the biopsy punch tools that have been used by others to obtain cylindrical geometries with prescribed diameters [38]. In addition, mammalian tissues contain many cell types of various dimensions, each with their own different permeability properties [4]. Recent advancements in precision slicers, such as vibratomes, have been developed to aid in the sectioning of live tissues without using methods requiring freezing or dehydration of the tissue [45]. However, standard practices for sectioning still need to be developed. To facilitate the creation of slicing and measurement techniques for tissues, a reference standard for tissues is imperative for identifying and minimizing sources of error throughout methodology development and optimization.

### **1.5 Desirable reference standard characteristics**

A reference standard is defined as “an artifact that embodies the quantity of interest in a way that ties its values to the reference base” [46]. In the context of studying CPA diffusivity, a reference standard would repeatedly yield the same diffusion coefficient for specified single CPA or mixture of CPAs if measured by the same methodology. As stated in the NIST standard reference materials

catalog, reference standards are used in various industries and academia to facilitate the calibration of instruments, verify measurement results, and develop measurement methodology [47]. In addition, traceability must be established by considering the uncertainty of measured properties and relating these materials to existing references, such as national standards or international standards [48, 49]. The use of a reference standard for CPA diffusion studies using the FTIR would aid in the identification of sources of error in the measurement methodology during development.

Current efforts towards a reference standard for tissues have primarily focused on creating tissue “phantoms” which simulate the optical properties found in human or animal tissue. They are used to test system designs, optimize the signal to noise ratio in established systems, maintain quality control, and compare results between systems, laboratories, and investigators [50, 51]. While the focus was not to create a reference standard, Bernemann et al. (2010) investigated the diffusion of DMSO into collagen scaffolds, which are commonly used in tissue engineering applications, to allow prediction of the time required to reach a homogeneous distribution of DMSO throughout the scaffolds [52]. Alternatively, polyethylene glycol (PEG) and poly(D,L-lactic-co-glycolic acid) (PLGA) microspheres were used to develop an analog which mimics cellular structure in tumors and the diffusion of water in the tissue for use in diffusion weighted imaging (DWI) experiments [53]. In addition, gel structures consisting of carrageenan, agarose, sodium alginate, or sucrose have been used for DWI. However, no standard quality control regulations or guidelines for DWI reference materials and none of these materials have been quantified or characterized adequately to be considered reference standards [54].

In the context of studying diffusion, a reference standard for tissues that would allow casting or slicing to repeatable dimensions with a predictable geometry, would improve the accuracy of input parameters, such as sample thickness, used in models to estimate the diffusion coefficient. In

addition, the composition throughout the reference standard material would be homogeneous to ensure diffusion throughout the material is consistent. Thus, variability in the estimated diffusion coefficient from inconsistencies in the reference material would be minimized or removed, enabling any remaining experimental uncertainty to be identified. With this knowledge, the variability in the  $D_{\text{eff}}$  value of tissue samples can then be estimated more accurately. The characteristics of particular interest in studying diffusion of CPAs into a reference standard are:

1. Stable properties over time with minimal to no effect from the environment during storage.  
Alternatively, the properties or effect from the environment can be controlled or measured quantitatively.
2. Has an index of refraction like that of tissue (~1.4)
3. Easy and inexpensive to manufacture.
4. Can be easily transported to different testing or experimental sites if necessary.
5. Has diffusion properties in the range of tissues of interest (testicular tissues in this work)

It should be noted that Intralipid 20% in water, India ink, agar, polyester and polyurethane resin, gelatin, polyacrylamide and polyvinyl alcohol hydrogels, and room-temperature-vulcanizing silicone have shown potential for use as reference standards, but none have been characterized and quantified enough for established reference standard use [50, 51].

## **CHAPTER 2 OVERVIEW OF EXPERIMENTAL DESIGN**

### **2.1 Rationale**

To maximize the success of cryopreservation processing of tissues, CPA diffusion and toxicity models have recently been developed [6-8]. These models enable a prediction of viability outcomes, given appropriate transport and toxicity data, and can be used to run simulations of the effects of different loading conditions. However, the models rely on good input data, including mass diffusion coefficients, and indicators of toxicity. Diffusion parameters of DMSO and a few common vitrification solutions have been identified for ovarian tissues [21], bone marrow [42], and articular cartilage [23, 24] but comprehensive diffusion data is lacking. Furthermore, because of the lack of available data, the toxicity cost function developed by Davidson et al. (2015), while yielding important process improvements, considers the use of a single component rather than the mixtures of CPAs that have become more common [7]. Benson et al. (2018) modified this toxicity cost function for use with thin tissues, but additional diffusion data is necessary to allow application to a wider range of tissue types.

The diffusion models that are used for parameter estimation are generally based on well-prescribed, simple geometries, but soft tissues are highly deformable which makes cutting and maintaining specific geometries difficult. Most current work involving sectioning of tissues and measurement of diffusion phenomena has been performed on hard tissues, which maintain their form throughout cutting [21, 23, 24, 28, 40, 41]. However, hard tissue diffusion behavior is not indicative of soft tissue behavior and methodology to create tolerated or measurable sections of soft tissues is needed. Production of a tissue analog with good dimensional repeatability after cutting to a specific geometry, as well as a composition, density, and structure with diffusion behavior comparable to that of tissues would enable identification and mitigation of sources of error or variability present during experimental procedures. Development of such a reference

standard would also facilitate the calibration of equipment and methodology within and between laboratories.

## **2.2 Goals and outcomes**

The main objective of this work was to determine the diffusivity of dimethyl sulfoxide (DMSO) in fresh testicular tissue at ambient and cold temperatures. In addition, to ensure that sources of error were identified and removed or accounted for, a reference material was created and used to test the developed diffusion study methodology.

## **2.3 Specific aims**

To accomplish the above goals and outcomes, the following specific aims were proposed:

**Aim 1** Develop a homogenous reference standard to support methodology development to measure transport characteristics of soft biological tissues.

The within-sample and sample-to-sample variability of tissues with respect to cellular composition, density, and structure can result in a high degree of variability when measuring unknown tissue transport properties, which is further complicated by anisotropy effects when sectioning from larger samples. To ensure that methodology and instrumentation are validated prior to measurement of complex tissues, especially soft tissues that are hard to section and handle, a suitable reference standard with known and reproducible properties is needed.

Two candidate materials were chosen for evaluation as reference standards. Alginate is commonly used in 3D cell culture systems due to its compatibility with cells. There is a priori knowledge of diffusion behavior of heavy metal salts [55] and sugar [56, 57] into alginate, studied using sorption and reaction methods, respectively. These constructs have also been demonstrated to be straightforward to manufacture for microphysiological systems [42, 55-66]. Agarose was also

evaluated because it has been used to model microbial biofilms and cytoplasm in cells [67]. Though most commonly used for gel electrophoresis to separate DNA and RNA, agarose has also been used in live cell imaging, to encapsulate mesenchymal cells and rat islets, and has been studied for its potential in aiding the healing of cartilage [68-70]. In addition, low melting point agarose can be quickly formed and sliced to a desired thickness using protocols developed for use with a microtome (Precisionary Instruments, LLC, MA, USA).

To determine CPA diffusivity in these reference materials, alginate-gelatin and agarose were exposed to known concentrations of CPAs on one side of a specimen with well estimated thicknesses, and FTIR was used to monitor the appearance of the CPA on the opposing side, as a function of time [22, 38, 39]. Integration of CPA specific peaks in the spectra allowed fitting of data to a mass diffusion equation. Thus, estimation of diffusivity was possible at room temperature as well as 4°C. The variability of data was analyzed by comparing averages and standard deviations between batches as well as between replicates within the same batch. The creation of a reference standard, which mimics the properties of native tissue and can be quickly and repeatedly manufactured in labs while yielding consistent properties, supports the identification of sources of error in methodology development and the transfer of technology between users. In turn, faster and more accurate investigation within the materials and process design space is possible.

**Aim 2** Develop an apparatus and methodology to enable continuous temperature control during exposure of tissues to CPAs for FTIR.

Current methods for exposing tissues to CPAs for FTIR analysis have utilized simple containers made from basic lab supplies which, while allowing easy exposure of CPAs, do not allow temperature control [22, 38, 39]. However, the diffusion time required for CPAs into tissues is dependent on temperature in addition to concentration, and CPAs are often added at low

temperatures. A chamber which allows continuous temperature control while maintaining a 1-dimensional diffusion environment was developed to facilitate the use of FTIR to study diffusion at different temperatures during exposure of tissues to common CPAs. With temperature control, it will be possible to gain a better understanding of the relationship between the diffusion behavior and the temperature of a sample, providing valuable information for optimizing CPA loading.

**Aim 3** Application of FTIR methodology to determine the temperature dependent mass diffusivity of DMSO in testicular tissue.

Temperature-dependent CPA diffusion coefficients are necessary for the efficient application of CPA loading simulation models for preservation processing [7, 8]. Testicular tissue slices were exposed to DMSO using the methodology outlined in Aim 1 to allow diffusion throughout the tissues. Loading of CPAs was conducted at 4°C and 22°C (room temperature) and analyzed by FTIR to determine diffusivity coefficients at each of these temperatures. The variability of data was analyzed by determining the standard deviations of replicates within the same batch as well as measurements between batches, where applicable. The determination of CPA diffusion characteristics in fresh soft tissue will aid the application of existing diffusion models to a wider range of tissues and facilitate optimization of CPA loading conditions to minimize CPA toxicity.

## **CHAPTER 3 GENERAL MATERIALS AND METHODOLOGY**

### **3.1 Density measurements**

The density of alginate-gelatin, agarose, and testicular tissue was estimated using volume displacement techniques. With an estimate of density, the sample thickness can be estimated from a geometrical model of the sample and the mass of individual samples, the latter being a measurement that is easily acquired in the lab. A 25 mL graduated cylinder with 0.5mL increment markings was used to determine the density of alginate-gelatin and agarose samples and a 50 mL graduated cylinder with 1mL markings was used to determine the density of testicular tissue.

A batch of alginate-gelatin was prepared. A known volume of PBS was added to the 25mL graduated cylinder. Three alginate-gelatin samples were blotted on a glass petri dish to remove excess PBS. The set of 3 alginate-gelatin samples was weighed and placed in the graduated cylinder. The volume of PBS displaced by the alginate-gelatin was noted. This process was repeated for the remaining 3 sets of 3 alginate-gelatin samples each. The density of alginate-gelatin was determined by dividing the mass of each set of alginate-gelatin samples by the volume of PBS displaced and averaging the densities of all 4 sets.

This same process was used to determine the density of agarose using 2 batches, each separated into 7 replicate sets of 4 agarose samples. In previous work in the Biostability Lab, testes were prepared for density measurements by removing the tunica albuginea and epididymis. A known volume of PBS was added to the 50mL graduated cylinder. A testis was blotted on a glass petri dish to remove excess PBS, weighed, and placed in the graduated cylinder. The volume of PBS displaced by the testis was noted, and the testis was stored once more. This process was repeated for all remaining testes in a collection day.

### 3.2 Estimation thickness from mass and density measurements

The average density of all samples was then used to determine the theoretical thicknesses of samples assuming a cylindrical geometry as defined in Equation 4.

$$L = \frac{m}{\pi\rho\left(\frac{d}{2}\right)^2} \quad (\text{Eqn 4})$$

In Equation 4,  $L$  is the thickness of the sample,  $m$  is the mass,  $\rho$  is the average density, and  $d$  is the diameter. Diameters of 10mm and 8mm were assumed for alginate-gelatin and agarose before packing into the sample holder. Diameters of 8mm and 7.4mm were assumed for alginate-gelatin and agarose after packing. The average density determined using 163 testes across 15 days was used to determine the theoretical thickness of testicular tissue samples assuming a cylindrical geometry with a diameter of 8mm for before packing and 6mm after packing.

### 3.3 Estimation of sample thicknesses

As thickness is an essential input to the model for diffusion kinetics, the thickness before and after compaction into the sample holder was determined in parallel metrology studies for alginate-gelatin, agarose, and testicular tissue. An ATOS Scanbox 4105 employing the triple scan principle was used to scan each material before and after packing into the sample holder.

A batch of alginate-gelatin was cast using methodology that will be described in Section 4.1.2. Since the alginate-gelatin is transparent at least 7 reference points were placed on the center and around the top surface to allow registration of the top surface by the ATOS Scanbox before compacting into the sample holder. The distance from the surface that the alginate-gelatin rested on during scanning and each reference point was estimated, as shown in Figure 2.



Figure 2 Reference points were used to register the top surface of the alginate-gelatin using the ATOS Scanbox (left). The thickness was estimated as the distance between the surface below the alginate-gelatin and the reference points (right). The thickness of the reference points was removed to define the thickness of the alginate-gelatin alone at each point.

After initial measurements, each alginate-gelatin sample was packed into an 8mm diameter ring inside the sample holder to simulate the diffusion testing conditions. After packing into the sample holder, a small circular piece of paper was placed on the top of the alginate-gelatin inside to provide more surface area for the ATOS Scanbox to visualize. A single point at the center of the top surface identified was used to estimate the height after packing as can be observed in Figure 3.

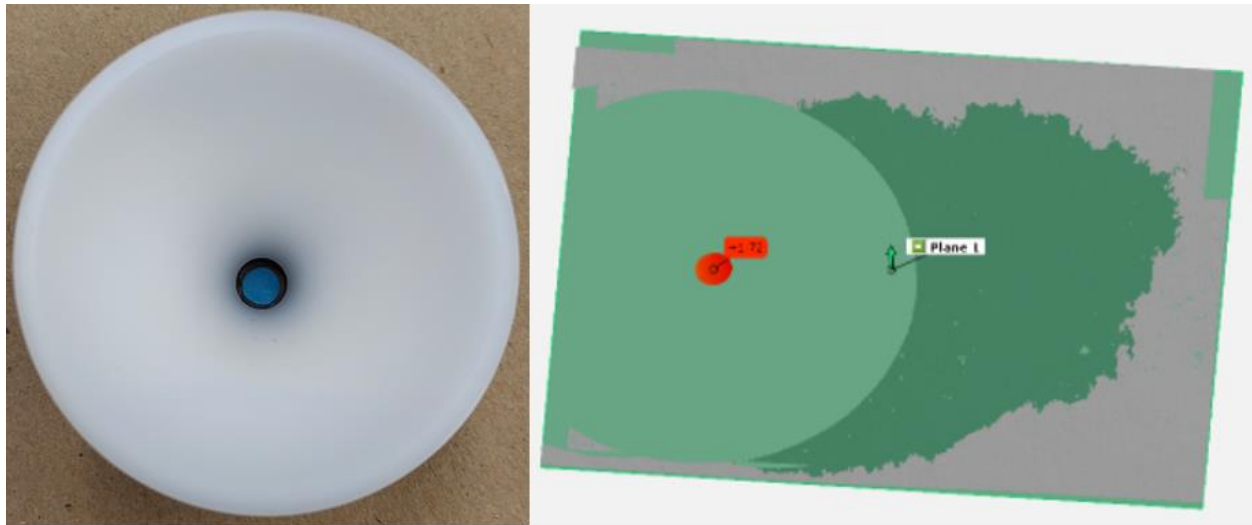


Figure 3 A small piece of paper was used to register the top surface after packing (left). A point at the center of the surface defined the thickness of the alginate-gelatin after packing (right). The thickness of the paper slip was removed to define the thickness of the alginate-gelatin only.

Similarly, a batch each of agarose and testicular tissue were prepared as will be described in Sections 4.2.2 and 5.2. Each agarose or testicular tissue sample was stored in an individual well of a 12-well plate. Agarose samples were stored with 750 $\mu$ L of PBS and testicular tissue samples were stored with 2 mL of PBS to keep each sample from drying. To maximize the surface area registered by the ATOS Scanbox for each sample, a hole punch was used to obtain paper sections that were placed on the top surface before compacting into the sample holder. Once a scan of all samples was obtained, the agarose and testicular tissue were stored in the PBS to prevent drying before packing in the sample holder. Agarose samples were packed into a 7.4mm diameter and testicular tissue samples were packed into a 6mm diameter inside the sample holder to simulate the diffusion testing conditions as shown in Figure 4.

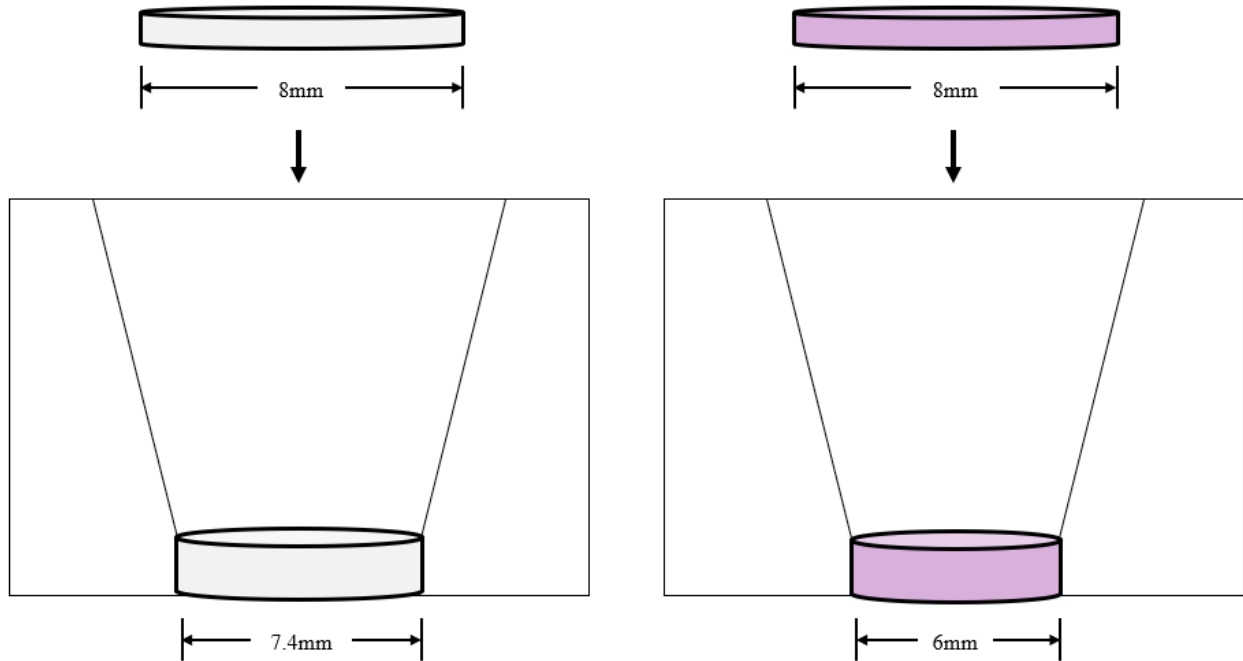


Figure 4 Agarose (left) and testicular tissue (right) were compacted into rings inside the sample holder with inner diameters of 7.4mm and 6mm, respectively.

After packing into the sample holder, a fresh small circular piece of paper was placed on the top of the sample inside for the ATOS Scanbox to visualize the top surface. Six points (agarose) or five points (testicular tissue) were set on the top of each surface defined by the ATOS Scanbox, and the distance from the surface that the sample rested on during scanning and each point was estimated. The thickness of the paper slips was removed from each point to define the thickness of the agarose or testicular tissue only.

### 3.4 FTIR testing

Fourier transform infrared (FTIR) spectroscopy is used to identify materials or species within samples. Infrared (IR) radiation passes through a sample, and some is absorbed. A spectrum is generated which displays the absorption or transmission of IR radiation [71]. Attenuated total reflectance (ATR) is a sampling method for FTIR utilizing a crystal with a high refractive index and used for measuring IR spectra for surfaces, thick materials, or strongly absorbing materials

[72]. A laser is used to pass infrared light of different wavelengths through a crystal and an ATR attachment directs the laser into a sample from below. Absorbance at each wavelength is calculated by integrating values across a sensing window. The sensing window cross-sectional area, the refractive indexes of the samples and crystal, the geometry of the sample and the concentration of a diffusing species are accounted for in the equation provided by Fieldson and Barbari (1993) and described in detail in Section 1.3.2. Unique absorption peaks are used to identify different substances and many have been identified for common CPAs at specific wavelengths, such as 950  $\text{cm}^{-1}$  for DMSO [22, 38, 39, 72]. The full-scale spectral responses from 4000  $\text{cm}^{-1}$  to 900  $\text{cm}^{-1}$  for alginate-gelatin, agarose, testicular tissue, and 3.1M DMSO are shown in Figure 5, Figure 6, Figure 7, and Figure 8, respectively. Peak bands are highlighted in gray for each spectrum. Common bands attributed to water can be observed in the full-scale spectral responses for all sample types from 2800 to 3700  $\text{cm}^{-1}$ , which contains the O-H stretching bands, and from 1500 to 1740  $\text{cm}^{-1}$ , resulting from the bending absorption of water [73]. Alginate contains bands from 1400 to 1490  $\text{cm}^{-1}$ , associated with C-N stretching, and from 1000 to 1080  $\text{cm}^{-1}$ , due to C-H stretching [74]. Agarose exhibits a C-H stretching band from 1015 to 1080  $\text{cm}^{-1}$ . However, feline testicular tissue does not have any additional peaks beyond the water peaks. Finally, DMSO contains two O-H bending peaks from 1310 to 1380  $\text{cm}^{-1}$  and from 1395 to 1440  $\text{cm}^{-1}$ , a S=O stretching peak from 980 to 1070  $\text{cm}^{-1}$ , and the unique DMSO peak from 930 to 970  $\text{cm}^{-1}$  used to quantify absorbance for DMSO during diffusion studies [75].

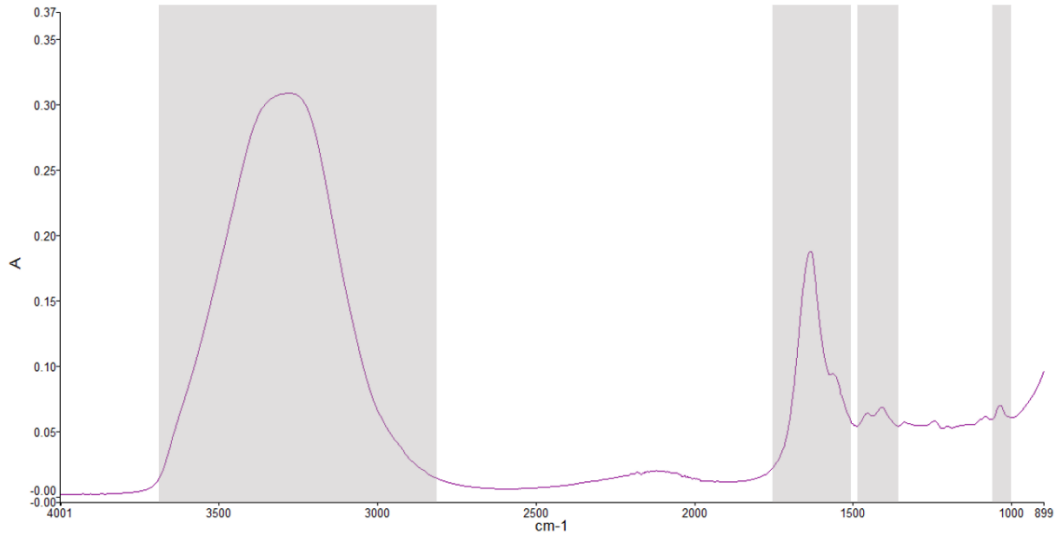


Figure 5 Full-scale spectral response from  $4000\text{ cm}^{-1}$  to  $900\text{ cm}^{-1}$  for alginate-gelatin. Bands unique to alginate exist from  $1400$  to  $1490\text{ cm}^{-1}$ , associated with C-N stretching, and from  $1000$  to  $1080\text{ cm}^{-1}$ , associated with C-H stretching [74].

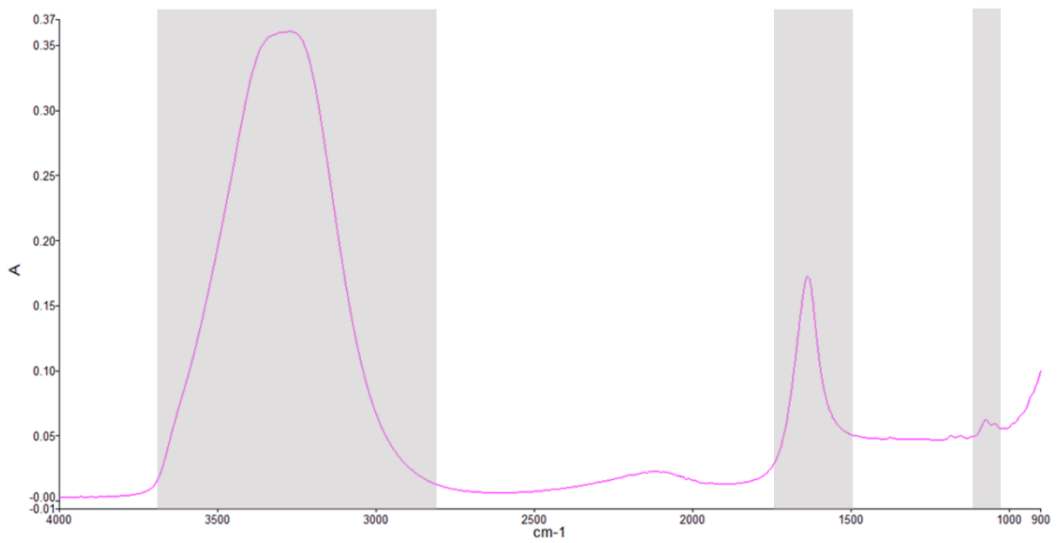


Figure 6 Full-scale spectral response from  $4000\text{ cm}^{-1}$  to  $900\text{ cm}^{-1}$  for agarose. The band from  $1015$  to  $1080\text{ cm}^{-1}$  is associated with C-H stretching.

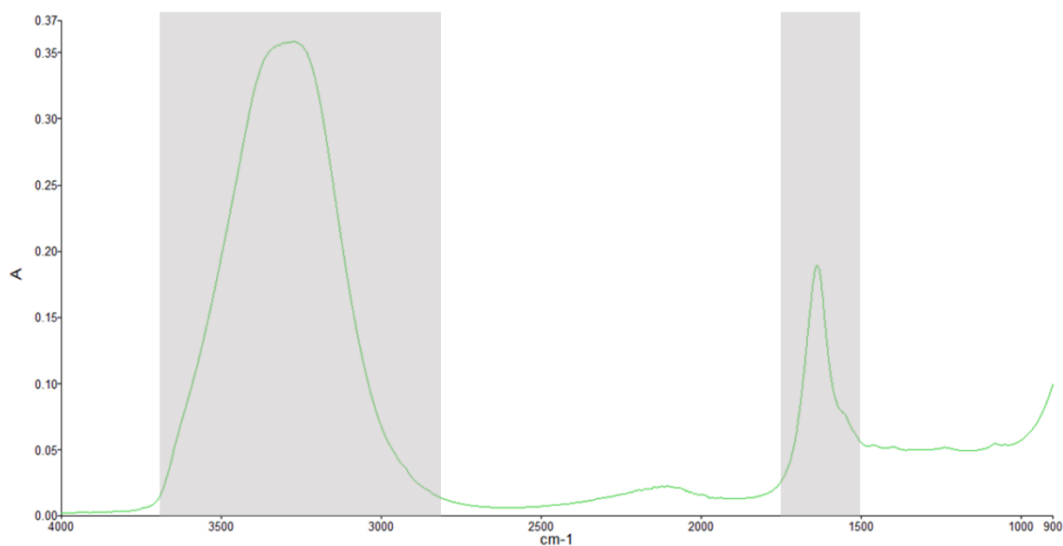


Figure 7 Full-scale spectral response from  $4000\text{ cm}^{-1}$  to  $900\text{ cm}^{-1}$  for testicular tissue. Only the water peaks can be observed for feline testicular tissue.

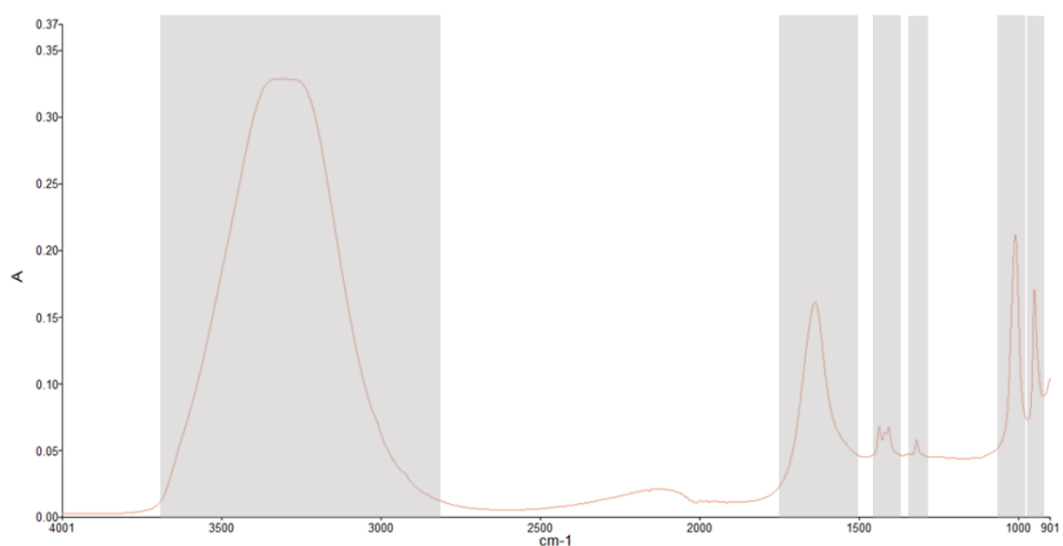


Figure 8 Full-scale spectral response from  $4000\text{ cm}^{-1}$  to  $900\text{ cm}^{-1}$  for 3.1M DMSO. Peaks from  $1310$  to  $1380\text{ cm}^{-1}$  and from  $1395$  to  $1440\text{ cm}^{-1}$  indicate O-H bending. A S=O stretching peak can be observed from  $980$  to  $1070\text{ cm}^{-1}$ , and the unique DMSO peak from  $930$  to  $970\text{ cm}^{-1}$  is used to quantify absorbance for DMSO during diffusion studies [75].

The absorbance can be quantified by calculating the area under the curve for wavelength bands centered at the characteristic wavelength. As the characteristic wavelength for 3.1M DMSO,  $950\text{ cm}^{-1}$ , is in the fingerprint region of the spectra, the background spectral responses from  $1500\text{ cm}^{-1}$  to  $900\text{ cm}^{-1}$  for alginate-gelatin, agarose, testicular tissue, and 3.1M DMSO are shown in Figure

9, Figure 10, Figure 11, and Figure 12, respectively. The bands in this region for each sample type are marked in gray.

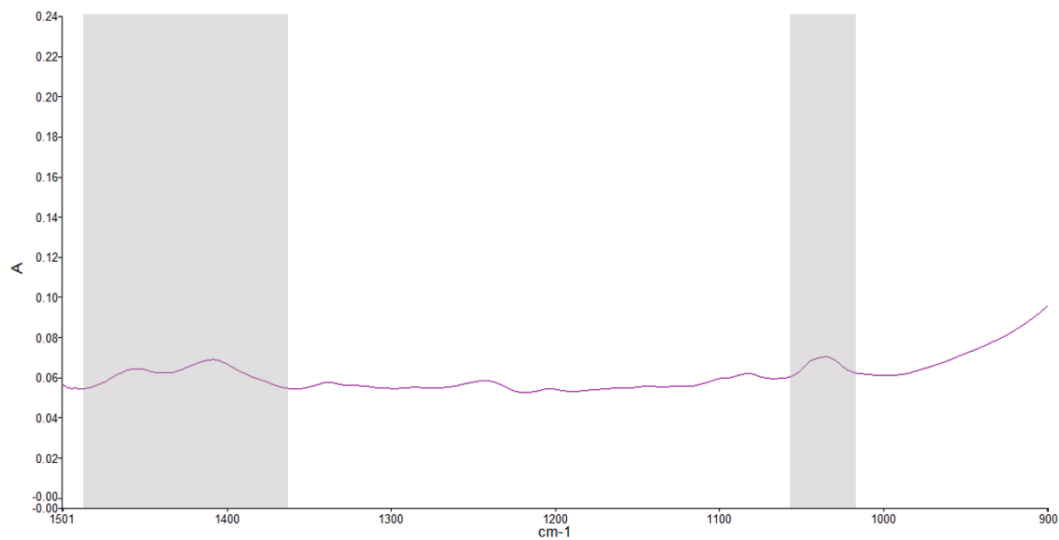


Figure 9 Fingerprint region spectral response from 1500  $\text{cm}^{-1}$  to 900  $\text{cm}^{-1}$  for alginate-gelatin.

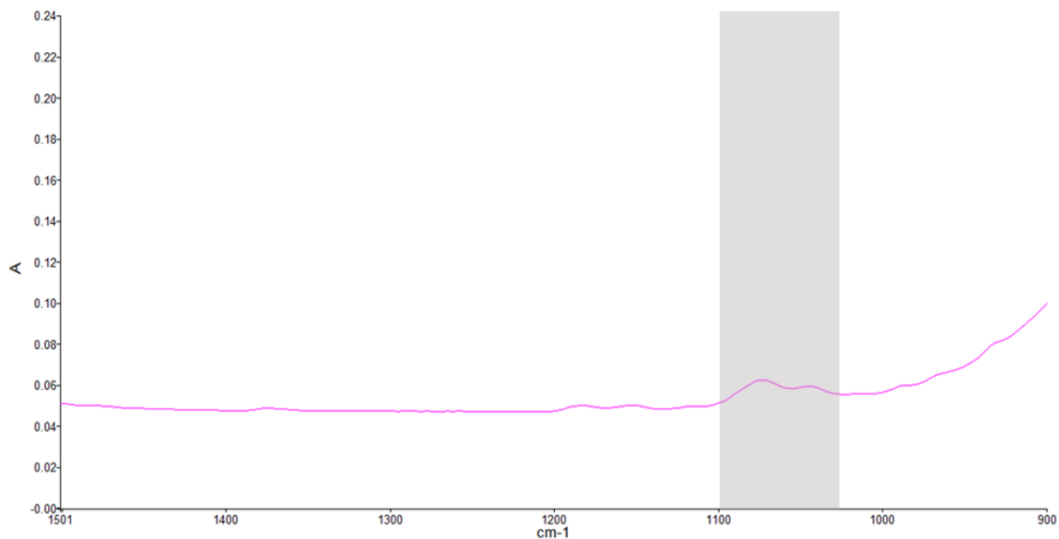


Figure 10 Fingerprint region spectral response from 1500  $\text{cm}^{-1}$  to 900  $\text{cm}^{-1}$  for agarose.

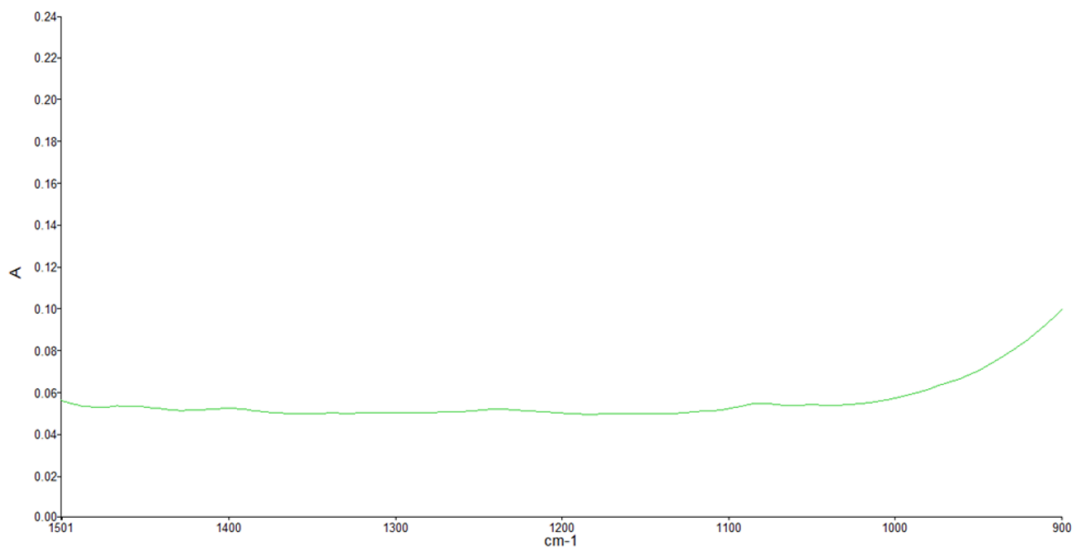


Figure 11 Fingerprint region spectral response from  $1500\text{ cm}^{-1}$  to  $900\text{ cm}^{-1}$  for testicular tissue.

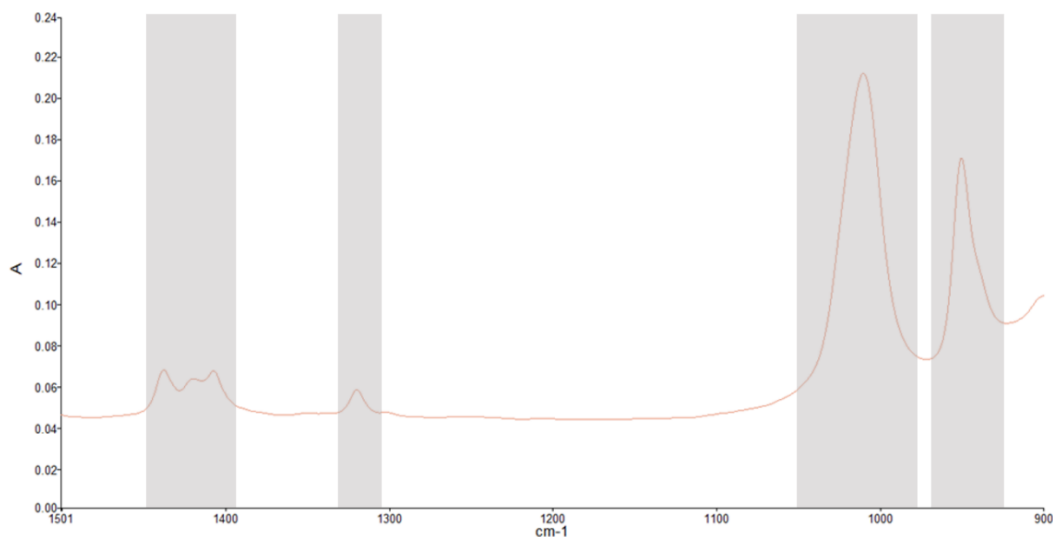


Figure 12 Fingerprint region spectral response from  $1500\text{ cm}^{-1}$  to  $900\text{ cm}^{-1}$  for 3.1M DMSO.

The resolution can decrease as background noise increases when using ATR-FTIR to analyze samples at lower wavenumbers [76]. However, low spectral responses can be observed at  $950\text{cm}^{-1}$  in the fingerprint regions of the spectra for alginate-gelatin, agarose, and testicular tissue. Furthermore, the first scan in a time series is used as a background scan for each sample to perform background correction on all spectra in a time series.

As ATR-FTIR reports the absorbance at the surface, ensuring good contact between the sample and the sensing window is imperative to obtaining accurate spectra. For hard or rough samples, it is often recommended that slight pressure be applied to the sample to maintain contact with the sensing window. A sample would appear to have a heterogeneous distribution across the sensing window if good contact is not maintained [77, 78]. Thus, the absorbance would be weaker or absorbances associated with different atomic behavior, such as the C-H or O-H stretching bands, may not appear at all. For hard and rough samples, it is recommended to use a preview function within the analysis software to apply pressure on a sample until at least 70% transmittance is achieved to ensure sufficient contact between the sample and the sensing window [79]. However, for soft or smooth samples, applying pressure to ensure contact is not necessary as tissues have been shown to self-adhere to the sensing window [78, 80]. For extremely thin tissues, such as skin samples, suspension in a water droplet allows the sample to be centered over the sensing window and removal of the water between the tissue and the sensing window ensures sufficient contact [78]. As the alginate-gelatin, agarose, and testicular tissue are to be compacted into the sample holder on the sensing window, the slight pressure applied during compaction and the weight of each sample is expected to maintain sufficient contact throughout each diffusion study.

During the diffusion studies, the absorbance values at a characteristic wavenumber increase as CPA concentration in a sample increases. The increasing absorbance values are recorded over time to generate a curve which can be fit to the diffusion model developed by Barbari and Fieldson (1993) to predict the effective diffusion coefficient for a CPA into a sample, as described previously in section 1.3.2 [10, 11].

Diffusion studies were conducted using a Frontier (PerkinElmer, MA, USA) with an Gladi-ATR attachment (Pike Technologies, WI, USA) to collect absorbance spectra for DMSO using a

wavelength band from  $970\text{ cm}^{-1}$  to  $930\text{ cm}^{-1}$  as the DMSO diffused into alginate-gelatin, agarose, or testicular tissue. A single sample of alginate-gelatin (nominal 10mm diameter), agarose (nominal 8mm diameter), or testicular tissue (nominal 8mm diameter) was weighed and compacted into the corresponding ring in the sample holder to prevent leaking around the edges. Rings with inner diameters of 8mm, 7.4mm, and 6mm were used inside the sample holder for alginate-gelatin, agarose, and testicular tissue, respectively. A volume of 2.5 mL of a 3.1M DMSO in 1X PBS solution was pipetted into a sample holder, described in detail in Section 6.2, immediately prior to data collection.

TimeBase 10 software, purchased from Perkin-Elmer (MA, USA), was used to collect SingleBeam spectra for wavelengths of  $4000\text{ cm}^{-1}$  to  $900\text{ cm}^{-1}$  every minute using 8 co-added interferograms with a resolution of  $4\text{ cm}^{-1}$ . A schematic of the data collection setup is shown in Figure 13. A detailed schematic of the sample holder is included in Section 6.2.

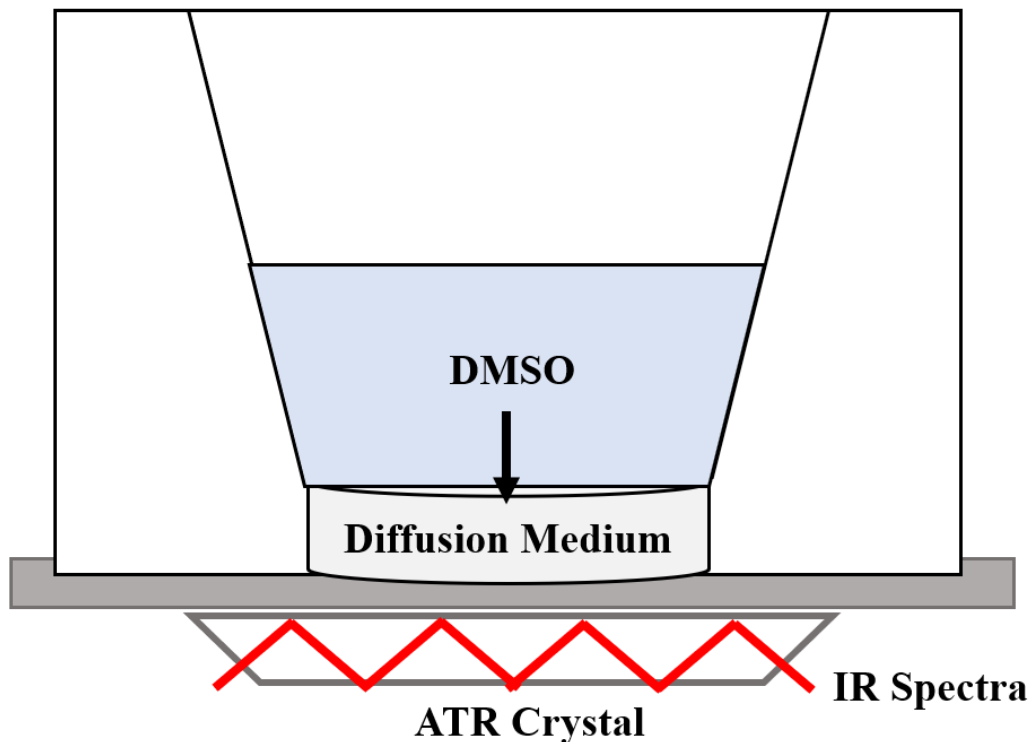


Figure 13 Diffusion study ATR-FTIR setup

The 3.1M DMSO was allowed to diffuse into the sample for 2 hours while spectra were collected. A Kimtech wipe with 70% ethanol was used to clean the ATR attachment surface after disposal of each sample and before a new diffusion study began. After 2 hours, spectra were exported from TimeBase 10 for processing in Spectrum IR (Perkin Elmer, MA, USA). To perform background correction and convert from energy to %transmittance, all spectra in a time series were ratioed to the first spectrum in the time series. An automatic function in Spectrum IR was used to convert all spectra to absorbance units. Absorbance was quantified by calculating the area under the curve from wavelengths of  $970\text{cm}^{-1}$  to  $930\text{ cm}^{-1}$  for each spectrum in the time series for alginate-gelatin and agarose. To resolve complexity introduced by testicular tissue as a biological sample for the  $950\text{cm}^{-1}$  peak and identify a clear DMSO peak, a deconvolution step was added after converting to absorbance from %transmittance for testicular tissue absorbance time series. The area under

the curve for the DMSO peak was calculated from wavelengths of 957 to 943  $\text{cm}^{-1}$ . The absorbance values were plotted versus time to provide the experimental curves for fitting the equation provided by Fieldson and Barbari (1993). The absorbance values for four sodium alginate-gelatins were collected in 1 day to observe any changes in the diffusion kinetics which may indicate changes in the alginate-gelatin over time. Absorbance values for three agarose or three testicular tissue samples were collected in a single day of diffusion studies.

### 3.5 Diffusion coefficients estimation program

Depending on the diffusion characteristics, samples may or may not reach chemical equilibrium during the 2-hour data collection period. This impacts how the data is normalized for subsequent parameter estimation procedures. Samples were considered equilibrated if the percent difference of the final absorbance values was less than 1%. A 1-parameter estimation program was created in Excel to estimate the diffusion coefficient using a least square fitting algorithm for equilibrated datasets. Absorbance values in equilibrated datasets were normalized to the final absorbance value in the time series. The thickness and material parameters, such as the refractive index of the sample, were used as inputs and the diffusion coefficient was changed manually to reduce the mean square error as the indicator of fit. The mean square error was calculated using Equation 5.

$$MSE = \frac{1}{n} \sum_{i=1}^n (y_i - \hat{y}_i)^2 \quad (\text{Eqn 5})$$

For datasets which did not reach equilibrium, a 2-parameter estimation Excel program was used to fit the absorbance data and simultaneously estimate the effective diffusion coefficient,  $D_{\text{eff}}$ , and the equilibrium absorbance value,  $A_{\infty}$ . The final absorbance value in the diffusion study was used as an initial guess for the equilibrium absorbance value and  $D_{\text{eff}}$  was changed manually to reduce the mean square error as the indicator of fit. Once a minimum mean square error was reached, the

equilibrium absorbance value was changed to further reduce the error values. At least three iterations were necessary to reach a global minimum.

## **CHAPTER 4 DEVELOPMENT OF A REFERENCE STANDARD FOR CPA DIFFUSION IN SOFT TISSUES**

### **4.1 Alginate-gelatin reference material**

#### **4.1.1 Rationale**

Biological tissues vary in composition and geometry. They contain various cell types with different permeability parameters, and have varied cellular arrangements, leading to different porosities and diffusion behavior [4, 9]. Furthermore, soft tissues are easily deformable and do not easily hold their structure after sectioning. Thus, highly reproducible diffusion data for use in parameter estimation experiments are difficult to produce. The creation of a reference material, which mimics the properties of native tissue, but which can be quickly and repeatedly manufactured in labs, while yielding consistent properties, would allow identification of sources of error in methodology development and support user training and technology transfer. In turn, faster and more accurate investigation within the materials and process design space would be possible. The ability to generate materials with a uniform composition and predictable, easily quantifiable geometries (e.g. thin discs with consistent thicknesses) would be highly desirable for methodology development.

Alginate cross-linked with gelatin has been used for encapsulating cells and creating micro-physiological systems, and thus has potential for development into a reference standard [55, 58, 59, 74]. Samp measured the stiffness and toughness of alginate and gelatin scaffolds with various percentages of crosslinking [63]. They discovered that mixing gelatin and alginate can increase the toughness while maintaining the Young's modulus. The lowest elastic modulus was 260 kPa for the 50 wt% samples, indicating an acceptable stiffness which will allow uniform slicing and sample heights to be achieved. Despite frequent use for encapsulating cells, it has mainly been used for in-vitro cell culture [62, 66]. Recent work has turned toward preservation [65], but CPA diffusivity values are not yet readily available. Changing the cross-linking density by controlling

the concentrations of sodium alginate in the alginate-gelatin samples may yield the ability to tune the properties of the alginate-gelatin to mimic different soft tissues. Thus, alginate-gelatin could serve as a reference material for studying diffusion in various tissue types, including testicular tissue, if manufacturing methods can be optimized and diffusion coefficients determined.

#### **4.1.2 Casting materials and methods**

Alginic acid sodium salt from brown algae with medium viscosity, sodium tetraborate decahydrate of Reagent 99.5% quality, and Type A gelatin from porcine skin with gel strength of 300 were purchased from Sigma-Aldrich (MO, USA). Histological grade reagent alcohol was purchased from Fisher Chemical (MA, USA). A silicone EMS round cavity casting mold with 10mm diameter and 1.8mm depth was purchased from Electron Microscopy Sciences (PA, USA). The EMS casting mold was heated on a plate warmer to 37°C. The sodium tetraborate decahydrate was used to create 0.1M borax solution using pure water and a volumetric flask. Pure water was heated to 37°C and the gelatin was added to create a 15% (w/v) gelatin solution. The alginic acid was added to the reagent alcohol to create a 20% (w/v) alginate solution. This solution was stirred with a stir bar for 5 minutes. After stirring for 5 minutes, a sufficient amount of the borax solution was added to create a 20% (v/v) solution of alginate in borax. The alginate-borax solution was suspended in a water bath at 37°C and stirred for 5 minutes with a stir bar.

The alginate-borax solution and gelatin solution were then mixed in a 1:1 ratio in a separate container and poured over the EMS casting mold until all wells in the mold were filled and a thin film of alginate-gelatin solution covered the top surface of the mold. The solution was allowed to cool for at least 40 minutes to ensure the solution had completely solidified. A thin polymer fiber was drawn across the top of each well, even with the surface of the mold, to remove the excess alginate-gelatin composition and create a uniform height for all alginate-gelatin samples. Each

well was considered one sample and the mass of each sample was recorded in grams. A schematic of the casting procedures is shown in Figure 14.

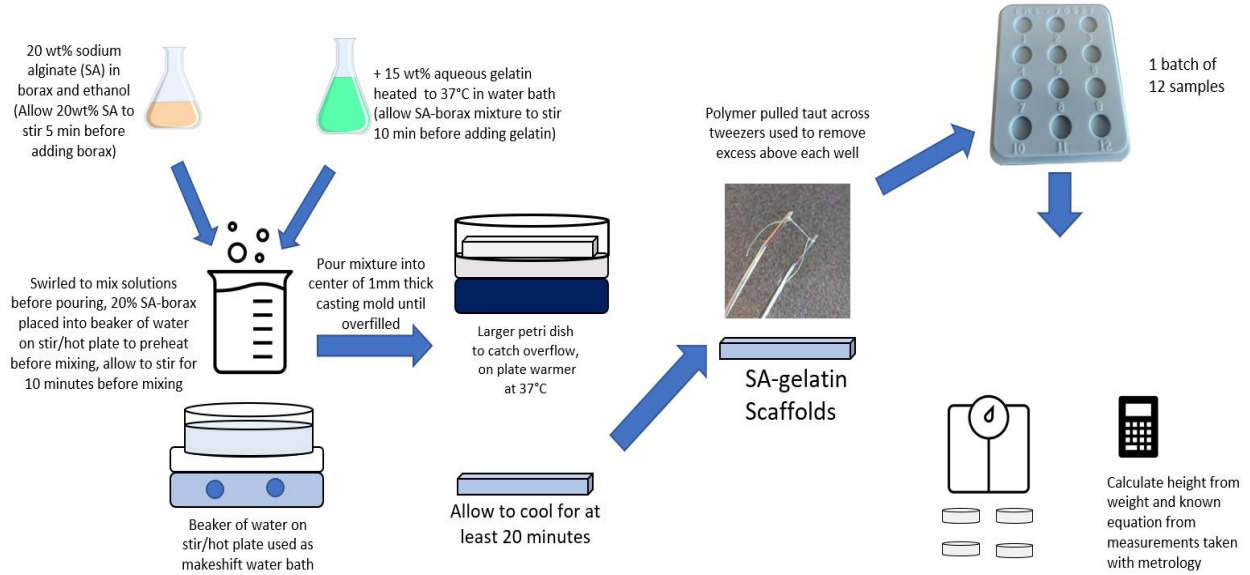


Figure 14 Casting procedures for ~1.8mm thick alginate-gelatin samples for diffusion studies

### 4.1.3 Estimating the thickness of alginate-gelatin

The thickness estimated at each point on top of the alginate-gelatin surface that were measured in the metrology study are shown in Table 2 and center points are highlighted in green.

Table 2 Estimated thickness of alginate-gelatin (n=12) in mm, determined at various points on the top surface, measured directly after trimming, before placement into the sample holder. The center point of each SA-gel is highlighted in green

Point \ SA-gel	1	2	3	4	5	6	7	8	9	10	11	12
1	1.04	1.07	1.62	1.19	1.25	1.59	0.70	0.85	1.83	0.92	0.79	1.19
2	1.09	0.99	1.93	1.20	1.14	1.39	0.72	0.74	1.77	0.92	0.78	1.16
3	1.21	1.02	1.70	1.54	1.42	1.70	0.85	1.19	2.09	1.17	1.17	1.38
4	0.90	0.81	1.63	1.28	1.29	1.46	0.76	0.99	1.70	0.81	0.88	1.24
5	1.08	0.67	1.92	1.35	1.06	1.35	0.62	0.78	1.65	0.97	0.96	1.13
6	1.13	0.92	1.60	1.30	1.14	1.32	0.76	0.85	1.80	1.00	0.89	1.05
7	1.01	0.77	1.36	1.34	1.23	1.38	0.87	0.90	1.89	0.85	1.10	1.28
8	0.88	0.85	1.43	1.23	1.28	1.42	0.94	0.94	1.86			1.19
9		0.98	1.55									
<b>Average</b>	1.05	0.90	1.64	1.31	1.23	1.46	0.78	0.91	1.83	0.95	0.94	1.21
<b>St. Dev.</b>	0.11	0.13	0.19	0.11	0.11	0.13	0.10	0.14	0.13	0.12	0.15	0.10
<b>St. Dev. (%)</b>	10.7	14.6	11.8	8.6	9.1	8.9	13.2	15.5	7.3	12.3	15.8	8.3

Some uncertainty in the thickness measurements is expected. The ATOS Scanbox has a maximum measurement uncertainty of 0.1mm which can be used to calculate the standard uncertainty of the measurement. The standard uncertainty is calculated using the following equation:

$$\text{Standard uncertainty} = \frac{\text{Measurement uncertainty}}{\sqrt{3}}$$

in which the measurement uncertainty is a reported tolerance value or estimated as half of the increment markings on the measurement instrument. Thus, the ATOS Scanbox had a standard uncertainty of 0.058mm. The calipers used to measure the thickness of the reference points and the paper slip placed on top of the alginate-gelatin had a measurement uncertainty of 0.01mm resulting in a standard uncertainty of 0.0058mm. The combined standard uncertainty would be 0.058mm from the measurement instruments. However, the within-sample standard deviations ranged from 0.10mm to 0.19mm with an average standard deviation of 0.13mm, which exceeds the combined standard uncertainty. Thus, there is moderate within-sample variation in the thicknesses of the alginate-gelatin. However, the within-sample variation in thickness is consistent

from sample-to-sample, especially given the low-tech methodology used for trimming excess alginate-gelatin from the mold.

The within-sample point values were then averaged to give the overall sample thickness value. The average SA-gel thicknesses ranged from 0.78mm to 1.83mm with an overall average thickness and standard deviation of  $1.2 \pm 0.3$ mm prior to packing, which is considerably higher than the within-sample variation. In addition, the depth of the EMS casting mold was 1.8mm, yet only one sample had a thickness just above 1.8mm. The remaining samples had consistently lower thicknesses, which could indicate that samples were dehydrating mildly resulting in slight contraction. Alternatively, the pressure applied to the tweezers during trimming could affect the sample-to-sample variation. If even slightly more pressure downwards was applied when trimming excess alginate-gelatin over one well in the mold versus another, the thickness would be reduced for the well over which more pressure was applied.

While there was considerable sample-to-sample variation in the thickness, the masses of the individual samples ranged from 0.1130g to 0.1392g with an average of  $0.1244 \pm 0.008$ g (6.7% standard deviation). Thus, smaller sample-to-sample variation in the thicknesses and higher reproducibility were expected. Nevertheless, alginate-gelatin can be quickly and efficiently manufactured using the casting methodology outlined in Section 4.1.2 as it does not require specialized equipment and is not time-consuming. Thus, the described methodology can be used to create alginate-gelatin as a reference material for applications which require less control over the thickness of samples.

Samples were then packed into the sample holder and ATOS measurements were taken again. A height increase was expected because the sample was prepared with a diameter of 10 mm but then placed into an 8 mm cylinder for testing. The alginate-gelatin was determined to compact to

thicknesses of  $1.7\text{mm} \pm 0.2\text{mm}$  (12.9% standard deviation) inside the sample holder. The increased standard deviation variability in the force applied by the researcher during packing. These samples are being packed by hand using custom plungers, thus variation in the force applied by the researcher can contribute to different levels of compression and affect the thickness measurements after packing.

The theoretical thicknesses were determined from mass measurements assuming a cylindrical geometry and the average density as described in Section 3.2. The average density for alginate-gelatin was determined to be  $1.25\text{ g/mL}$  using the methods detailed in Section 3.1. The theoretical thicknesses provide reasonable estimates of the thicknesses prior to packing into the sample holder as can be seen when comparing with the experimental center point thicknesses on the left of Figure 15. However, after packing the theoretical thicknesses were overestimated compared to the experimental thicknesses in all but one case as can be seen in the right of Figure 15. While some height change was expected because the alginate-gelatin is deformable, the amount of expected compaction was unknown. Reliable thickness measurement after packing could thus not be obtained from mass measurements on prepared samples using only a geometrical relationship. Thickness measurements using the ATOS Scanbox cannot be easily obtained for every alginate-gelatin sample prepared, especially before use in diffusion studies. As such, a correlation line was fit to the SA-gel thickness values after packing in the sample holder. Although the correlation between thickness after packing and mass was lower than expected, this equation of this line was used to estimate the thickness after packing. The estimated heights from this equation were used in the FTIR diffusion model to estimate the diffusion coefficients.

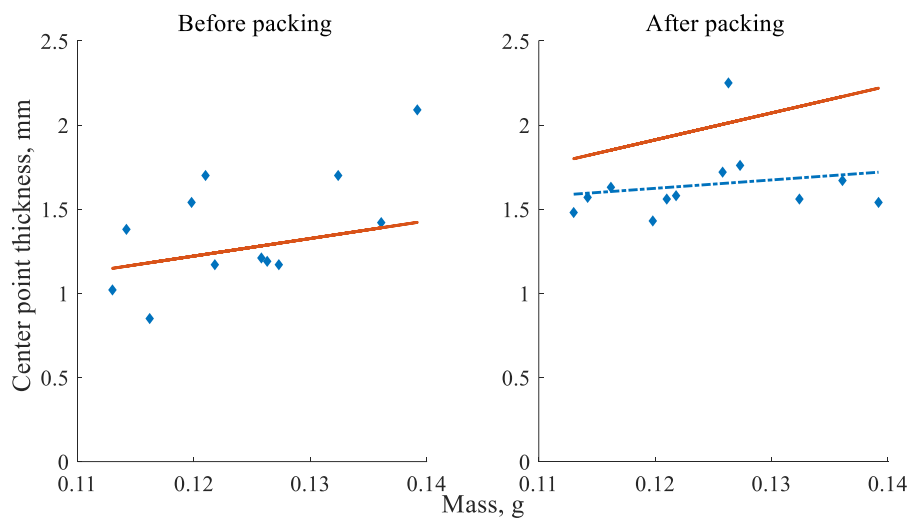


Figure 15 A comparison of the theoretical and experimental thicknesses before (left) and after (right) packing in sample holder for alginate-gelatin. A solid orange line represents the theoretical thicknesses before and after packing. Experimental thicknesses are shown as blue diamonds. The correlation line for the experimental thicknesses after packing in the sample holder is represented by a blue dashed line, equation: thickness = 4.97\*mass in grams + 1.03 mm ( $R^2 = 0.0389$ ).

#### 4.1.4 Estimated diffusion coefficients in alginate-gelatin

A fresh batch of alginate-gelatin was created and FTIR spectra were collected while samples were exposed to 3.1M DMSO as described in Section 3.4. Absorption time series were collected for four sequential samples over a period of 8 hours to determine if the alginate-gelatin aged over time that affected the absorption. As no systematic change in absorbance curves was observed the samples do not appear to be degrading or aging within the time period explored.

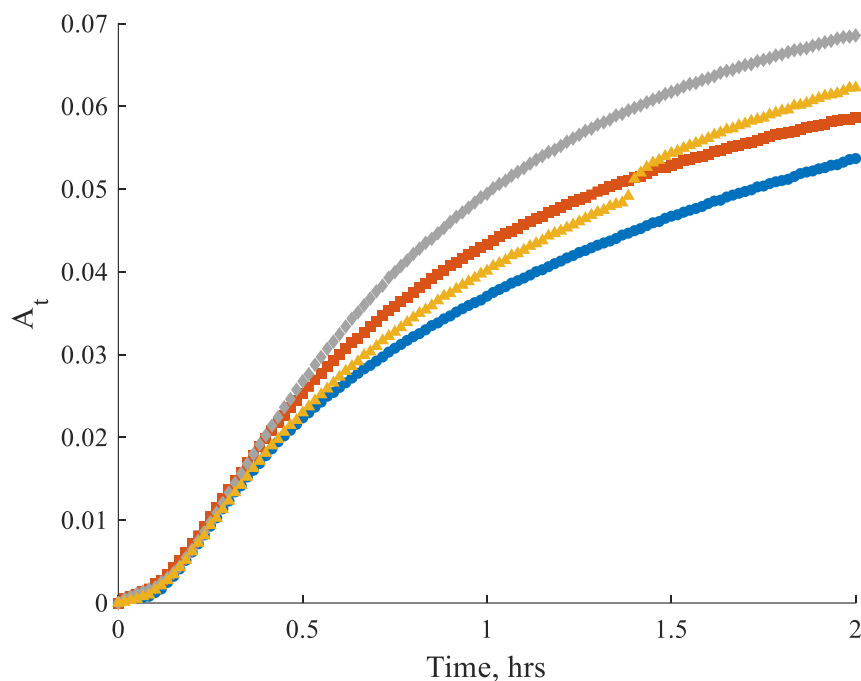


Figure 16 Absorbance as a function of time for different samples of alginate-gelatin from the same preparation batch, exposed to DMSO. Sample 1 (blue circles), 2 (orange squares), 3 (gray diamonds), and 4 (yellow triangles) were processed in time exposure.

Plotting the absorption as a function of time before normalization also showed that the alginate-gelatin had not reached an equilibrium absorbance value within 2 hours, as shown in Figure 16. As such, the 2-parameter estimation Excel program was used to fit the absorbance data. As described in the previous section, the thickness used for estimation was determined from the sample mass, using the equation developed from optical measurements on equivalently prepared alginate-gelatin samples. When plotting the predicted and experimental absorbance values on the same axes as shown in Figure 17 some minor mismatching of data shape was observed.

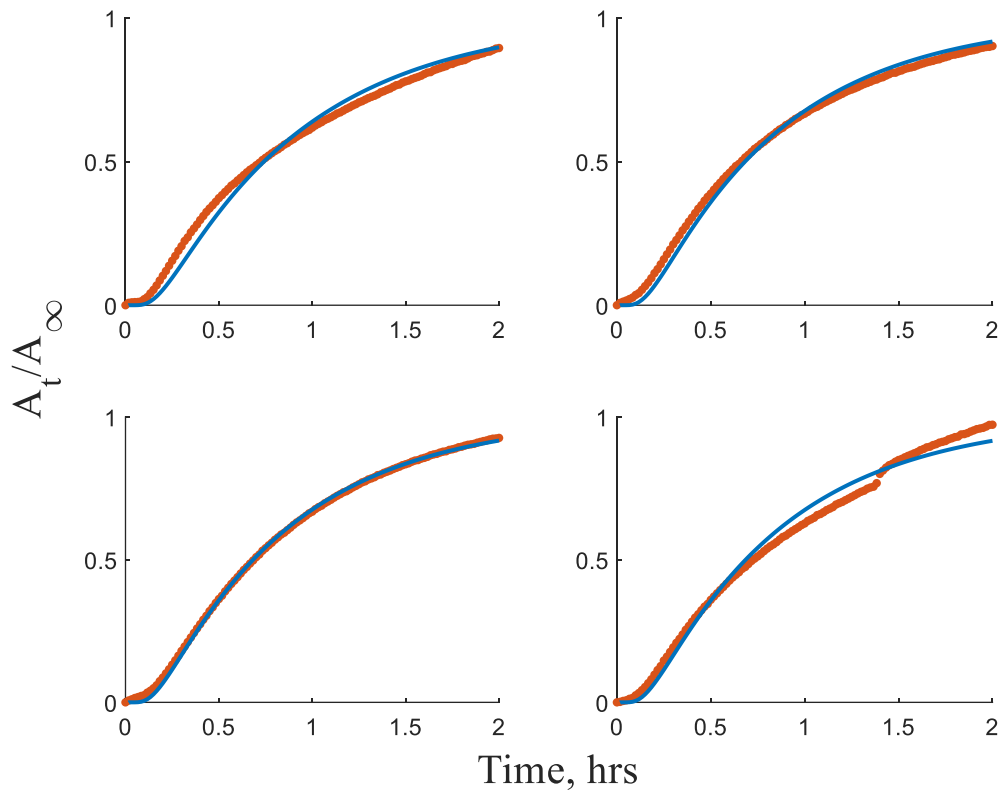


Figure 17 Diffusion coefficient estimation fits for alginate-gelatin sample 1 (top left), 2 (top right), 3 (bottom left), and 4 (bottom right). The experimental values are indicated by orange circles, the predicted values are represented by the blue line.

It should be noted that sample 4, does show a sudden increase in absorbance just before 1.5 hours of data collection. This sudden increase could indicate possible relaxation in the sample or a slight leak. Thus, the diffusion coefficient for sample 4 may have been lower than estimated. The final diffusion coefficients, equilibrium absorbance values, and associated error values are summarized in Table 3. The average  $D_{\text{eff}}$  value was determined to be  $4.3 \pm 0.3 \times 10^{-6} \text{ cm}^2/\text{s}$  (7% standard deviation). The average  $A_{\infty}$  value was  $0.07 \pm 0.01$  (9.0% standard deviation).

Table 3 Diffusion Coefficients and Equilibrium Absorbances for Alginate-gelatin

<b>D<sub>eff</sub> [x10<sup>-6</sup> cm<sup>2</sup>/s]</b>	<b>A<sub>∞</sub></b>	<b>Sum of Squares [x10<sup>-4</sup>]</b>	<b>Mean Square Error [x 10<sup>-6</sup>]</b>
4.1	0.060	4.5	3.75
4.5	0.065	2.95	2.46
4.6	0.074	0.49	0.41
4.0	0.064	5.64	4.70

The effective diffusion coefficient was in the range of diffusivity values for DMSO in porcine collagen scaffolds,  $2.4 \times 10^{-6} \text{ cm}^2/\text{s}$ , and sucrose in alginate containing yeast cells,  $4.05 \times 10^{-6} \text{ cm}^2/\text{s}$  [52, 57]. Additionally, the alginate-gelatin shows comparable effective diffusion coefficients to that of DMSO in tissues such as pulmonary arterial valve tissue,  $3.02 \times 10^{-6} \text{ cm}^2/\text{s}$  [22], and porcine articular cartilage,  $3.1 \times 10^{-6} \text{ cm}^2/\text{s}$  [30].

## 4.2 Agarose

### 4.2.1 Rationale

Low melting point agarose can be quickly mixed with a buffer solution and cast to a desired shape. Currently, low-melting point agarose is used to ensure uniform pressure around tissue samples during slicing with a precision slicer. The use of a precision slicer and biopsy punch can also facilitate the creation of thin agarose slices which can be cut to a cylindrical geometry. As such, agarose shows potential as a reference material that can be cut to prescribed thicknesses in the mm to sub-mm range, which can facilitate estimation of diffusion coefficients on thinner sections which require less time to process.

### 4.2.2 Materials and methods

Low melting point agarose tablets of 0.5 agarose LE were purchased from Precisionary Instruments LLC (MA, USA). Agarose tablets were dissolved in 25mL phosphate buffer solution

to produce a 2% (w/v) agarose solution. The solution was heated in a microwave for 10 seconds and gently stirred by hand. This process was repeated twice more. Then the solution was heated for 5 seconds and gently stirred by hand. This process was repeated 3-4 more times or until the solution became clear. A bulk pipette tip was used to pipette the clear agarose solution into a 20mm diameter specimen tube and a cooling block was wrapped around the specimen tube to facilitate quick and even solidification of the agarose. The specimen tube was inserted into a VF-500-0Z Microtome which was set to oscillation level 7 and advance level 3. One tube of agarose was considered a slicing batch, and a new steel blade was used every 2 slicing batches. A step-down calibration method was employed to ensure slices were 1mm (1000  $\mu\text{m}$ ) thick. The Microtome was set to 1200  $\mu\text{m}$  initially and the agarose was sliced. Once a slice was obtained which did not show signs of striations or marks from being sliced, the Microtome thickness was decreased to 1100  $\mu\text{m}$ . This process was repeated, decreasing the thickness to 1050  $\mu\text{m}$  and finally 1000  $\mu\text{m}$  each time a slice without striations or other marks from slicing were obtained. A schematic of the casting and slicing procedure is shown in Figure 18.

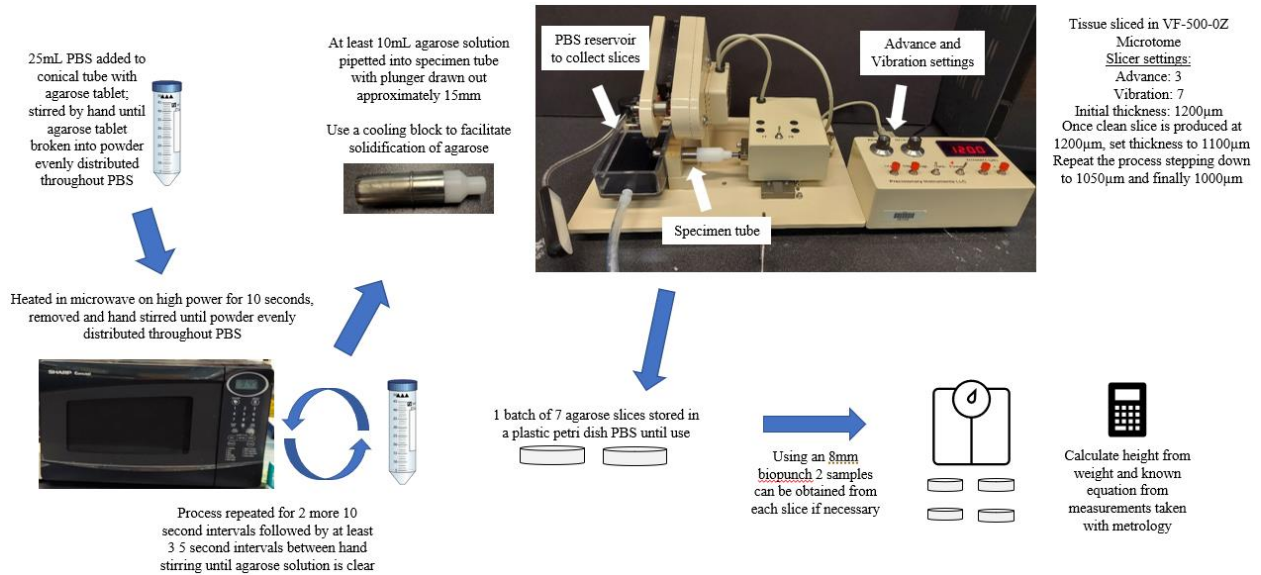


Figure 18 Casting procedures for ~1mm thick agarose samples for diffusion studies

### 4.2.3 Estimating thickness of agarose

The thickness estimated at each point on top of the agarose surface prior to packing into the sample holder measured during the metrology study are shown in Table 4 and center points are highlighted in green.

Table 4 Estimated thickness of agarose (n=12) in mm, determined at various points on the top surface, measured directly after slicing and punching, before placement into the sample holder. The center point of each agarose is highlighted in green.

Point \ Sample	1	2	3	4	5	6	7	8	9	10	11	12
1	1.00	0.84	1.10	0.82	0.93	0.86	1.16	1.09	0.76	0.86	1.12	1.15
2	1.00	0.87	1.09	0.73	0.96	0.81	1.08	0.96	0.60	0.79	0.83	0.97
3	0.97	0.83	0.97	0.82	0.80	0.97	1.08	0.96	0.61	0.76	0.97	0.92
4	1.14	0.87	0.98	0.81	0.87	1.10	1.19	1.00	0.75	0.83	1.02	0.95
5	1.10	0.74	0.96	0.89	1.00	0.96	1.18	0.93	0.69	0.77	0.98	1.02
6	0.94	0.81	0.99	0.76	0.86	0.84	1.08	0.95	0.68	0.75	0.90	0.94
<b>Average</b>	1.03	0.83	1.02	0.81	0.90	0.92	1.13	0.98	0.68	0.79	0.97	0.99
<b>St. Dev.</b>	0.08	0.05	0.06	0.06	0.07	0.11	0.05	0.06	0.07	0.04	0.10	0.08
<b>St. Dev. (%)</b>	7.6	5.9	6.2	6.9	8.1	11.7	4.8	5.9	9.9	5.4	10.3	8.5

As with, alginate-gelatin the individual sample standard deviations were larger than the combined standard uncertainty, 0.058mm, in most cases. However, the within-sample variation for agarose

was considerably lower than for alginate-gelatin, with 3 samples having standard deviations less than the measurement uncertainty. The individual standard-deviations ranged from 0.04mm to 0.11mm with an average value of 0.07mm. Though this indicates some within-sample variation for the remaining samples that cannot be attributed to measurement uncertainty, the variation is less than for alginate-gelatin. In addition, this variation is more consistent sample-to-sample than for alginate-gelatin. This is to be expected as a precision slicer was used to prepare the agarose.

The within-sample thicknesses were again averaged to give the overall average thickness value. The average thicknesses ranged from 0.68 to 1.13mm with an overall thickness of  $0.9 \pm 0.1$ mm. Though use of a precision slicer was expected to eliminate within-sample and reduce sample-to-sample variation, the thicknesses were near but less than the nominal 1mm setting with less variation than was observed for alginate-gelatin samples. The small variation in thickness is consistent with small variation in the masses, which ranged from 0.0430 to 0.0485g with an average mass of  $0.0458 \pm 0.002$ g (4.3% standard deviation). Thus, the slicing methodology described in Section 4.2.2 can be used to create agarose as a reference material for applications in which greater control of the thickness is necessary.

As mentioned in Section 3.3, multiple points on the top surface of the agarose were used to estimate the thickness after packing into the sample holder. The resulting thickness estimated at each point on the surface of the agarose is shown in Table 5 and center points are highlighted in green.

Table 5 Estimated thickness of agarose (n=12) in mm, determined at various points on the top surface, measured after placement into the sample holder. The center point of each agarose is highlighted in green.

Point \ Sample	1	2	3	4	5	6	7	8	9	10	11	12
1	1.04	0.93	1.18	1.06	1.09	0.96	0.81	1.06	0.95	0.99	0.87	1.10
2	1.21	1.23	1.25	1.17	1.15	0.99	0.84	1.00	0.99	1.12	0.97	1.56
3	0.96	1.22	1.24	1.04	1.09	1.09	0.90	1.13	1.00	1.22	0.88	1.22
4	1.01	0.91	1.04	1.02	1.10	1.14	0.94	1.36	0.96	1.13	0.87	1.17
5	1.07	1.06	1.35	1.11	1.25	1.33	1.15	1.18	1.17	1.03	0.97	1.26
6	1.27	1.16	1.26	1.22	1.17	1.02	1.03	1.15	1.16	0.96	1.11	1.34
<b>Average</b>	1.09	1.09	1.22	1.10	1.14	1.09	0.95	1.15	1.04	1.08	0.95	1.28
<b>St. Dev.</b>	0.12	0.14	0.10	0.08	0.06	0.14	0.13	0.12	0.10	0.10	0.09	0.16
<b>St. Dev. (%)</b>	11.0	13.0	8.5	7.1	5.5	12.5	13.4	10.7	9.6	9.2	9.9	12.7

After packing the within-sample variation increases considerably with individual standard deviations ranging from 0.06 to 0.16mm and an average standard deviation of 0.11mm. Thus, the within-sample variation after packing is nearly double that of the combined standard uncertainty, indicating higher variation in the thickness after packing. However, the sample-to-sample variation remains low for agarose. It should be noted that, as with alginate-gelatin, placement of the paper slips and possible variation in pressure applied when packing by hand using custom plungers will also cause some uncertainty and variation in the thickness measurements. The agarose was determined to compact to average thicknesses of  $1.1 \pm 0.1$ mm (12.8% standard deviation) inside the sample holder. Thus, the sample-to-sample variation in the thicknesses after packing into the sample holder of agarose was comparable to that of alginate-gelatin.

The theoretical thicknesses, determined using an average density of 1.58 g/mL and the mass of samples, consistently underestimate the thickness of the agarose before and after packing as can be seen in Figure 19. As described in Section 3.1, density measurements were recorded using volume displacement methods. However, as agarose is a porous material, it is possible that the density is overestimated as the agarose samples absorbed some of the PBS in the graduated

cylinder which would then decrease the thickness estimations. As such, though there was a smaller correlation between mass and thickness after packing than expected, the equation of a correlation line fit to the average thicknesses after packing into the sample holder was used to estimate the thickness for samples used in diffusion studies.

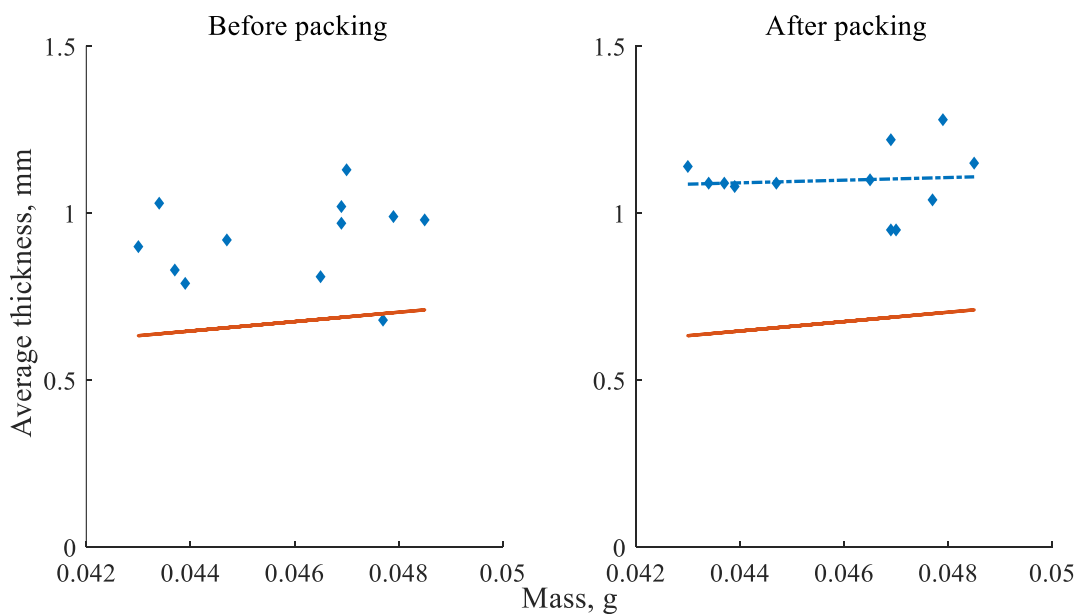


Figure 19 A comparison of the theoretical and average experimental thicknesses of agarose before (left) and after (right) packing in sample holder. A solid orange line represents the theoretical thicknesses before and after packing. Experimental thicknesses are shown as blue diamonds. The correlation line for the experimental thicknesses after packing in the sample holder is represented by a blue dashed line, thickness =  $3.46 \cdot \text{weight in grams} + 0.94 \text{ mm}$  ( $R^2 = 0.005$ ).

#### 4.2.4 Estimated diffusion coefficients in agarose at 22°C

A fresh batch of agarose was prepared, and three samples were exposed to 3.1 M DMSO as described in Section 3.4 in sequence over the course of 6 hours. Spectra were collected for each sample and absorbance values were plotted over time. Plotting the absorbance values before normalizing showed that the agarose had reached an equilibrium absorbance as can be observed visually in Figure 20. This same trend was observed in batches 2 and 3 for agarose. As such, the absorbance values were normalized to the final value in the time series. The effective diffusion

coefficient and the equilibrium absorbance value were estimated by fitting the normalized absorbance values in a 1-parameter estimation Excel program. The thickness used for estimation was determined from the sample mass, using the equation developed from optical measurements on equivalently prepared agarose samples. The final absorbance value in the diffusion study was used for the equilibrium absorbance value and the diffusion coefficient was changed manually to reduce the error. The mean square error was used as an indicator of fit.

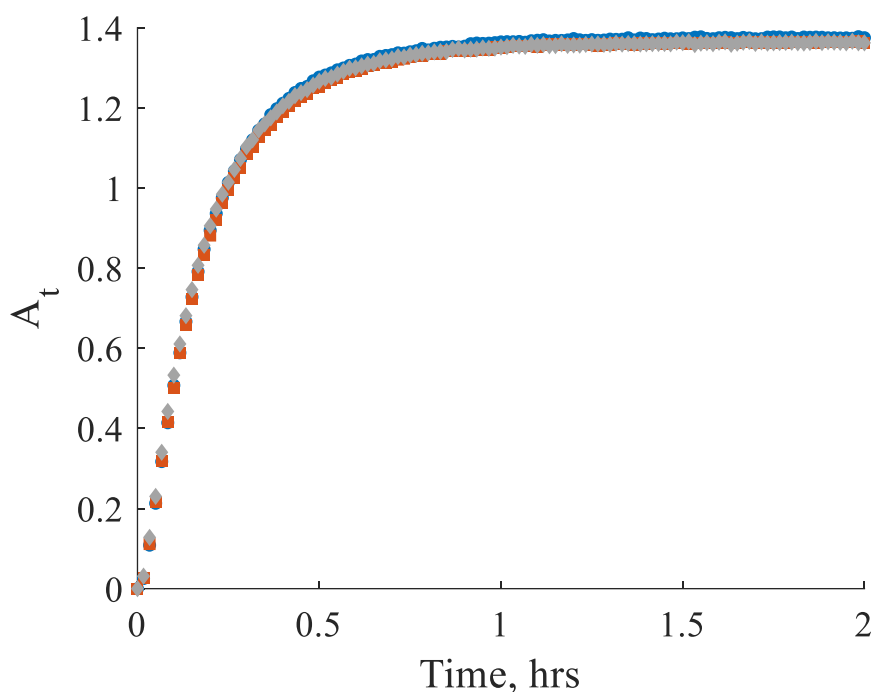


Figure 20 Absorbance as a function of time for agarose exposed to DMSO obtained at 22°C. The data represents three individual samples (blue circles, orange squares, and gray diamonds) from a single preparation batch.

Plotting the predicted absorbances values for each replicate in batch 1, it can be observed that the predicted absorbances reach equilibrium slightly ahead of the experimental data, as shown in Figure 21. This trend can be observed in all 9 diffusion studies conducted at room temperature.

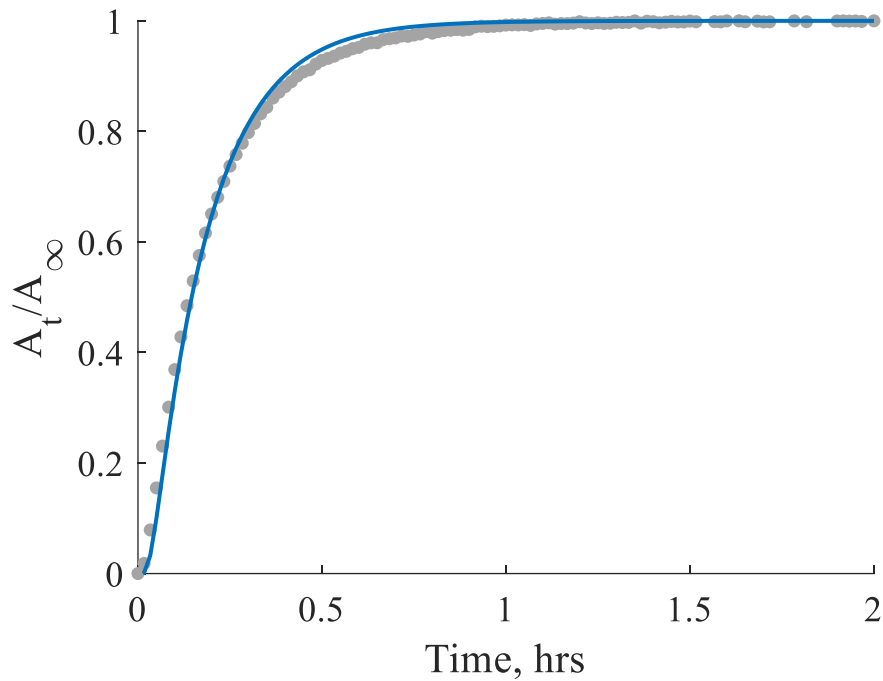


Figure 21 Absorbance data fit to determine  $D_{\text{eff}}$  for agarose batch 1 sample 1 at 22°C. Experimental absorbances are indicated by gray circles, and predicted values are represented by the blue line.

Plotting and examining the residuals, as shown in Figure 22, clearly displays a pattern of initial underestimation for early absorbance values, particularly in the first 15 minutes of data collection, followed by overestimation until the model approaches equilibrium at 1 hour of data collection. However, the maximum differences between the predicted and experimental absorbance values remain less than 0.08.

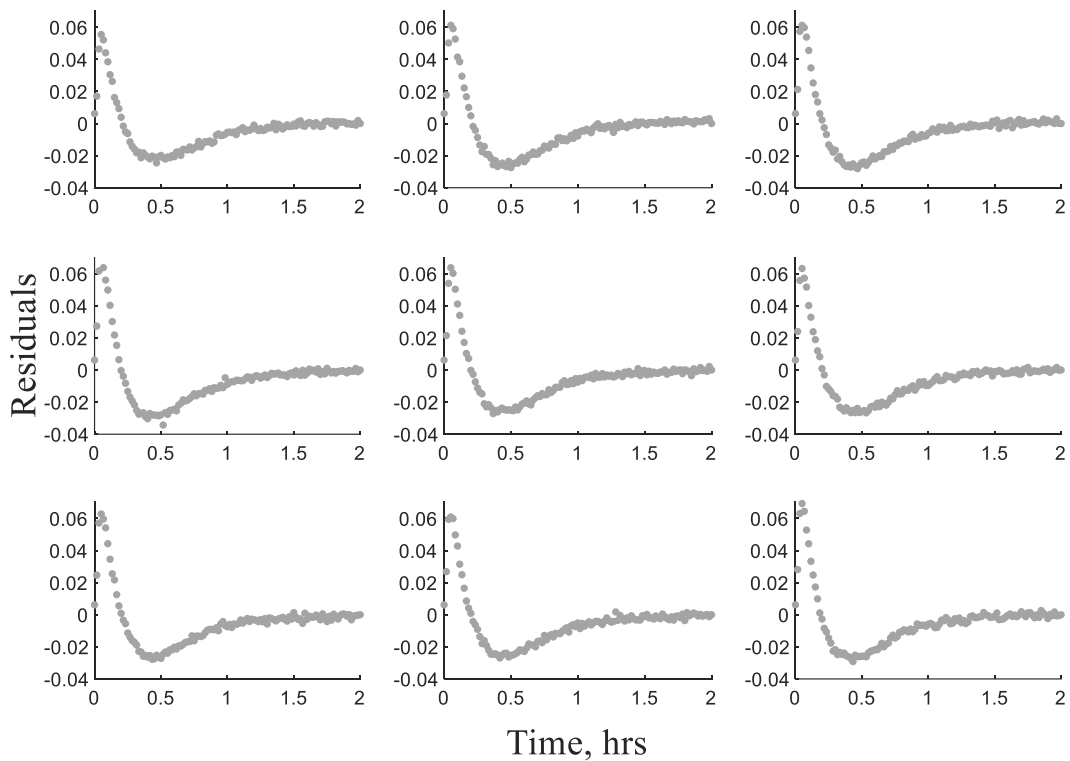


Figure 22 Residual plots for absorbance value fits obtained for three agarose samples across three batches at 22°C. Each row is a different batch, and each column is a different sample within each batch.

The estimated diffusion coefficients are summarized in Table 6. The corresponding equilibrium absorbance values, minimum sum of squares, and minimum mean square error for each sample are summarized in Table 22 in the Appendix.

Table 6 Diffusion Coefficients [ $\times 10^{-6} \text{ cm}^2/\text{s}$ ] for Agarose Obtained at Room Temperature

Sample # \ Batch #	1	2	3	Average	St. Dev.	St. Dev. (%)
1	8.9	9.1	9.1	9.1	0.1	2
2	8.8	9.3	9.2	9.1	0.3	3
3	9.2	9.4	9.5	9.4	0.1	2
<b>Average</b>	9.0	9.3	9.3			
<b>St. Dev.</b>	0.2	0.1	0.2			
<b>St. Dev. (%)</b>	2	1	2			

The average effective diffusion coefficient of all nine replicates was  $9.2 \pm 0.2 \times 10^{-6} \text{ cm}^2/\text{s}$  (2% standard deviation). This is much higher than the reported diffusivity for Dextran 4400 MW in agarose,  $1.35 \times 10^{-6} \text{ cm}^2/\text{s}$  [81], DMSO in collagen,  $2.4 \times 10^{-6} \text{ cm}^2/\text{s}$  [52], and the values for DMSO in alginate-gelatin reported within this work. However, the diffusion coefficients for reproductive tissue, such as ovarian tissue ( $11 \times 10^{-6} \text{ cm}^2/\text{s}$  at  $4^\circ\text{C}$  and  $14 \times 10^{-6} \text{ cm}^2/\text{s}$  at  $27^\circ\text{C}$  for human ovarian tissues or  $15.7 \times 10^{-6} \text{ cm}^2/\text{s}$  at  $22^\circ\text{C}$  for porcine ovarian tissue), are nearly double that of agarose at room temperature [21, 28].

Nevertheless, the sum of square errors were less than 0.05 and the mean square errors are less than 0.0004 for all nine replicates. Furthermore, the percent standard deviations for all batches and for individual samples across all batches are less than 5%. The within-sample and sample-to-sample variability for diffusion coefficient estimates is very low. Thus, agarose is the preferred material for use as a reference material for diffusion studies.

Independent two-sided t-tests were conducted using IBM SPSS Statistics 28 (IBM, Armonk, NY) to compare the average effective diffusion coefficients between batches as well as between replicates within the same batch. Equal variances between all batches and a significance value of  $\alpha = 0.05$  were assumed. No significant differences were found between batch 1 and 2 ( $p = 0.098$ ), batch 1 and 3 ( $p = 0.148$ ), or batch 2 and 3 ( $p = 0.940$ ). Equal variances were also assumed between all replicates. No significant differences were found when comparing the averages of the first and second replicates ( $p = 0.739$ ), first and third replicates ( $p = 0.054$ ), or second and third replicates ( $p = 0.054$ ). To further validate the effective diffusion coefficients, an average diffusion coefficient for batch 1 was used to fit against the six absorbance datasets from batches 2 and 3. This process was repeated using the average  $D_{\text{eff}}$  for batch 2 to fit against absorbances from batches 1 and 3,

then the average  $D_{\text{eff}}$  for batch 3 to fit against absorbances from batches 1 and 2. The sum of squares and mean square error were recorded for each fit and are summarized in Table 7.

Table 7 Comparison between average effective diffusion coefficients from individual batches and fits with other agarose absorbance data for validation of agarose effective diffusion coefficients at 22°C

Average $D_{\text{eff}}$ Source Batch #	Average $D_{\text{eff}} \times 10^{-6}$ [cm <sup>2</sup> /s]	Fit Batch #	Fit Sample #	SS [x 10 <sup>-2</sup> ]	MSE [x 10 <sup>-4</sup> ]
1	9.0	2	1	4.54	3.78
			2	3.93	3.28
			3	4.12	3.43
		3	1	3.64	3.03
			2	3.62	3.02
			3	4.81	4.01
2	9.3	1	1	3.28	2.73
			2	4.31	3.59
			3	3.51	2.93
		3	1	3.63	3.02
			2	3.47	2.89
			3	3.98	3.32
3	9.3	1	1	3.25	2.71
			2	4.27	3.56
			3	3.51	2.93
		2	1	4.50	3.75
			2	3.41	2.84
			3	3.56	2.97

All sum of squares error values were less than 0.05, and all mean square error values were less than 0.0004. Thus, the average diffusion coefficients from individual batches fit the remaining absorbance datasets closely. This is further apparent when examining the residuals for each fit shown in Figure 23, Figure 24, and Figure 25. Only one fit exceeds maximum differences of 0.08 between the predicted and experimental absorbance values. In this case, the maximum difference was 0.083 between the predicted and experimental absorbance values.

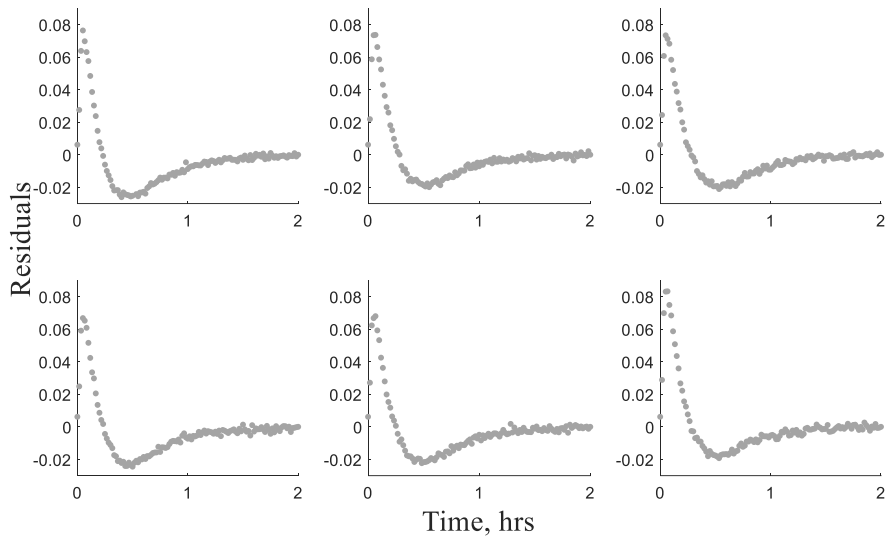


Figure 23 Residual plots for validation of the average effective diffusion coefficient for batch 1 of agarose obtained at 22°C using batches 2 (top row) and 3 (bottom row) absorbance time series. Each column is a different sample in each batch.

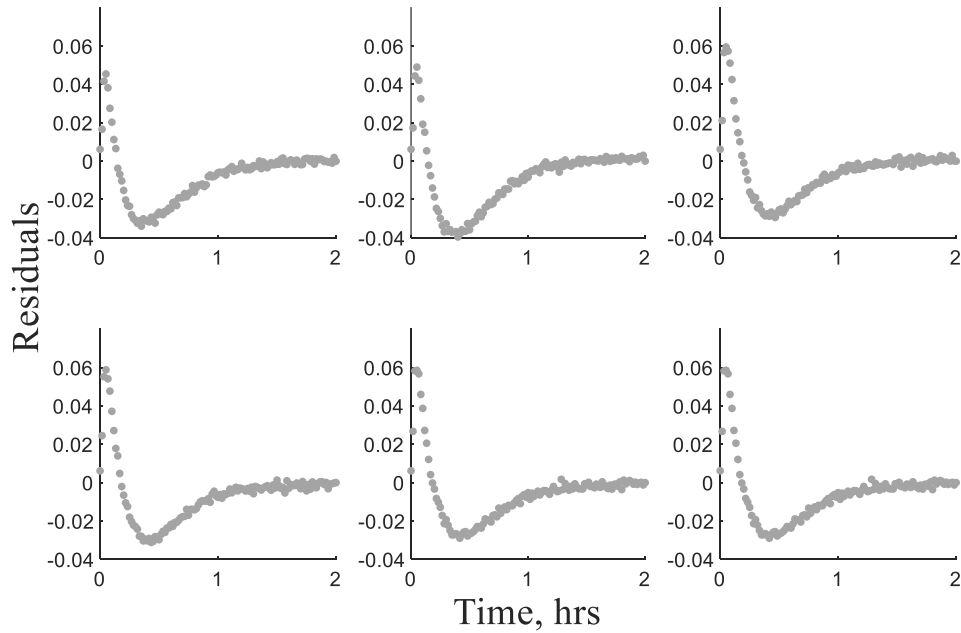


Figure 24 Residual plots for validation of the average effective diffusion coefficient for batch 2 of agarose obtained at 22°C using batches 1 (top row) and 3 (bottom row) absorbance time series. Each column is a different sample in each batch.

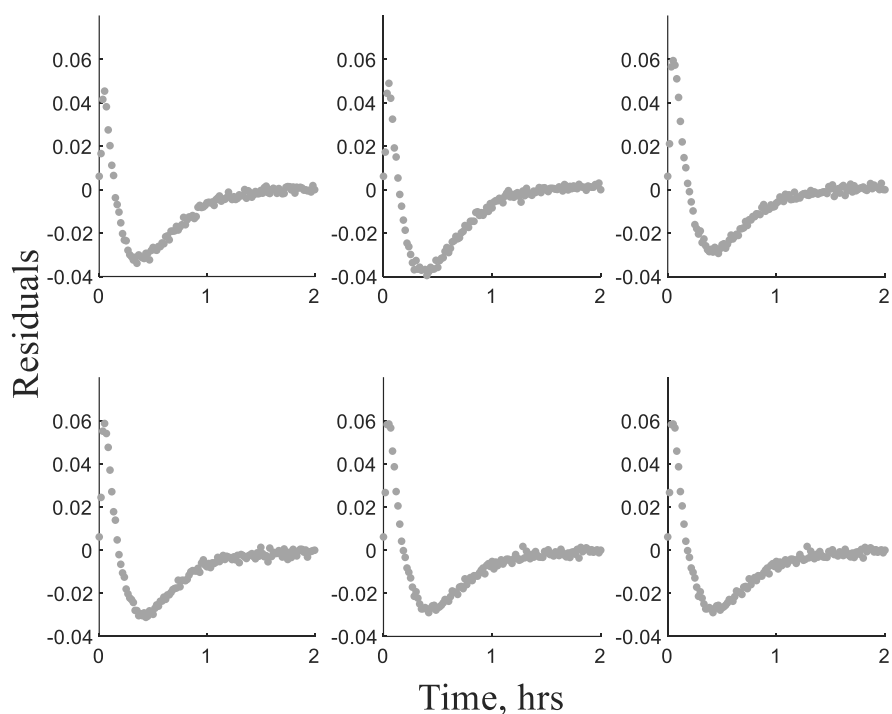


Figure 25 Residual plots for validation of the average effective diffusion coefficient for batch 2 of agarose obtained at 22°C using batches 1 (top row) and 2 (bottom row) absorbance time series. Each column is a different sample in each batch.

Finally, an average diffusion coefficient was calculated using sample 1 from each batch and used to fit against the six absorbance datasets for samples 2 and 3 from all batches. This process was also repeated using the average  $D_{\text{eff}}$  for sample 2 from each batch to fit against absorbances for samples 1 and 2 across all batches, then the average  $D_{\text{eff}}$  for sample 3 from each batch to fit against absorbances for samples 1 and 2 across all batches. The sum of squares and mean square error were recorded for each fit and are summarized in Table 8.

Table 8 Comparison between average effective diffusion coefficients from individual samples and fits with other agarose absorbance data for validation of effective diffusion coefficients at 22°C

Average $D_{\text{eff}}$ Source Sample #	Average $D_{\text{eff}} \times 10^{-6}$ [ $\text{cm}^2/\text{s}$ ]	Fit Sample #	Fit Batch #	SS [ $\times 10^{-2}$ ]	MSE [ $\times 10^{-4}$ ]
1	9.0	2	1	3.66	3.05
			2	3.72	3.10
			3	3.52	2.93
		3	1	3.60	3.00
			2	3.90	3.25
			3	4.52	3.77
2	9.1	1	1	2.88	2.40
			2	4.44	3.70
			3	3.54	2.95
		3	1	3.54	2.95
			2	3.76	3.13
			3	4.33	3.60
3	9.4	1	1	3.52	2.94
			2	4.61	3.84
			3	3.74	3.11
		2	1	5.40	4.50
			2	3.39	2.83
			3	3.44	2.87

All sum of squares error values were approximately 0.05 or less, and all mean square error values were less than 0.0005. Thus, the average diffusion coefficients from individual samples also fit the remaining agarose absorbance datasets closely. Examining the residuals for the fits to validate the average effective diffusion coefficients for each sample in Figure 26, Figure 27, and Figure 28 reveals a similar pattern to validation of the average  $D_{\text{eff}}$  for each batch. In the one case that exceeds a maximum difference of 0.08, the maximum difference value was 0.081. As such, the pooled average effective diffusion coefficient for all nine samples,  $9.2 \pm 0.2 \times 10^{-6} \text{ cm}^2/\text{s}$ , can be used as a comparison when transferring the FTIR diffusion study methodology between users in the same lab as well as between labs.

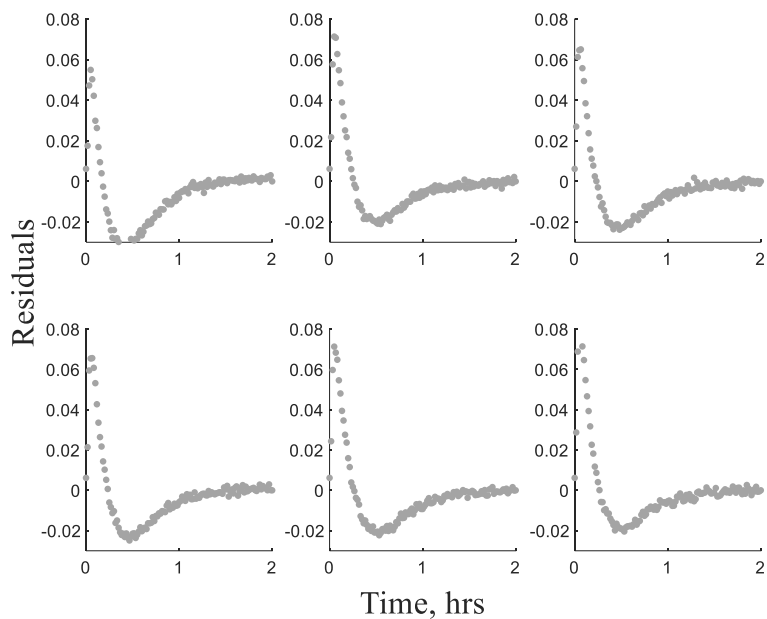


Figure 26 Residual plots for validation of the average effective diffusion coefficient for sample 1 across all batches of agarose obtained at 22°C using the absorbance time series for samples 2 (top row) and 3 (bottom row) across all batches. Each column represents a different batch.

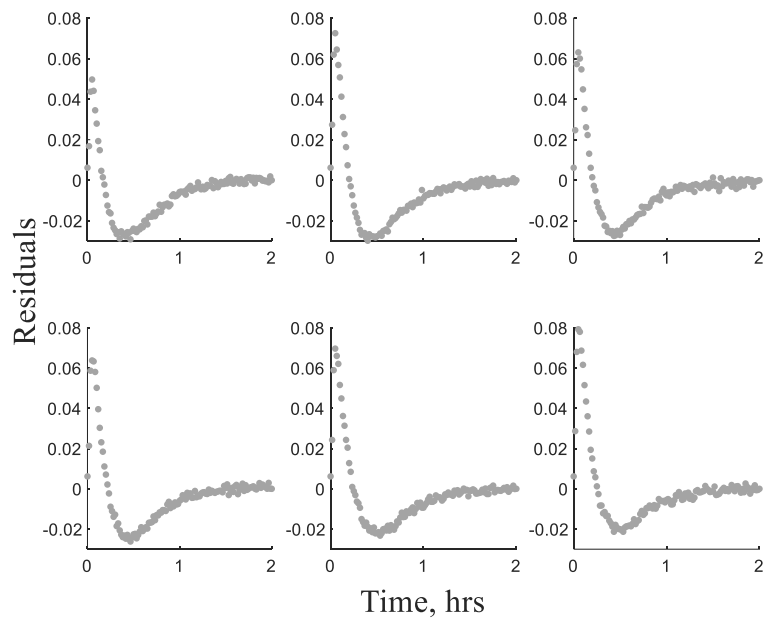


Figure 27 Residual plots for validation of the average effective diffusion coefficient for sample 2 across all batches of agarose obtained at 22°C using the absorbance time series for samples 1 (top row) and 3 (bottom row) across all batches. Each column represents a different batch.

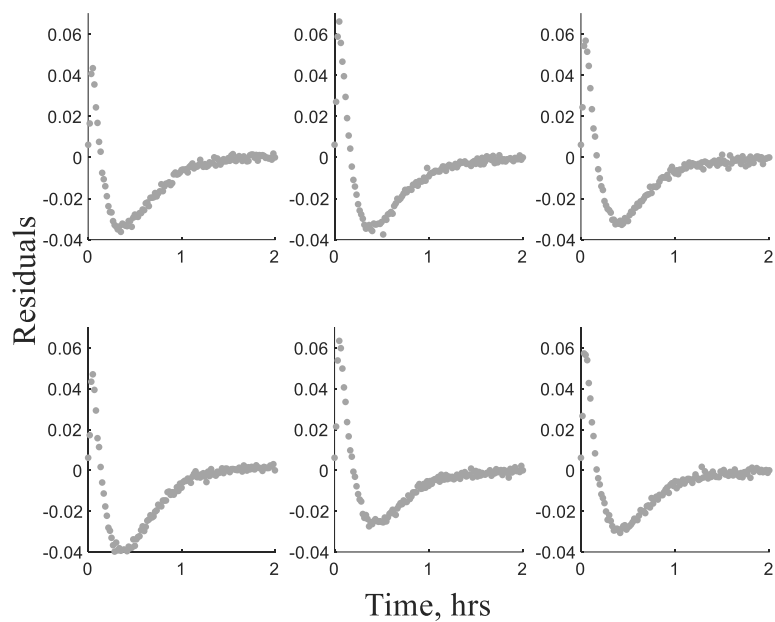


Figure 28 Residual plots for validation of the average effective diffusion coefficient for sample 3 across all batches of agarose obtained at 22°C using the absorbance time series for samples 1 (top row) and 2 (bottom row) across all batches. Each column represents a different batch.

## **CHAPTER 5 DETERMINATION OF EFFECTIVE DIFFUSIVITY FOR TESTICULAR TISSUES USING FTIR**

### **5.1 Rationale**

CPA diffusion coefficients at various temperatures have been determined in several types of tissues [21, 22, 24, 27-32, 38, 57] as summarized in sections 1.3.1 and 1.3.2. While many of these tissues are soft tissues, the only diffusion coefficients determined for reproductive tissue thus far have been for ovarian tissue. As such, the development of procedures for measuring diffusion through fresh soft tissue samples will aid the application of existing diffusion models to a wider range of tissues, including testicular tissue. In turn, integrated optimization will be enabled for material and process parameters.

### **5.2 Slicing materials and methods**

Feline testes that were discarded from routine sterilization procedures were acquired from Cabarrus Spay and Neuter Clinic (NC, USA). They were stored in 150mL PBS and transported in an insulated container with 2 ice packs. The tunica albuginea and epididymis were removed to prepare testes for slicing in the Microtome. Low melting point agarose tablets were dissolved in 25mL phosphate buffer solution to produce a 2% (w/v) agarose solution as previously described. As testes are ovoid in shape, one end perpendicular to the major axis of the testis was sliced off to provide a flat surface and instant bonding adhesive was used to secure the testis to the 20mm diameter specimen tube plunger. A bulk pipette tip was used to pipette the clear agarose solution into the specimen tube until approximately 2-3mm of agarose solution was above the testis in the specimen tube, and a cooling block was wrapped around the specimen tube to facilitate quick and even solidification of the agarose around the testis. The specimen tube was inserted into the VF-500-0Z Microtome which was set to oscillation level 7 and advance level 3. One testis was considered a slicing batch, and a new steel blade was used every 2 slicing batches. A step-down

calibration method was employed to ensure slices were 1mm (1000  $\mu$ m) thick. The Microtome was set to 1200  $\mu$ m initially and the agarose above the testis in the specimen tube was sliced. Once a slice was obtained which did not show signs of striations or marks from being sliced, the Microtome thickness was decreased to 1100  $\mu$ m. This process was repeated, decreasing the thickness to 1050  $\mu$ m and finally 1000  $\mu$ m each time a slice without striations or other marks from slicing were obtained.

### 5.3 Estimating thickness of testicular tissue inside sample holder

The optical measurements for estimating thickness were repeated for a batch of testicular tissue. The resulting points before packing into the sample holder are shown in Table 9 and the center point for each testicular tissue is highlighted in green.

Table 9 Estimated thickness of testicular tissue (n=8) in mm, determined at various points on the top surface, measured directly after slicing and punching, before placement into the sample holder. The center point of each testicular tissue is highlighted in green.

Point \ Sample	1	2	3	4	5	6	7	8
<b>1</b>	1.50	1.96	1.81	1.81	1.35	2.09	1.96	1.39
<b>2</b>	1.80	2.01	1.93	1.35	1.39	2.43	1.77	1.27
<b>3</b>	1.90	2.35	2.11	1.07	1.41	2.14	1.50	0.97
<b>4</b>	1.47	2.01	2.90	1.43	0.97	2.37	1.26	1.34
<b>5</b>	1.66	2.02	2.07	1.46	1.18	2.21	1.71	1.17
<b>6</b>	1.69	2.63	1.10	1.17	2.25	1.66	1.28	1.97
<b>Average</b>	1.67	2.16	1.99	1.38	1.43	2.15	1.58	1.35
<b>St. Dev.</b>	0.17	0.27	0.58	0.26	0.44	0.27	0.28	0.34
<b>St. Dev. (%)</b>	10.0	12.4	29.2	18.7	30.7	12.7	17.8	25.0

The within-sample variation is much higher for testicular tissue than for agarose despite the use of a precision slicer. The individual standard deviations range from 0.17 to 0.58mm with an average of 0.33mm, which is more than 5 times that of the combined standard uncertainty. While some uncertainty would be added considering the reliance on placement of the paper slips, this is a much larger variation than expected. Though, the higher sample-to-sample variation is to be expected as

the sample masses range from 0.0618 to 0.1074g with an average of  $0.0830 \pm 0.020$  (24% standard deviation). While the precision slicer likely reduced the within-sample and sample-to-sample variation in thickness compared to manual cutting methods, the testicular tissue was highly deformable and difficult to handle in general. Testes often were visually pressed towards the bottom of the specimen tube despite the use of agarose to maintain pressure around the testis in the tube. In addition, the tendency for testes to deform during slicing may in part explain the fact that all samples were thicker than the nominal 1mm setting on the precision slicer.

Averaging the within-sample point values to obtain overall sample thickness values resulted in average thicknesses ranging from 1.35 to 2.16mm with an average of  $1.7 \pm 0.5$  (26% standard deviation) prior to packing which is only slightly greater than the standard deviation for alginate-gelatin but much greater than for agarose. In addition, this standard deviation is only slightly larger than the variation in sample masses. In fact, the sample-to-sample variation is nearly 7 times larger than that of agarose and is 4 times as large as alginate-gelatin.

The thickness estimated at each point on the surface of the testicular tissue after packing into the sample holder is shown in Table 10 and the center point for each testicular tissue sample is highlighted in green.

Table 10 Estimated thickness of testicular tissue (n=8) in mm, determined at various points on the top surface, measured after placement into the sample holder. The center point of each testicular tissue is highlighted in green.

Point \ Sample	1	2	3	4	5	6	7	8
1	0.76	2.04	2.28	2.94	1.6	2.59	2.74	2.94
2	1.05	2.18	1.91	2.43	1.57	2.39	0.94	2.43
3	1.17	1.62	2.37	2.72	1.85	2.38	2.1	2.72
4	1.17	1.65	2.31	1.22	1.32	4.19	2.58	1.22
5	0.98	1.96	2.6	1.59	1.63	2.75	2.67	1.59
6	0.93	1.77	2.12	1.8	1.32	2.13	1.11	1.8
<b>Average</b>	1.01	1.87	2.27	2.12	1.55	2.74	2.02	2.12
<b>St. Dev.</b>	0.16	0.23	0.23	0.68	0.20	0.74	0.81	0.68
<b>St. Dev. (%)</b>	15.5	12.1	10.3	32.2	13.1	27.1	39.9	32.2

The within-sample variation increased after packing with standard deviations ranging from 0.16 to 0.81mm and an average standard deviation of 0.47mm. As such, the within-sample variation increased to more than 8 times the combined standard uncertainty. While an increase in within-sample variation is to be expected after packing as seen in agarose, the sample-to-sample variation increased to more than double that before packing. Though, it should be noted that packing the testicular tissue by hand using custom plungers would contribute to the larger increase in within-sample and sample-to-sample variation.

The testicular tissue was determined to compact to average thicknesses of  $2 \pm 0.7$ mm (35% standard deviation) inside the sample holder. Similar to agarose, the theoretical thicknesses, determined using an average density of 1.22 g/mL, before packing consistently underestimate the actual thicknesses for testicular tissue, as can be observed in the left of Figure 29. However, the theoretical values overestimate the thicknesses of the testicular tissue samples after packing in the sample holder in most cases, as shown in the right of Figure 29. Thus, as with agarose, the equation of a correlation line fit to the average thicknesses after packing into the sample holder was used to estimate the thickness for samples used in diffusion studies.

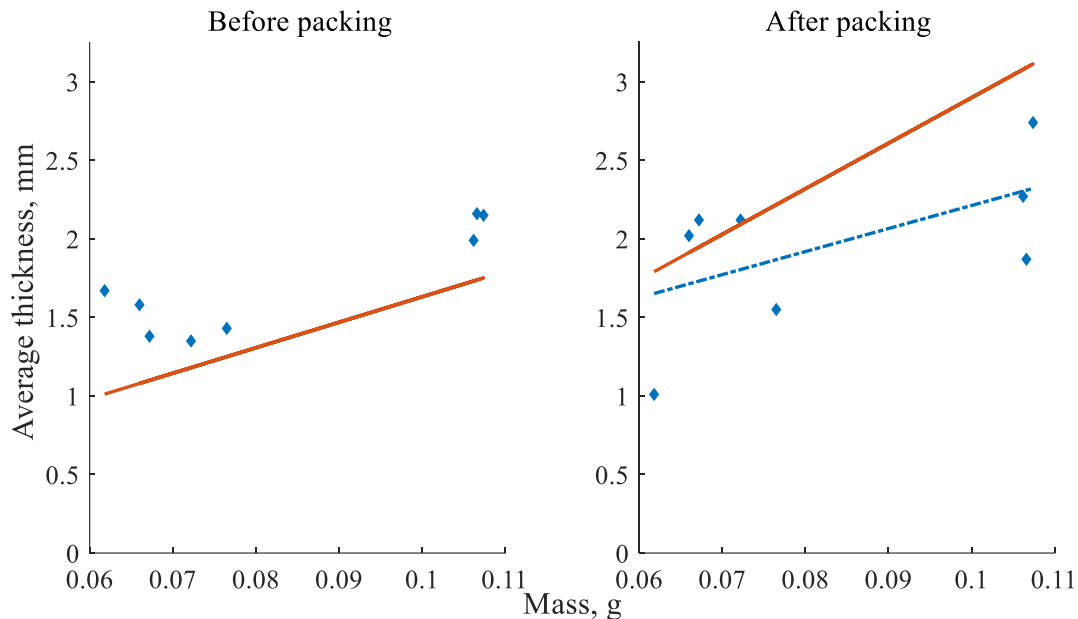


Figure 29 A comparison of the theoretical and average experimental thicknesses before (left) and after (right) packing in sample holder for testicular tissue. A solid orange line represents the theoretical thicknesses before packing. Experimental thicknesses are shown as blue diamonds. The correlation line for the experimental thicknesses after packing in the sample holder is represented by a blue dashed line, equation: thickness = 14.7\*weight in grams + 0.75 mm ( $R^2 = 0.3323$ ).

### 5.3.1 Estimated diffusion coefficients in testicular tissue at 22°C

A fresh batch of testicular tissue was prepared, and three sequential samples were exposed to DMSO over a period of 6 hours. FTIR spectra were collected for each sample and absorbance values were plotted over time. Only one of the nine testicular tissue slices reached an equilibrium absorbance at room temperature as can be observed visually in Figure 30. As such, the 1-parameter estimation Excel program was used to estimate the effective diffusion coefficient for the first testis slice. Diffusion coefficients for all testicular tissues were determined using the 2-parameter estimation program in Excel to fit for the effective diffusion coefficient and the equilibrium absorbance value. The thickness used for estimation was determined from the sample mass, using the equation developed from optical measurements on equivalently prepared testicular tissue samples. The final absorbance value in the diffusion study was used as an initial guess for the

equilibrium absorbance value and the diffusion coefficient and equilibrium absorbance values were manually changed in several iterations to reduce the error. The sum of squares and mean square error were used as indicators of fit.

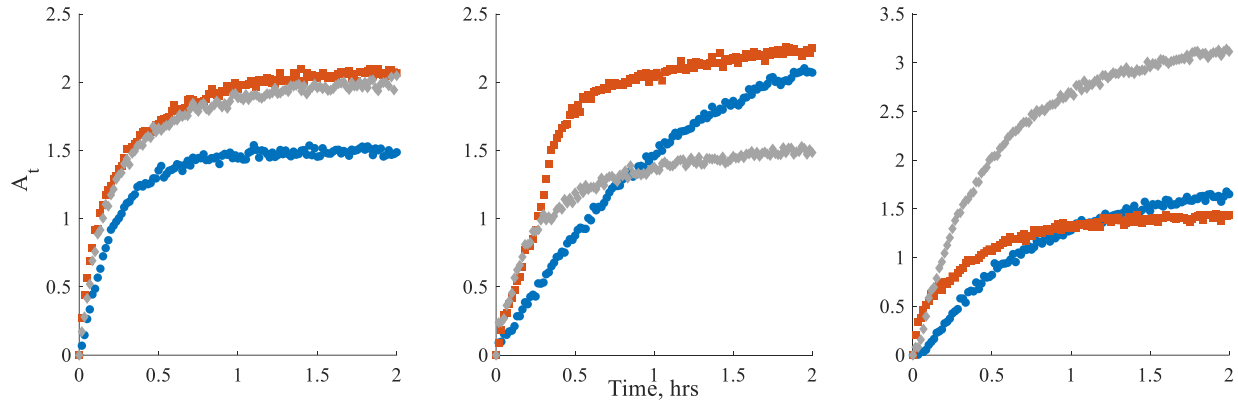


Figure 30 Absorbance as a function of time obtained at 22°C for different samples of testicular tissue across three collection days 1 (left), 2 (middle), and 3 (right). For each day, samples 1, 2, and 3 are represented by blue circles, orange squares, and gray diamonds, respectively.

The plots of the predicted and experimental absorbance values displayed in Figure 31 show that the predicted absorbances for day 1 reached equilibrium faster than the experimental data. Though, this trend was also observed for agarose at 22°C, there is a much greater mismatch for testicular tissues between the predicted and experimental absorbance values. Again, this trend can be observed in several of the nine diffusion studies conducted at room temperature.

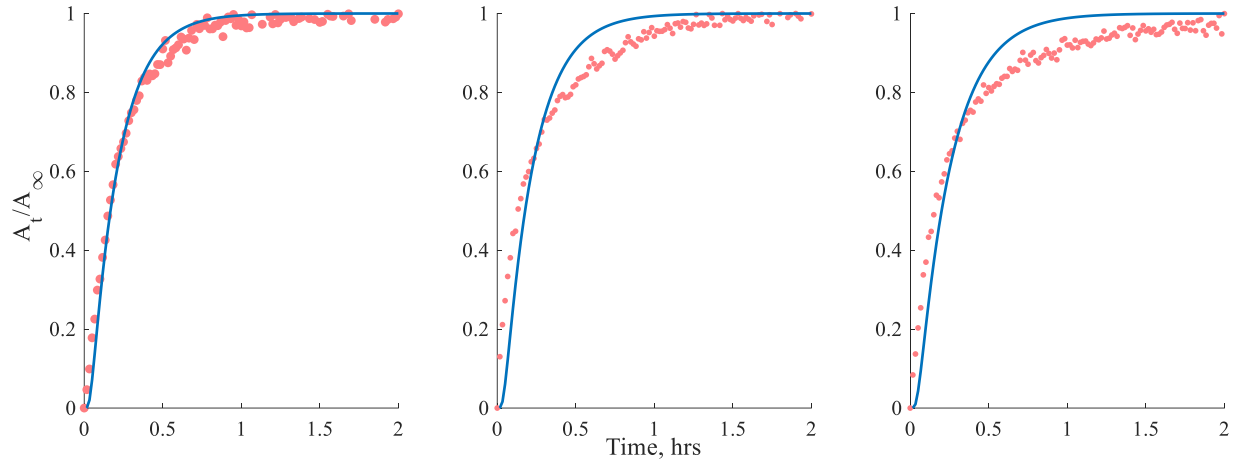


Figure 31 Absorbance data fit to determine  $D_{\text{eff}}$  for testicular tissue collection day 1 samples 1 (left), 2 (middle), and 3 (right). Experimental absorbance values are indicated by pink circles and predicted absorbance values are represented by the blue line.

The residuals in Figure 32 for all nine fits show a similar pattern to that observed for agarose. The model underestimates the absorbance values for the first 15 minutes of data collection. However, the model often overestimates the absorbance values for the remainder of the two-hour data collection window for testicular tissue rather than approaching zero as the experimental and predicted absorbance values both approach equilibrium. In addition, much larger maximum differences can be observed for testicular tissue, reaching a maximum difference of 0.37 for one case.

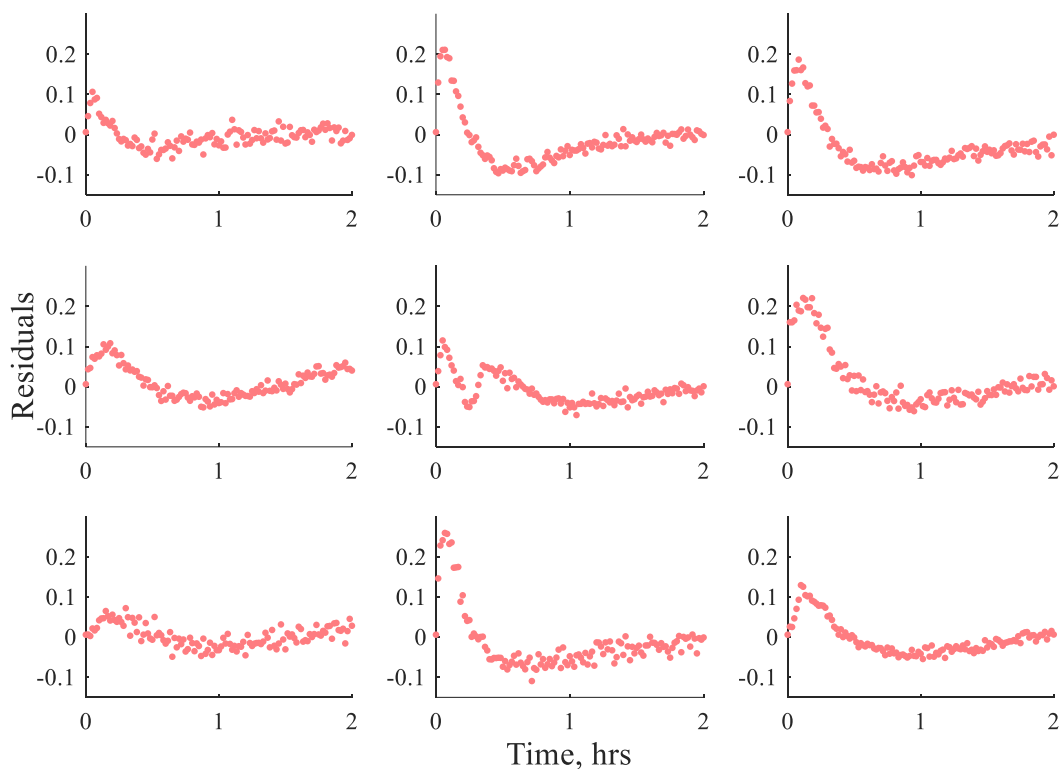


Figure 32 Residual plots for normalized absorbance value generated during estimation of the diffusion coefficient for DMSO in testicular tissue at 22°C. Each row is a different collection day and each column is a different sample for each collection day.

The final diffusion coefficients for each sample are summarized in Table 11. The diffusion coefficients are organized by day and sample. Each day consisted of a fresh batch of testes collected and sliced. The corresponding equilibrium absorbance values, minimum sum of squares, and mean square errors are summarized in Table 23 in the Appendix. At least three iterations were necessary to reach a global minimum in the 2-parameter estimation program.

Table 11 Diffusion coefficients [ $\times 10^{-6} \text{ cm}^2/\text{s}$ ] for fresh testicular tissue obtained at room temperature for three separate days

<b>Sample # \ Batch #</b>	<b>1</b>	<b>2</b>	<b>3</b>
<b>1</b>	15	5	7
<b>2</b>	12	13	11
<b>3</b>	12	13	8
<b>Average</b>	13	10	9
<b>St. Dev.</b>	2	5	2
<b>St. Dev. (%)</b>	13	45	24

The average effective diffusion coefficient of all nine testicular tissues was  $11 \pm 3 \times 10^{-6} \text{ cm}^2/\text{s}$  (31% standard deviation). While this is much higher than diffusivity values for DMSO in pulmonary arterial valves,  $3.02 \times 10^{-6} \text{ cm}^2/\text{s}$  [22], and human articular cartilage at  $27^\circ\text{C}$ ,  $6.8 \times 10^{-6} \text{ cm}^2/\text{s}$  [27], it is less than the diffusivity values for DMSO in other reproductive tissues, such as porcine ovarian tissue,  $15.7 \times 10^{-6} \text{ cm}^2/\text{s}$  [21], or the simulated value for human ovarian tissue,  $11 \times 10^{-6} \text{ cm}^2/\text{s}$  [28].

Independent two-sided t-tests were conducted using SPSS to compare the average effective diffusion coefficients between collection days. Equal variances between all collection days and a significance value of  $\alpha = 0.05$  were assumed. No significant differences were found when comparing between collection days 1 and 2 ( $p = 0.445$ ), days 1 and 3 ( $p = 0.052$ ), or days 2 and 3 ( $p = 0.588$ ). To validate the effective diffusion coefficients, the average effective diffusion coefficient for collection day 1 was used to fit against the six absorbance datasets from collection days 2 and 3. This process was repeated using the average  $D_{\text{eff}}$  for collection day 2 to fit against absorbances from days 1 and 3, then the average  $D_{\text{eff}}$  for day 3 to fit against absorbances from days 1 and 2. The sum of squares and mean square error were recorded for each fit and are summarized in Table 12.

Table 12 Comparison between average effective diffusion coefficients from individual collection days and fits with other testicular tissue absorbance data for validation of effective diffusion coefficients at 22°C

Average $D_{\text{eff}}$ Source Batch #	Average $D_{\text{eff}} \times 10^{-6}$ [cm <sup>2</sup> /s]	Fitting Day #	Fitting Sample #	SS	MSE [ $\times 10^{-2}$ ]
1	13	2	1	37.3	31.1
			2	0.816	0.680
			3	1.66	1.38
		3	1	9.97	8.31
			2	1.78	1.48
			3	14.0	11.6
2	10	1	1	1.65	1.37
			2	2.51	2.10
			3	2.66	2.21
		3	1	5.07	4.23
			2	1.49	1.24
			3	5.52	4.60
3	9	1	1	3.80	3.17
			2	4.06	3.38
			3	4.15	3.46
		2	1	17.0	14.2
			2	7.73	6.44
			3	6.58	5.48

The sum of squares error ranged from 0.816 to 37.3 for each fit. This pattern is further reflected in mean square error with values from 0.007 to 0.311. As can be seen visually in Figure 33, the average diffusion coefficients are overestimated for some of the nine diffusion coefficients and underestimated for others as is expected with the large standard deviation for all nine testicular tissue samples.

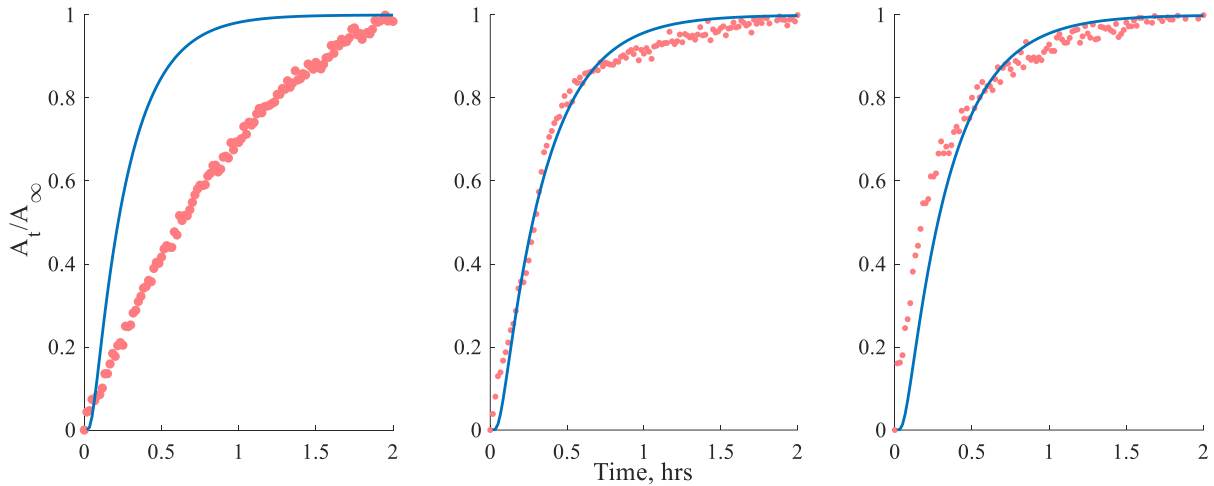


Figure 33 Absorbance as a function of time for testicular tissue collection day 2 samples 1 (left), 2 (middle), and 3 (right) fit using the average effective diffusion coefficient from collection day 1. Experimental values are indicated by pink circles, and predicted absorbance is represented by the blue line.

This pattern can also be observed in the residual plots for validation of the average effective diffusion coefficients for each collection day in Figure 34, Figure 35, and Figure 36. Again, large maximum differences can be seen, reaching a maximum difference of 0.49 when trying to estimate the first sample of collection day 2 using the average  $D_{\text{eff}}$  value from collection day 1. In addition, when fitting the absorbance data series for collection days 2 and 3 using the average diffusion coefficient from collection day 1, the predicted absorbance values are overestimated for half the absorbance time series and underestimated for the remaining time series. Fitting the absorbance time series from collection days 1 and 3 using the average  $D_{\text{eff}}$  from collection day 2 results also in half the time series being overestimated, but only two of the remaining absorbance time series being underestimated. Finally, five of the six absorbance series are overestimated when fitting collection days 1 and 2 with the average  $D_{\text{eff}}$  from collection day 3.

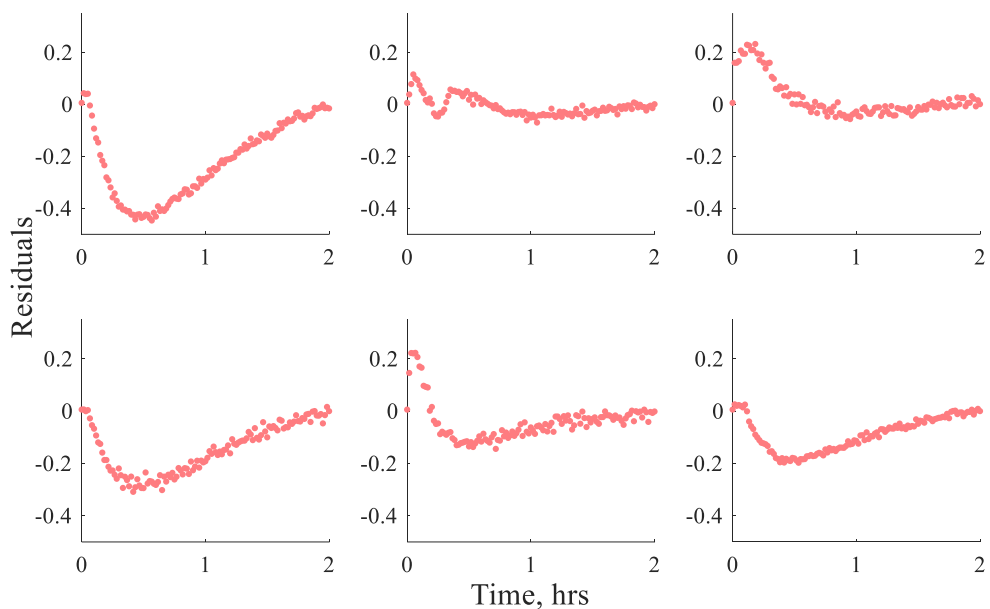


Figure 34 Residual plots for validation of the average effective diffusion coefficient for collection day 1 of testicular tissue obtained at 22°C using collection days 2 (top row) and 3 (bottom row) absorbance time series. Each column corresponds to a different sample on each collection day.

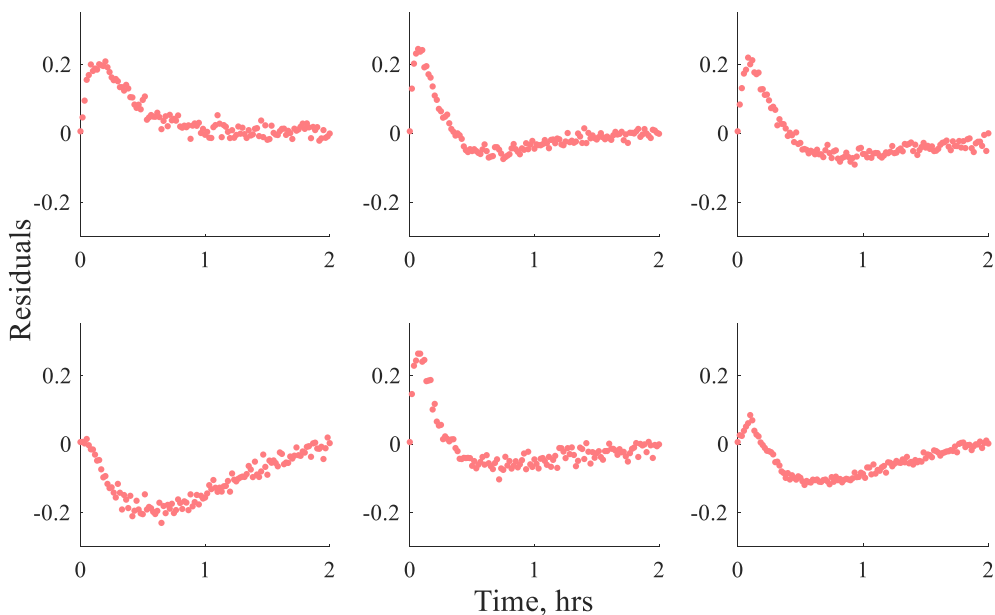


Figure 35 Residual plots for validation of the average effective diffusion coefficient for collection day 2 of testicular tissue obtained at 22°C using collection days 1 (top row) and 3 (bottom row) absorbance time series. Each column corresponds to a different sample on each collection day.

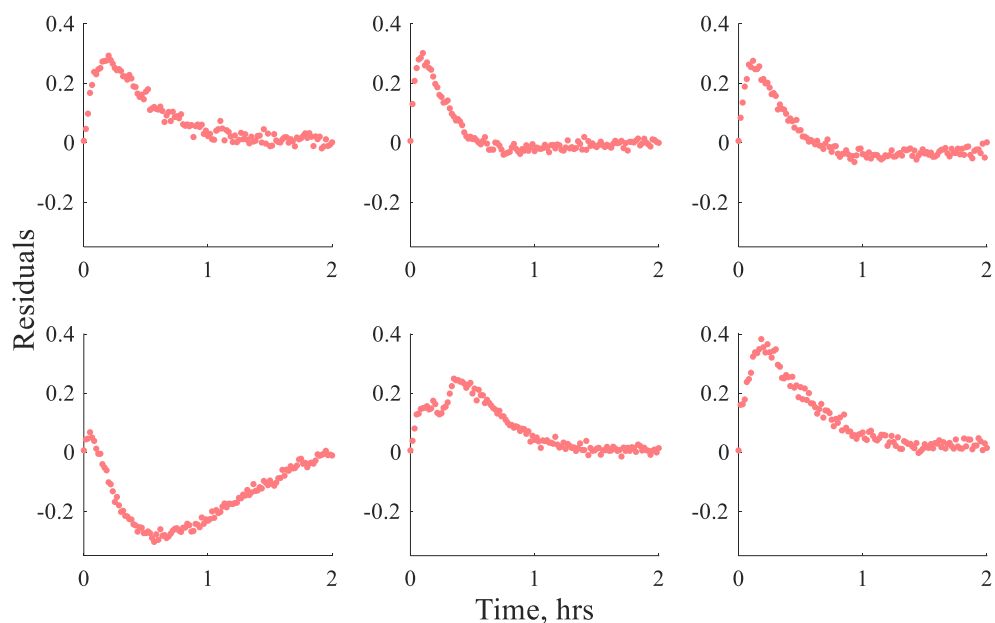


Figure 36 Residual plots for validation of the average effective diffusion coefficient for collection day 3 of testicular tissue obtained at 22°C using collection days 1 (top row) and 2 (bottom row) absorbance time series. Each column corresponds to a different sample on each collection day.

Thus, while the average effective diffusion coefficient of all nine testicular tissue samples can be used in planning future preservation studies and to estimate the time required to load DMSO into a testicular tissue sample, the variability inherent in the tissue must be considered. For example, the model developed by Fieldson and Barbari (1995) can be used to estimate the time required for a tissue sample exposed to DMSO to reach equilibrium using a known tissue thickness and  $D_{\text{eff}}$  and  $A_{\infty}$  values. Assuming the average thickness for testicular tissue determined using the ATOS Scanbox and the average effective diffusion coefficient and equilibrium absorbance of all nine samples, the required time to reach equilibrium (a normalized absorbance value of 0.9999) is 3 hours and 45 minutes. The times required to reach equilibrium for various cases based on decreasing or increasing the thickness,  $D_{\text{eff}}$ , and  $A_{\infty}$  by 1 standard deviation are summarized in Table 13. While less than 10 hours is required to reach equilibrium if the tissue slice is compacted

to 2.7mm inside the sample holder, a tissue of thickness 5mm, as was typical in many of the studies described in Section 1.3.1, requires 18 hours and 15 minutes to reach equilibrium even with the greatest effective diffusion coefficient. Similarly, if the greatest  $D_{\text{eff}}$ ,  $14 \text{ cm}^2/\text{s}$ , and the smallest  $A_{\infty}$ , 1.431, are used, 18 hours and 12 minutes are necessary for a 5mm thick testicular tissue slice to reach equilibrium.

Table 13 Estimated required time to reach equilibrium for testicular tissue at 22°C

Thickness, mm	$D_{\text{eff}} = 8 \text{ cm}^2/\text{s}$ $A_{\infty} = 1.431$	$D_{\text{eff}} = 11 \text{ cm}^2/\text{s}$ $A_{\infty} = 1.961$	$D_{\text{eff}} = 14 \text{ cm}^2/\text{s}$ $A_{\infty} = 2.491$
1.3	2 hrs 11 min	1 hr 35 min	1 hr 15 min
2	5 hrs 11 min	3 hrs 45 min	2 hrs 56 min
2.7	9 hrs 20 min	6 hrs 45 min	5 hrs 20 min
5	31 hrs 50 min	23 hrs 11 min	18 hrs 15 min

## **CHAPTER 6 DESIGN OF AN APPARATUS FOR TEMPERATURE-CONTROLLED CPA EXPOSURE FOR TISSUE**

### **6.1 Rationale**

Current methods for exposing tissues for FTIR analysis have utilized molds made from common lab materials which, while allowing easy exposure to CPAs, do not provide good features for temperature control [22, 38, 39, 82, 83]. However, the diffusion time required for CPAs into tissues is dependent on temperature in addition to concentration. A chamber which allows temperature control while maintaining a 1-dimensional diffusion environment is necessary to study diffusion phenomena at different temperatures during exposure of tissue to CPAs.

### **6.2 Development of a custom sample holder for 1-D CPA diffusion studies**

A sample holder was designed and machined out of acetal while a lid was machined out of aluminum to create a closed environment inside the sample holder. Current methods for introducing CPAs to samples on the FTIR use a sample holder made from common lab materials with a 6mm diameter to prevent leaking around the sides of the tissue. However, the current sample holders introduce a small amount of CPA (250 $\mu$ L) to the tissue [38, 39]. There is some concern about changes in the boundary condition at the top surface of the tissue as the small amount of CPA depletes while diffusing into the tissue. To prevent changes in the boundary condition, the sample holder was designed to hold at least 2.5mL of CPA to provide a large CPA reservoir. In addition, the holder design is compatible with rings of different inner diameters to accommodate different sample sizes and types. Rings with inner diameters of 6mm, 7.4mm, and 8mm were used for testicular tissue, agarose, and alginate-gelatin, respectively. The smaller inner diameters allowed slight compression of samples to prevent leaking around the edges of the materials. Acetal was chosen for ease of machining and its thermal insulation properties. Aluminum was chosen for the lid due to ready availability and ease of machining to a precise dimension to prevent the lid

from sticking to the chamber while also allowing a tight fit to maintain the environment inside the holder. A detailed engineering drawing of the custom holder dimensions is shown in Figure 37. Only the 8mm ring is shown as the only change between dimensions for the inner ring was the inner diameter. The sample is packed into the inner ring after placement on the FTIR surface over the sensing window. A foam insulation box with an open bottom was placed over the FTIR surface during all diffusion studies.

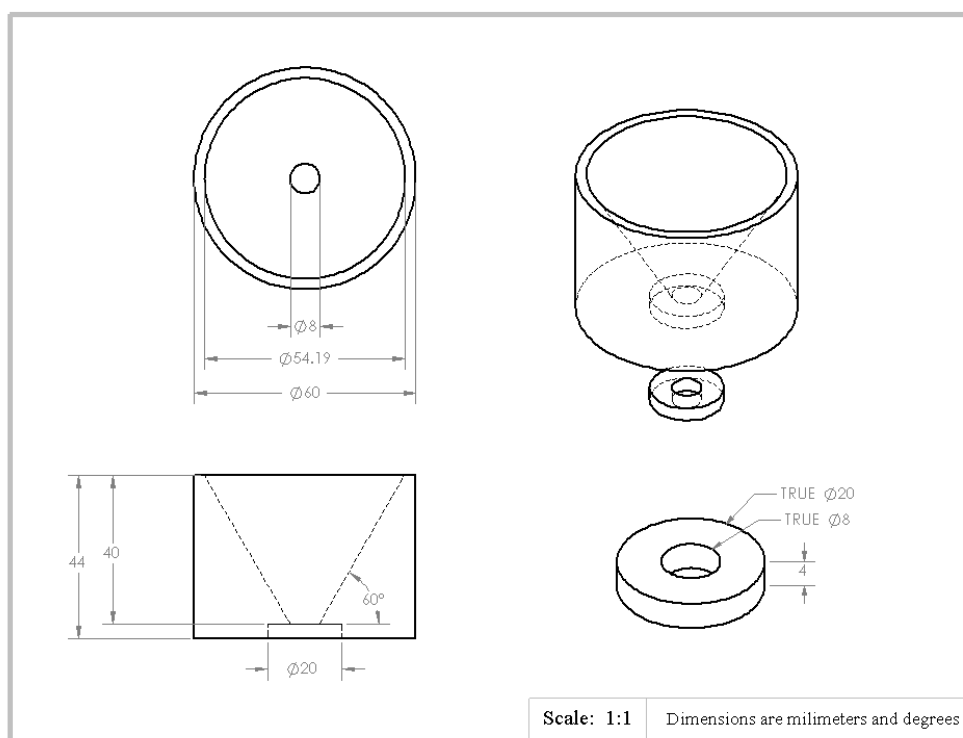


Figure 37 Design and dimensions for sample holder for CPA diffusion studies. Only the ring designed for alginate-gelatin is shown here. Two more rings with inner diameters of 6mm and 7.4mm were also machined from acetal for use with testicular tissue and agarose.

To validate that pressure effects remain negligible and do not need to be considered in the diffusion model despite the increase in CPA introduced on top of the sample, a scaling comparison with atmospheric pressure was performed. SolidWorks Student Edition 2022 (Waltham, MA) was used

to estimate the height of the DMSO inside the sample holder by constructing a solid placeholder inside the sample holder and setting the material density to  $1.1 \text{ g/cm}^3$ . The height was then adjusted until the volume was approximately 2.5mL at 12.65mm. The system for the scaling comparison is shown in Figure 38.

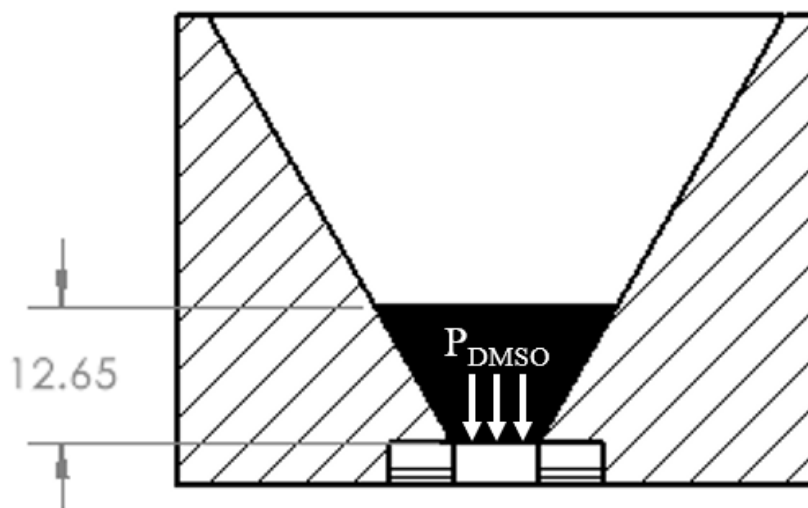


Figure 38 System diagram of scaling comparison for pressure introduced by DMSO on top of sample inside the holder.

The pressure of the DMSO was calculated as the product of the density of DMSO ( $1.1 \text{ g/cm}^3$ ), acceleration due to gravity ( $9.81 \text{ m/s}^2$ ), and the height of the DMSO inside the sample holder. The pressure of the DMSO on top of the sample was 137 Pa which is much less than atmospheric pressure (101,325 Pa). Thus, pressure effects do not need to be considered in the diffusion model.

### 6.3 Thermal control design and evaluating temperature profile

The main sources of heat to the sample holder during temperature control experiments were assumed to be radiation, convection from the air around the holder, and conduction from the FTIR surface. Foam insulation was purchased from Home Depot (NC USA) and cut into panels which were taped together such that all seams were covered and sealed to minimize environmental heat sources. A cooling circulation bath was connected to the existing liquid-jacket system embedded

around the sensing window of the Gladi-ATR attachment for the FTIR. This system was used to circulate 60% ethylene glycol in water through the liquid jacket system at temperatures below 4°C such that the temperature of the plate at the top surface was 4°C. Phase Change Materials (PCMs) were selected to provide further resistance to warming of the FTIR surface.

Phase Change Materials are certified to change phase at a specific temperature and have well characterized thermal properties. A lumped system solution for Fick's Second Law as applied for transient heat transfer was used to estimate the amount of PCM required to precool the surface of the Gladi-ATR attachment to 4°C within 15 minutes as well as to maintain the surface temperature of the Gladi-ATR attachment at 4°C for 1hr without considering the contribution of the circulation bath. Samples of PureTemp 4 were acquired from PureTemp LLC (MN, USA). Vacuum sealed bags were filled with amounts of PureTemp 4 necessary to total to 685mL for pre-cooling and 425mL for maintaining the surface temperature during the diffusion studies. Three sets of the vacuum sealed bags were created to allow a quick change between consecutive diffusion studies.

A diagram of the temperature control design is shown in Figure 39. Thermocouple placement is shown on the left, and PCM bag and sample holder placement are shown on the right. The thermocouple next to the sensing window was only placed on the FTIR surface during pre-cooling. During data collection, the thermocouple was removed from the FTIR surface and suspended just above the sample so it would rest in the 3.1M DMSO once added without interfering with the top boundary of the sample throughout the diffusion study.

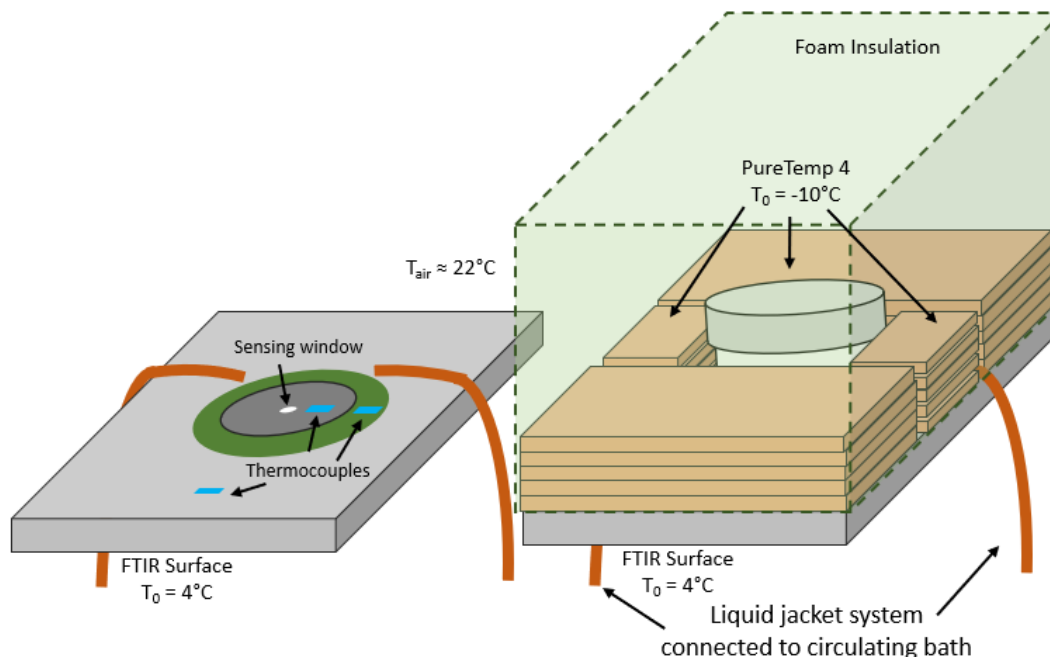


Figure 39 Thermal control design setup for diffusion studies with thermocouple placement (left) and PCM bag placement (right).

The sample holder and vacuum sealed bags of PureTemp 4 were stored in a  $-20^\circ\text{C}$  freezer for at least 2 hours before use. To evaluate the thermal profile of DMSO inside the sample holder and on the surface of the FTIR in two locations for at least one hour, three Type K thermocouples were attached to two Ames Instruments DTT-1372 thermocouple readers purchased from Harbor Freight (CA, USA). Three parallel diffusion studies were performed without collecting diffusion data, to allow monitoring and testing of the thermal control system multiple times for an hour each test. For use during each parallel study, agarose and 3.1M DMSO were prepared and stored in a  $4^\circ\text{C}$  refrigerator until use. The circulation bath was set to  $4^\circ\text{C}$  initially. The set temperature was slowly lowered as needed until the thermocouple placed on the central plate next to the sensing window read  $\sim 8^\circ\text{C}$ . The addition of the vacuum sealed bags of PureTemp 4 totaling 685mL precooled the surface of the FTIR to approximately  $4^\circ\text{C}$ . The circulation bath was never run below  $0^\circ\text{C}$  to prevent condensation and ice buildup on the tubing of the liquid-jacket system which could

allow liquid to leak into the sensing window or the Gladi-ATR attachment. The agarose was quickly weighed and loaded into the sample holder on the FTIR. An amount of 2.5mL of precooled 3.1M DMSO was added before the thermocouple was replaced in the liquid, the lid was quickly secured, and the foam insulation placed around the FTIR surface. The vacuum sealed bags of PureTemp 4 totaling 425mL were placed around the sample chamber prior to the addition of the sample and DMSO. The temperature of the DMSO and the two locations on the surface of the FTIR was recorded every 5 minutes.

An average thermal profile of three parallel diffusion studies is shown in Figure 40. The target temperature of 4°C is shown in green. The average temperature of the DMSO inside the sample holder, shown on the left, remains within a range of 4°C ± 2°C. The temperatures of the front surface of the FTIR and the ringed surface around the sensing window plate equilibrated within 30 minutes to ~10.1°C and ~12.6°C, respectively. Both average temperature profiles are shown on the right.

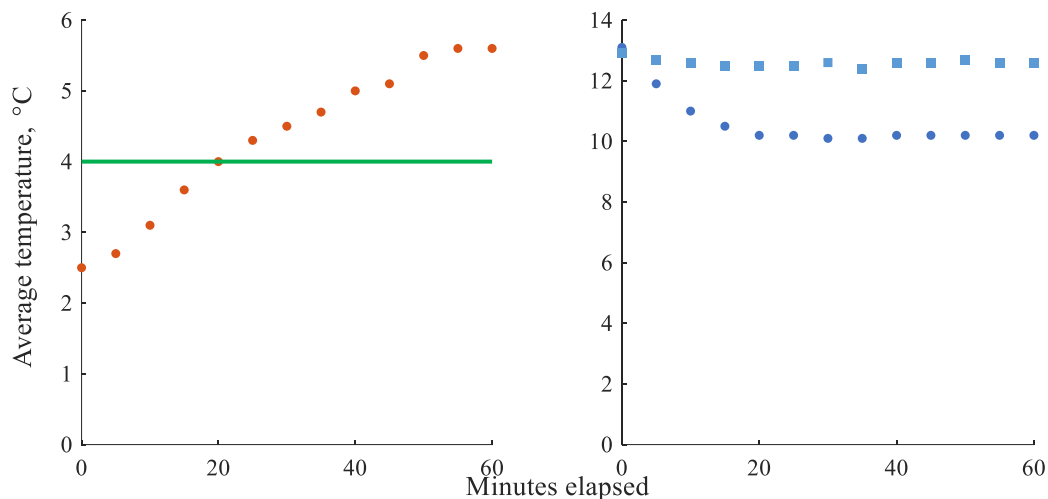


Figure 40 Average thermal profile of DMSO inside sample holder (left) the surface of FTIR (right) of three parallel thermal controlled diffusion studies. In the left figure, the experimental and target temperature values for the DMSO inside the sample holder are presented as orange circles and a green line, respectively. In the right figure, the temperatures for the front surface of the FTIR and the surface of the ring around the sensing window plate are represented by dark blue circles and light blue squares, respectively.

During the thermal studies a fourth thermocouple was added to monitor the temperature of the air inside the insulation. This setup was used to maintain and monitor the temperature of the DMSO and FTIR surface throughout all diffusion studies with temperature control.

## 6.4 Diffusivity measurements using temperature control

### 6.4.1 Estimating temperature dependent effective diffusion coefficient of agarose

Agarose and 3.1M DMSO were prepared and stored in a 4°C refrigerator until use. The circulation bath was set to 4°C initially. The set temperature was slowly lowered as needed until the thermocouple placed on the central plate next to the sensing window read ~8°C. The addition of the vacuum sealed bags of PureTemp 4 totaling 685mL precooled the surface of the FTIR to approximately 4°C. The agarose was quickly weighed and loaded into the sample holder on the FTIR. A volume of 2.5mL of precooled 3.1M DMSO was added before the thermocouple was replaced in the liquid, the lid was quickly secured, and the foam insulation placed around the FTIR

surface. The vacuum sealed bags of PureTemp 4 totaling 425mL were placed around the sample chamber prior to the addition of the sample and DMSO. The temperature of the DMSO, the two locations on the surface of the FTIR, and the air inside the insulation was recorded every 5 minutes throughout each study.

No agarose samples reached equilibrium at 4°C as shown in Figure 41. Thus, all effective diffusion coefficients for agarose were estimated using the 2-parameter estimation program in Excel to determine the effective diffusion coefficient and the equilibrium absorbance value. The thickness for each agarose sample was set to the thickness estimated with the equation based on the metrology measurements and the weight of each sample. The final absorbance value in the diffusion study was used as an initial guess for the equilibrium absorbance value and the diffusion coefficient and equilibrium absorbance values were manually changed in several iterations to reduce the error. The sum of squares and mean square error were used as indicators of fit.

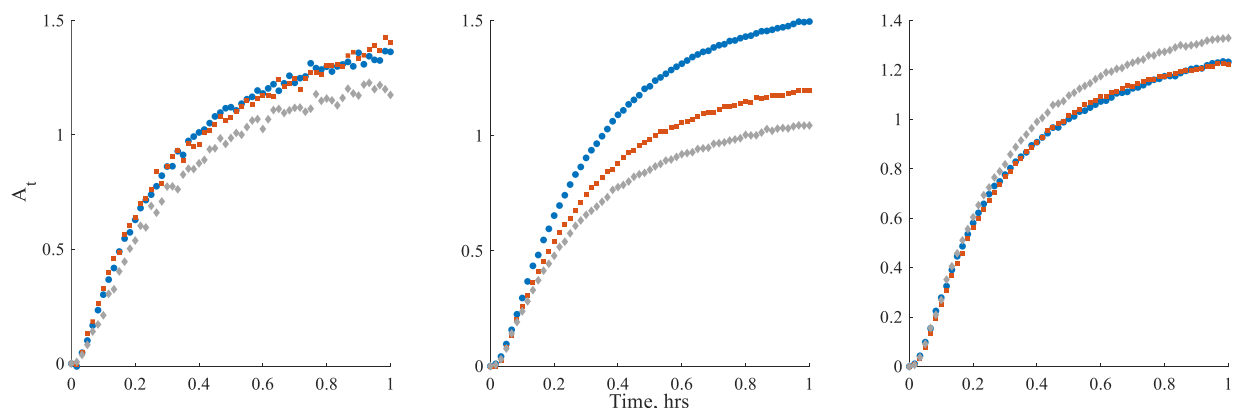


Figure 41 Absorbance as a function of time obtained at 4°C for different agarose samples from the same preparation batch. Batch 1 samples 1 (left), 2 (middle), and 3 (right). The first, second, and third samples in each batch are represented by blue circles, orange squares, and gray diamonds, respectively.

The predicted and experimental absorbance values obtained for agarose batch 1 samples 1, 2, and 3 at 4°C are shown in Figure 42. Though a larger mismatch can be observed for agarose at 4°C than at 22°C, the mismatch remains less than that observed for testicular tissue at 22°C.

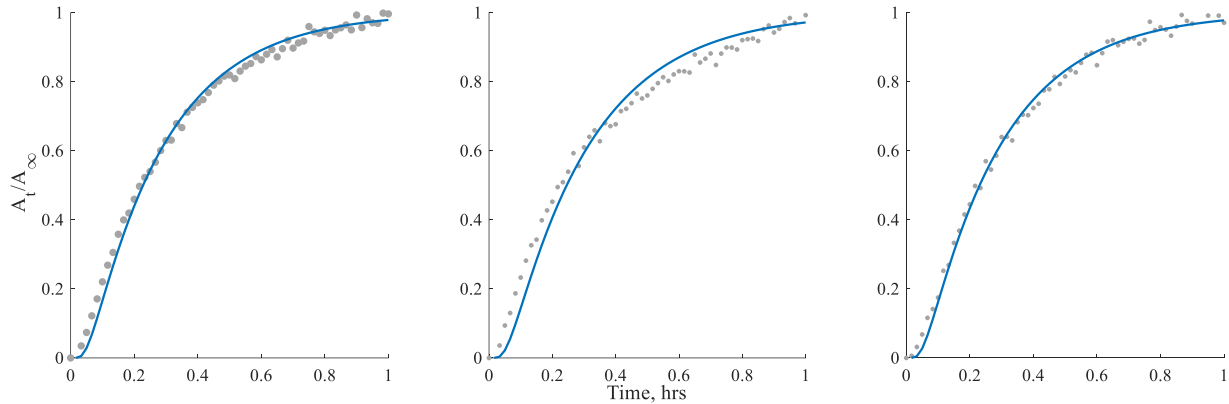


Figure 42 Diffusion coefficient estimation fits obtained at 4°C for agarose batch 1 samples 1 (left), 2 (middle), and 3 (right). Experimental absorbance values are indicated by gray circles, and predicted values are represented by the blue line.

As observed for the agarose fits obtained at 22°C, the absorbance value fits at 4°C have small maximum residual values, as shown in Figure 43. The maximum differences between the experimental and predicted absorbance values only exceed 0.09 in two cases, with a maximum difference of 0.15 when fitting Batch 1 Sample 2 and 0.1 when fitting Batch 3 Sample 1.

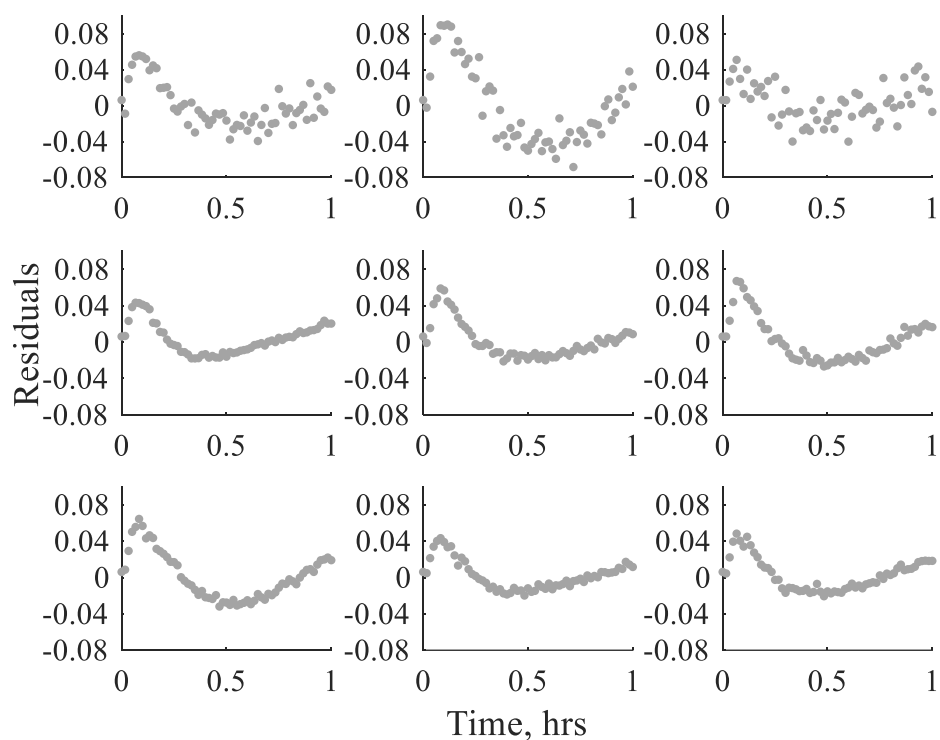


Figure 43 Residual plots for normalized absorbance value generated during estimation of the diffusion coefficient for DMSO in agarose at 4°C. Each row is a different batch, and each column is a different sample within each batch.

The final diffusion coefficients for each sample are summarized in Table 14. The corresponding equilibrium absorbance values, minimum sum of squares, and mean square errors are summarized in Table 24 in the Appendix. At least three iterations were necessary to reach a global minimum in the 2-parameter estimation program.

Table 14 Diffusion coefficients for agarose obtained at 4°C

Sample # \ Batch #	1	2	3	Average	St. Dev.	St. Dev. (%)
1	5.6	5.5	5.8	5.6	0.1	2
2	5.3	5.4	5.6	5.4	0.1	3
3	5.6	5.7	5.7	5.7	0.1	1
<b>Average</b>	5.5	5.6	5.7			
<b>St. Dev.</b>	0.2	0.2	0.1			
<b>St. Dev. (%)</b>	3	3	2			

The average effective diffusion coefficient was  $5.6 \times 10^{-6} \text{ cm}^2/\text{s} \pm 0.2 \text{ cm}^2/\text{s}$  (3% standard deviation). This is nearly double the diffusivity values for DMSO in porcine articular cartilage at 4°C,  $2.6 \times 10^{-6} \text{ cm}^2/\text{s}$  [30], and human articular cartilage,  $3.1 \times 10^{-6} \text{ cm}^2/\text{s}$  [27]. On the other hand, this is close to half the effective diffusion coefficient simulated for human ovarian tissue at 4°C,  $11 \times 10^{-6} \text{ cm}^2/\text{s}$  [28]. While the sum of squares and mean square errors increased from 22°C to 4°C, the only three sum of square error values were greater than 0.05, and 2 of those values were less than 0.07. Similarly, the mean square errors were less than 0.0008 for all replicates except for the three replicates with greater sum of square error values. The mean square error values for those three replicates were still less than 0.004 indicating all fits were very close to the experimental data. All standard deviations were less than 5%, indicating that the thermal control system could be effectively applied for studying the diffusion of CPAs into testicular tissue samples at decreased sample temperature.

Independent two-sided t-tests were conducted using SPSS to compare the average effective diffusion coefficients between batches as well as between replicates within the same batch at 4°C. Equal variances between all batches and a significance value of  $\alpha = 0.05$  were assumed. No significant differences were found between batch 1 and 2 ( $p = 0.675$ ), batch 1 and 3 ( $p = 0.202$ ), or batch 2 and 3 ( $p = 0.296$ ). Equal variances were also assumed between all replicates. No

significant differences were discovered when comparing the averages of the first and second replicates ( $p = 0.166$ ) or first and third replicates ( $p = 0.409$ ). However, a significant difference was found when comparing the averages of the second and third replicates ( $p = 0.045$ ). Validation was performed for agarose absorbance datasets obtained at 4°C as described in Section 4.2.4. The resultant sum of squares and mean square error when using the average effective diffusion coefficients from individual batches to fit all remaining absorbance datasets are summarized in Table 15.

Table 15 Comparison between average effective diffusion coefficients from individual batches and fits with other agarose absorbance data for validation of agarose effective diffusion coefficients at 4°C

Average $D_{\text{eff}}$ Source Batch #	Average $D_{\text{eff}} \times 10^{-6}$ [cm <sup>2</sup> /s]	Fit Batch #	Fit Sample #	SS [x 10 <sup>-2</sup> ]	MSE [x 10 <sup>-4</sup> ]
1	5.5	2	1	4.13	6.89
			2	3.62	6.03
			3	4.80	8.01
		3	1	7.72	12.9
			2	2.54	4.24
			3	3.96	6.59
2	5.6	1	1	6.72	11.2
			2	25.6	42.7
			3	4.35	7.25
		3	1	7.00	1.17
			2	2.41	4.01
			3	4.32	7.20
3	5.7	1	1	6.97	11.6
			2	28.4	47.4
			3	4.35	7.25
		2	1	5.33	8.88
			2	5.01	8.36
			3	3.85	6.42

All sum of squares error values were less than 0.08, and all mean square error values were less than 0.0013 with the exception of two fits. Nevertheless, the fits for batch 1 sample 2 using the

average  $D_{\text{eff}}$  values from batch 2 or from batch 3 had sum of squares errors less than 0.3 and mean square errors less than 0.005. The residuals further exhibit that the average  $D_{\text{eff}}$  values from individual batches fit the remaining absorbance datasets well as can be observed in Figure 44, Figure 45, and Figure 46.

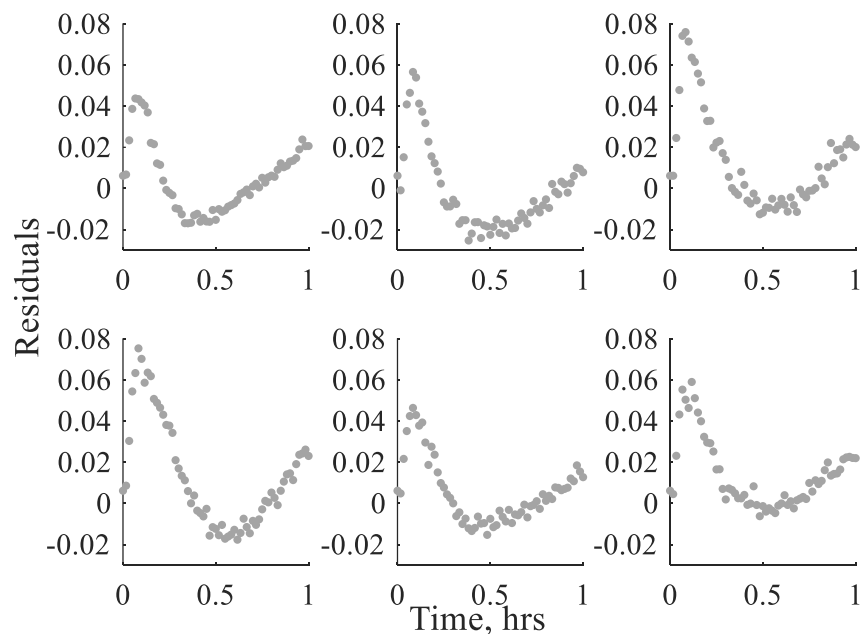


Figure 44 Residual plots for validation of the average effective diffusion coefficient for batch 1 of agarose obtained at 4°C using batches 2 (top row) and 3 (bottom row) absorbance time series. Each column corresponds to a different sample in each batch.

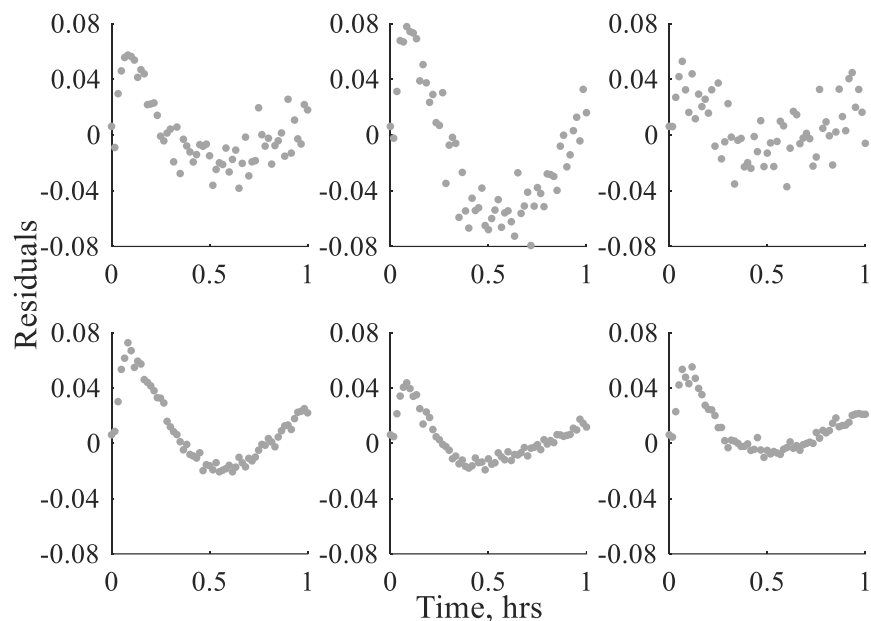


Figure 45 Residual plots for validation of the average effective diffusion coefficient for batch 2 of agarose obtained at 4°C using batches 1 (top row) and 3 (bottom row) absorbance time series. Each column corresponds to a different sample in each batch.

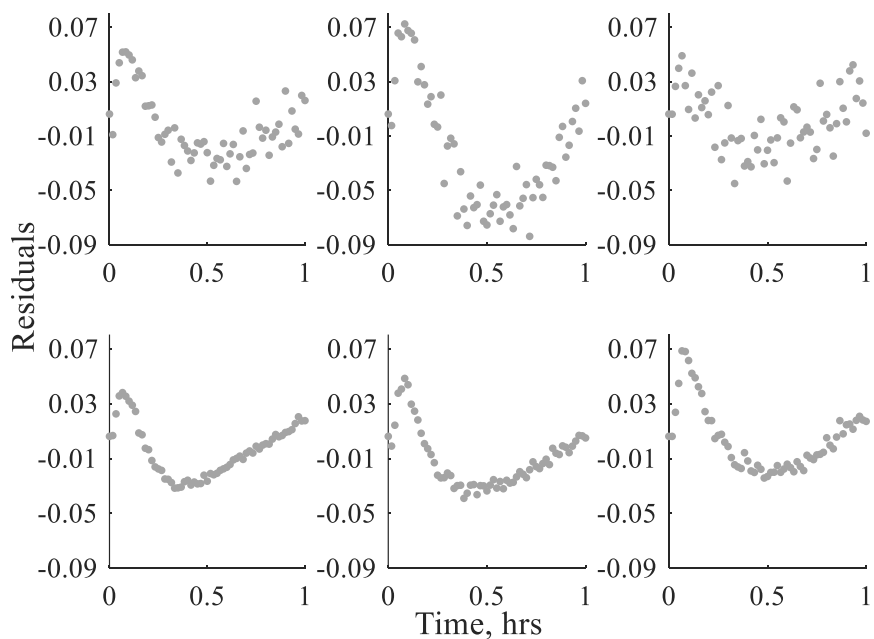


Figure 46 Residual plots for validation of the average effective diffusion coefficient for batch 3 of agarose obtained at 4°C using batches 1 (top row) and 2 (bottom row) absorbance time series. Each column corresponds to a different sample in each batch.

While four of the residual plots had values that exceeded 0.09, only two residual plots had values greater than 0.1. The first maximum difference was 0.1 when fitting batch 1 sample 1 using the average  $D_{\text{eff}}$  values for batch 2 and batch 3. The second maximum difference was 0.15 when fitting batch 1 sample 2 using the average  $D_{\text{eff}}$  values for batch 2 and batch 3. This process was repeated using average diffusion coefficients determined for individual samples to fit all remaining absorbance series as described in Section 4.2.4. The resultant sum of squares and mean squares error values are summarized in Table 16.

Table 16 Comparison between average effective diffusion coefficients from individual samples and fits with other agarose absorbance data for validation of agarose effective diffusion coefficients at 4°C

Average $D_{\text{eff}}$ Source Sample #	Average $D_{\text{eff}} \times 10^{-6}$ [ $\text{cm}^2/\text{s}$ ]	Fitting Sample #	Fitting Batch #	SS [ $\times 10^{-2}$ ]	MSE [ $\times 10^{-4}$ ]
1	5.6	2	1	26.8	44.7
			2	4.32	7.21
			3	2.46	4.10
		3	1	4.25	7.09
			2	4.04	6.73
			3	3.82	6.37
2	5.4	1	1	7.50	12.5
			2	4.38	7.30
			3	8.73	14.5
		3	1	5.21	8.68
			2	5.48	9.13
			3	6.21	10.4
3	5.7	1	1	6.69	11.2
			2	5.44	9.07
			3	6.17	10.3
		2	1	28.7	47.8
			2	5.11	8.52
			3	2.79	4.65

All sum of squares error values were less than 0.09, and all mean square error values were less than 0.0013 with the exception of two fits. Nevertheless, the fits for batch 1 sample 2 using the average  $D_{\text{eff}}$  values from sample 1 or from sample 3 had sum of squares errors less than 0.3 and mean square errors less than 0.005. The residuals for each fit are shown in Figure 47, Figure 48, and Figure 49. While seven fits had maximum differences between the experimental and predicted absorbance values exceeding 0.08, only two of those values were greater than 0.1. The maximum difference was 0.16 when fitting batch 1 sample 2 using either the average  $D_{\text{eff}}$  value for sample 1 across all batches or the average  $D_{\text{eff}}$  value for sample 3 across all batches.

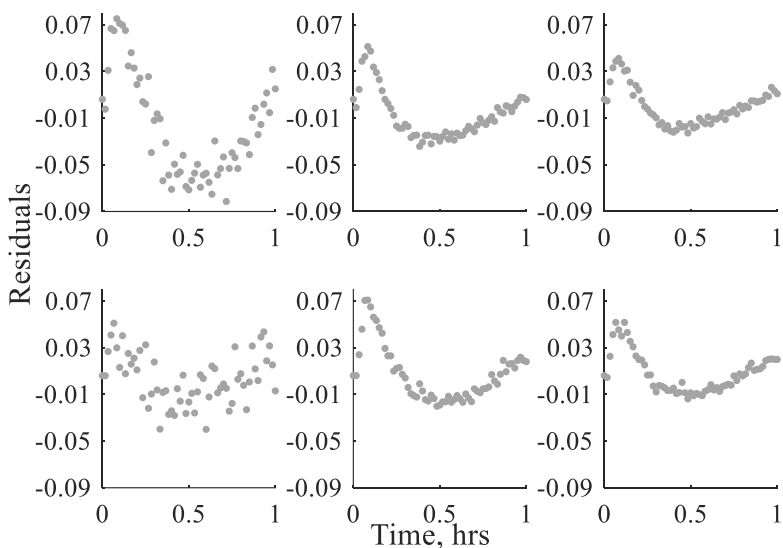


Figure 47 Residual plots for validation of the average effective diffusion coefficient for sample 1 across all batches of agarose obtained at 4°C using the absorbance time series for sample 2 (top row) and 3 (bottom row) across all batches. Each column represents a different batch.

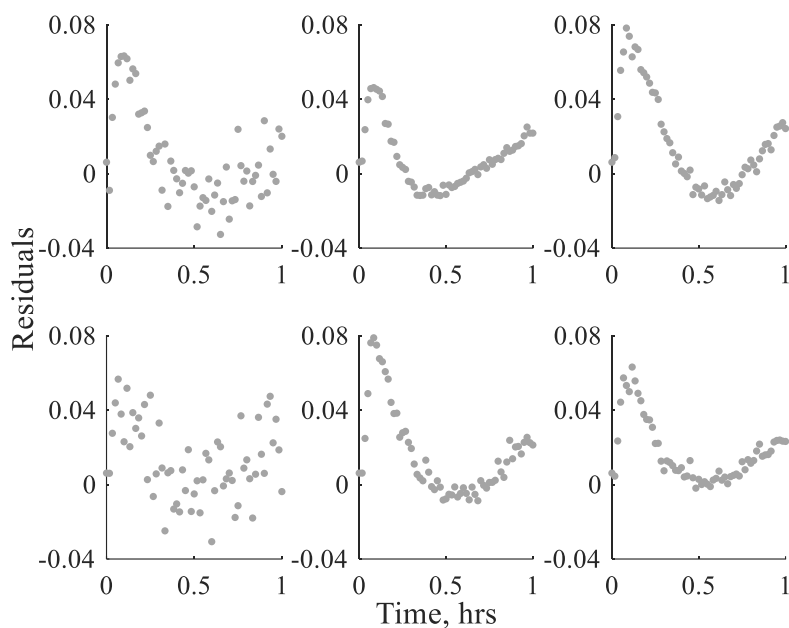


Figure 48 Residual plots for validation of the average effective diffusion coefficient for sample 2 across all batches of agarose obtained at 4°C using the absorbance time series for samples 1 (top row) and 3 (bottom row) across all batches. Each column represents a different batch.

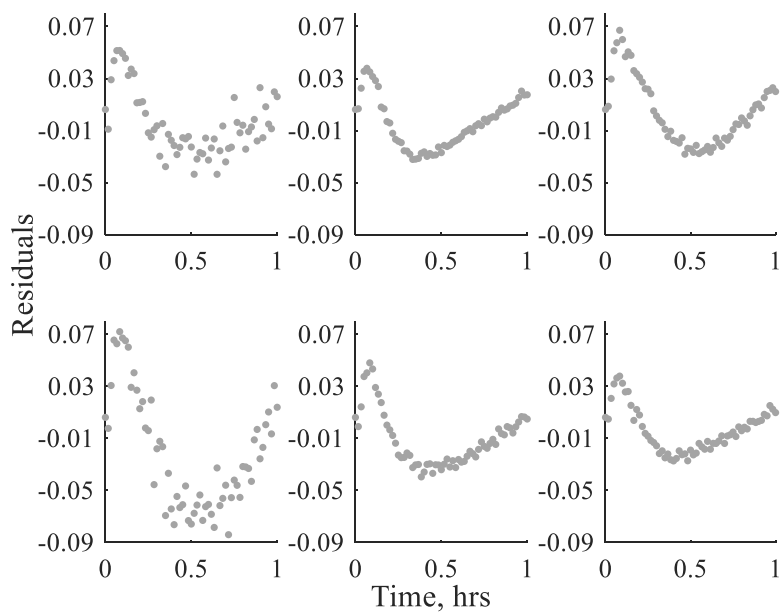


Figure 49 Residual plots for validation of the average effective diffusion coefficient for sample 3 across all batches of agarose obtained at 4°C using the absorbance time series for samples 1 (top row) and 2 (bottom row) across all batches. Each column represents a different batch.

Thus, the average diffusion coefficients from individual batches still fit the remaining absorbance datasets closely and the average effective diffusion coefficient of all nine agarose samples obtained at 4°C can be used as a reference value when applying this methodology in different labs and for different investigators.

#### **6.4.2 Estimating temperature dependent effective diffusion coefficient of testicular tissue**

On each testing day, testicular tissue samples and 3.1M DMSO were prepared and stored in a 4°C refrigerator until use. The circulation bath was set to 4°C initially. The set temperature was slowly lowered as needed until the thermocouple placed on the central plate next to the sensing window read ~8°C. The addition of the vacuum sealed bags of PureTemp 4 totaling 685mL precooled the surface of the FTIR to approximately 4°C. Each testis sample was quickly weighed and loaded into the sample holder on the FTIR. An amount of 2.5mL of precooled 3.1M DMSO was added before the thermocouple was replaced in the liquid, the lid was quickly secured, and the foam insulation placed around the FTIR surface. The vacuum sealed bags of PureTemp 4 totaling 425mL were placed around the sample chamber prior to the addition of the sample and DMSO. The temperature of the DMSO, the two locations on the surface of the FTIR, and the air inside the insulation was recorded every 5 minutes throughout each study.

No testicular tissues reached equilibrium at 4°C as shown in Figure 50. Thus,  $D_{\text{eff}}$  values for testicular tissue were obtained using the 2-parameter estimation program in Excel to determine the effective diffusion coefficient and the equilibrium absorbance value. The thickness was calculated using the equation from the ATOS Scanbox results and the weight of the testis sample. The final absorbance value in the diffusion study was used as an initial guess for the equilibrium absorbance value and the diffusion coefficient and equilibrium absorbance values were manually changed in

several iterations to reduce the error. The sum of squares and mean square error were used as indicators of fit.

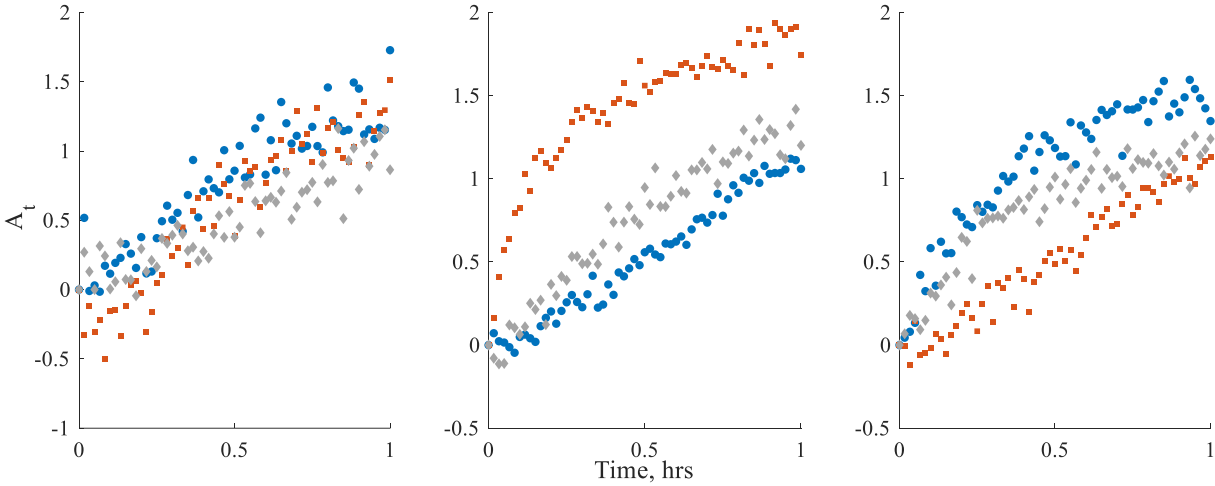


Figure 50 Absorbance as a function of time obtained at 4°C for testicular tissue days 1 (left), 2 (middle), and 3 (right). The first, second, and third sample each day are represented by blue circles, orange squares, and gray diamonds, respectively.

The predicted and experimental absorbance values for day 1 samples 1, 2, and 3 of testicular tissues obtained at 4°C are shown in Figure 51. While some scatter in absorbance values over time was observed for testicular tissue at 22°C, the scatter greatly increases at 4°C. As such, though the predicted values from the model by Fieldson and Barbari (1995) are centered in the scatter, the fits still show large mismatch to the experimental absorbance values.

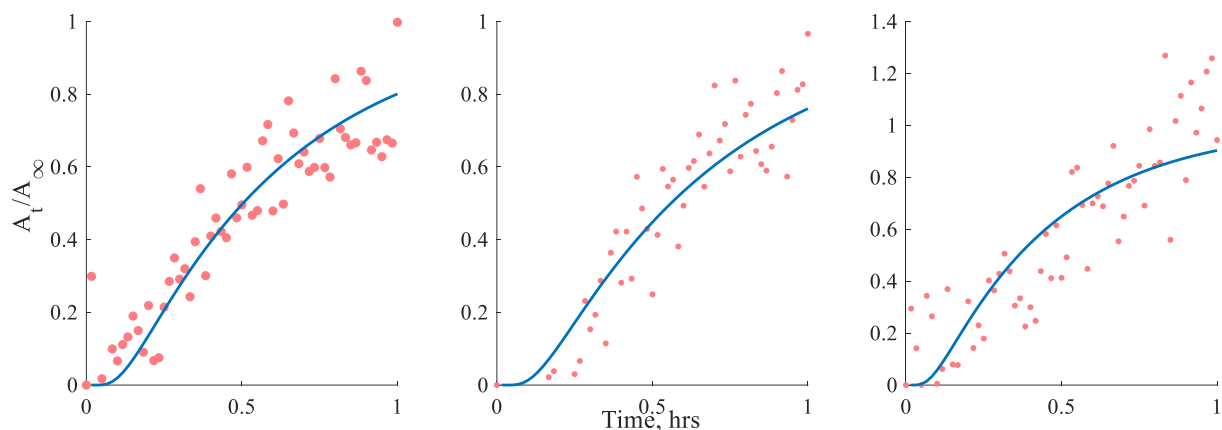


Figure 51 Diffusion coefficient estimation fits obtained at 4°C for testicular tissue collection day 1 samples 1 (left), 2 (middle), and 3 (right). Experimental absorbance values are indicated by pink circles, and predicted values are represented by the blue line.

The final diffusion coefficients for each sample are summarized in Table 17. The  $D_{\text{eff}}$  values are organized by day and sample, with each day constituting a fresh batch of testes. The corresponding equilibrium absorbance values, minimum sum of squares, and mean square errors are summarized in Table 25 in the Appendix. At least three iterations were necessary to reach a global minimum in the 2-parameter estimation program.

Table 17 Diffusion coefficients for testicular tissue obtained at 4°C for three separate days

Sample # \ Day #	1	2	3
1	5	3	16
2	4	21	3
3	6	7	11
<b>Average</b>	5	10	10
<b>St. Dev.</b>	1	9	7
<b>St. Dev. (%)</b>	20	91	66

The average effective diffusion coefficient was  $8 \pm 6 \text{ cm}^2/\text{s}$  (75% standard deviation). The diffusivity values for DMSO in porcine articular cartilage at 4°C,  $2.6 \times 10^{-6} \text{ cm}^2/\text{s}$  [30], and human

articular cartilage,  $3.1 \times 10^{-6} \text{ cm}^2/\text{s}$  [27], are less than half that of the testicular tissue diffusion coefficient. Nevertheless, the  $D_{\text{eff}}$  for testicular tissue is still less than that simulated for human ovarian tissue at  $4^\circ\text{C}$ ,  $11 \times 10^{-6} \text{ cm}^2/\text{s}$  [28]. As was observed at room temperature, the variation in the effective diffusion coefficient was greater than for agarose. However, the sample-to-sample variation is greater for the  $4^\circ\text{C}$  diffusion coefficient than for the  $22^\circ\text{C}$  diffusion coefficient for testicular tissues.

Independent two-sided t-tests were conducted using SPSS to compare the average effective diffusion coefficients between collection days. A significance value of  $\alpha = 0.05$  was used. Equal variances were assumed when comparing between collection days 1 and 3 as well as 2 and 3. However, equal variances were not assumed when comparing between collection days 1 and 2. No significant differences were found when comparing between collection days 1 and 2 ( $p = 0.438$ ), days 1 and 3 ( $p = 0.237$ ), or days 2 and 3 ( $p = 0.981$ ). The residuals for all nine fits are plotted in Figure 52. While the residuals exhibit greater scatter around zero, a similar pattern to that observed for absorbance data fits obtained at  $22^\circ\text{C}$  can be noted. Though only one maximum difference between the experimental and predicted absorbance values exceeds 0.5 at a value of 0.7 when fitting collection day 1 sample 3, with most maximum difference values remaining less than 0.4.

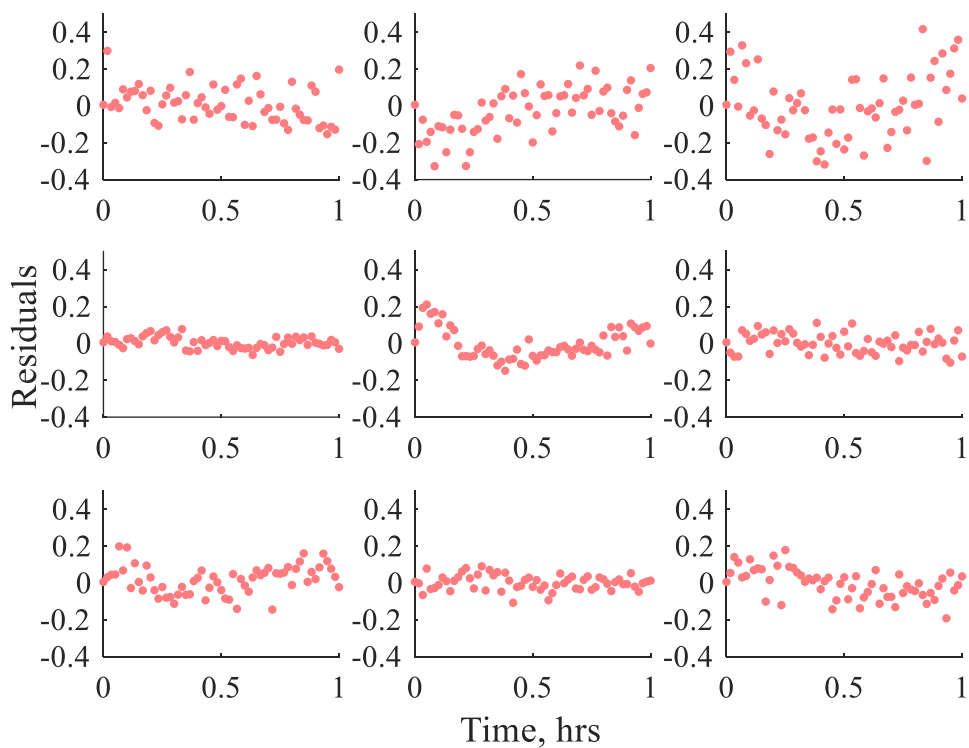


Figure 52 Residual plots for normalized absorbance value generated during estimation of the diffusion coefficient for DMSO in testicular tissue at 4°C. Each row is a different collection day, and each column is a different sample for each collection day.

Validation was also performed on testicular tissue absorbance series obtained at 4°C as described in Section 5.3.1. The sum of squares and mean square error values are summarized in Table 18.

Table 18 Comparison between average effective diffusion coefficients from individual collection days and fits with other testicular tissue absorbance data for validation of effective diffusion coefficients at 4°C

Average $D_{\text{eff}}$ Source Batch #	Average $D_{\text{eff}} \times 10^{-6}$ [cm <sup>2</sup> /s]	Fitting Day #	Fitting Sample #	SS	MSE [x 10 <sup>-2</sup> ]
1	5	2	1	6.19	10.3
			2	33.4	55.7
			3	2.07	3.45
		3	1	18.0	30.0
			2	4.93	8.21
			3	7.65	12.8
2	10	1	1	13.5	22.5
			2	18.9	31.5
			3	3.65	6.09
		3	1	2.68	4.46
			2	33.67	56.1
			3	0.654	1.09
3	10	1	1	13.0	21.7
			2	18.4	30.6
			3	3.54	5.91
		2	1	35.5	59.2
			2	7.74	12.9
			3	3.78	6.30

The sum of squares error ranged from 0.654 to 35.5 for each fit. This pattern is further reflected in mean square error with values from 0.011 to 0.592. Figure 53 shows that the trend for overestimation and underestimation of the effective diffusion coefficients for some of the individual samples observed at room temperature continues at 4°C with increased variability as expected with the larger standard deviation for the  $D_{\text{eff}}$  values of all nine testicular tissue samples.

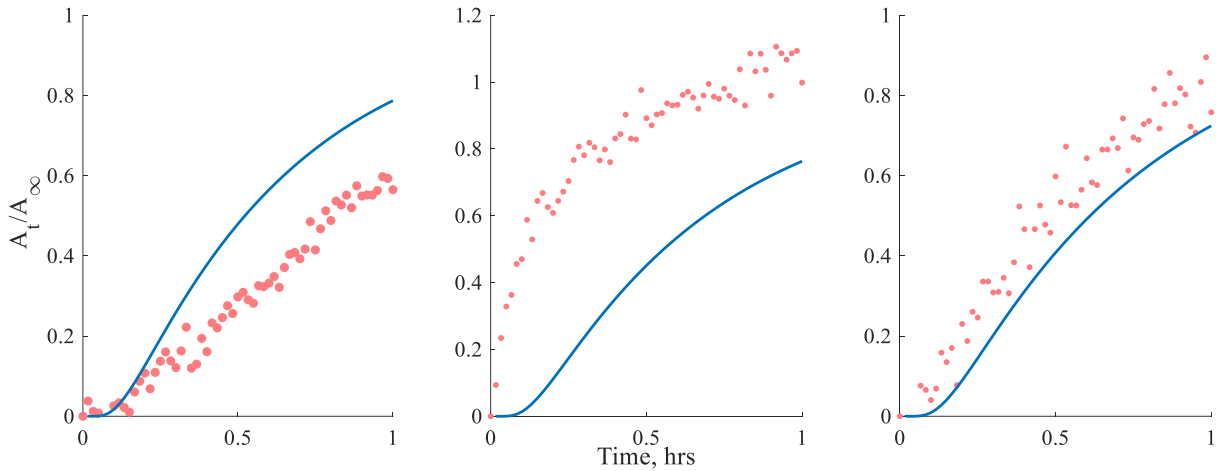


Figure 53 Absorbance data for testicular tissue collection day 2 samples 1 (left), 2 (middle), and 3 (right) fit using the average effective diffusion coefficient from collection day 1. Experimental values are indicated by pink circles and predicted values are represented by the blue line.

The residual plots for validation of the average effective diffusion coefficients for each collection day are shown in Figure 54, Figure 55, and Figure 56. Instead of the pattern of overestimating the initial absorbance values and overestimating the absorbance values after 15 minutes for each time series, average diffusion coefficients for each collection day tend to overestimate or underestimate entire absorbance series. When fitting the absorbance data series for collection day 2 and 3 using the average diffusion coefficient from collection day 1, the predicted absorbance values are larger than the experimental for four out of the six samples. However, when using either to the average  $D_{\text{eff}}$  from collection day 2 to fit the absorbance time series from collection days 1 and 3 or the average  $D_{\text{eff}}$  from collection day 3 to fit the absorbance time series from collection days 1 and 2, the predicted absorbance values for four of the six samples are underestimated.

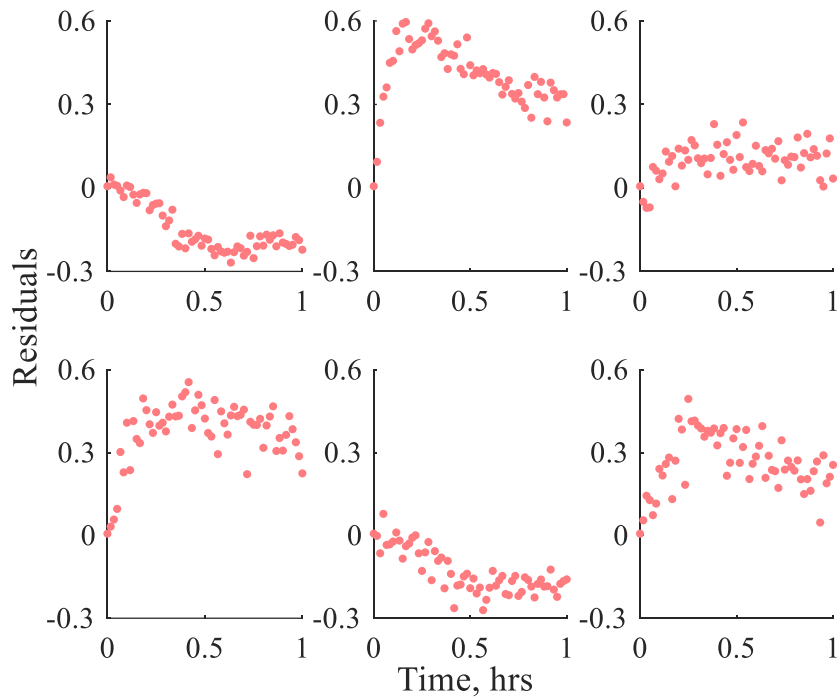


Figure 54 Residual plots for validation of the average effective diffusion coefficient for collection day 1 of testicular tissue obtained at 4°C using batches 2 (top row) and 3 (bottom row) absorbance time series. Each column corresponds to a different sample on each collection day.

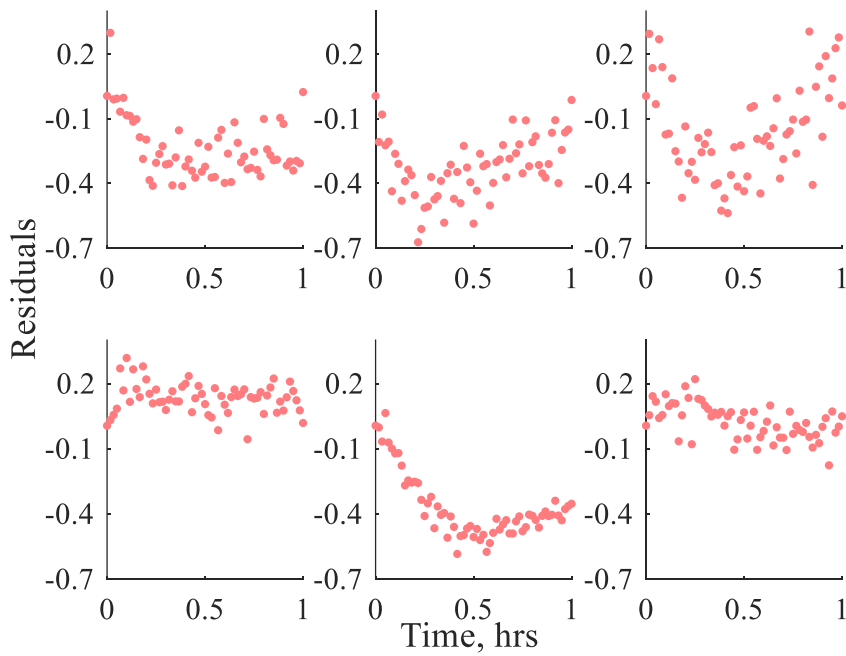


Figure 55 Residual plots for validation of the average effective diffusion coefficient for collection day 2 of testicular tissue obtained at 4°C using batches 1 (top row) and 3 (bottom row) absorbance time series. Each column corresponds to a different sample on each collection day.

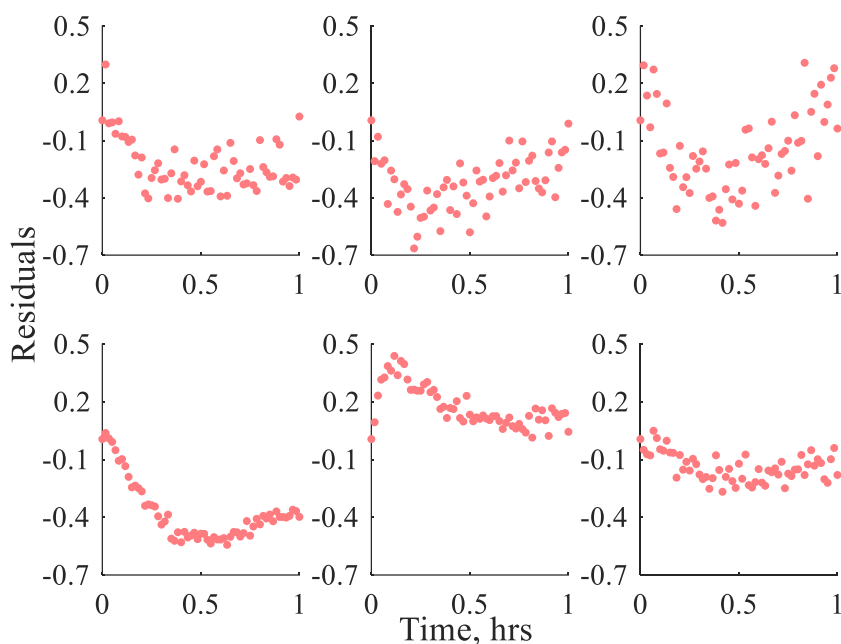


Figure 56 Residual plots for validation of the average effective diffusion coefficient for collection day 3 of testicular tissue obtained at 4°C using batches 1 (top row) and 2 (bottom row) absorbance time series. Each column corresponds to a different sample on each collection day.

If the average diffusion coefficient and average  $A_{\infty}$  for all nine testicular tissue samples at 4°C are used, the estimated time required for a 2mm thick testicular tissue sample to reach equilibrium is 5 hours and 10 minutes. The results from repeating the calculations to estimate the time required for testicular tissue slices to reach equilibrium from Section 5.3.1 using the  $D_{\text{eff}}$  and  $A_{\infty}$  values obtained at 4°C are summarized in Table 19. While the estimated times at the greatest possible diffusion coefficient are comparable to those at 22°C, the times necessary to reach equilibrium at the lower temperature for the average  $D_{\text{eff}}$  and  $A_{\infty}$  increase by at least half an hour even at a tissue thickness of 1.3mm. Even assuming the smallest equilibrium absorbance and greatest effective diffusion coefficient, the equilibration time required for a 5mm thickness only decreases by 5 minutes to 18 hours and 15 minutes.

Table 19 Estimated required time to reach equilibrium for testicular tissue at 4°C

Thickness, mm	$D_{\text{eff}} = 2 \text{ cm}^2/\text{s}$ $A_{\infty} = 1.227$	$D_{\text{eff}} = 8 \text{ cm}^2/\text{s}$ $A_{\infty} = 1.547$	$D_{\text{eff}} = 14 \text{ cm}^2/\text{s}$ $A_{\infty} = 1.867$
1.3	8 hrs 41 min	2 hrs 10 min	1 hr 15 min
2	20 hrs 26 min	5 hrs 10 min	2 hrs 56 min
2.7	37 hrs 11 min	9 hrs 20 min	5 hrs 20 min
5	5 days 7 hrs 30 min	31 hrs 50 min	18 hrs 20 min

### 6.4.3 Refinement of thermal monitoring system to support improvements in temperature control

Commercial type K thermocouples were used in the thermal control system for preliminary FTIR tests. While the thermocouples were insulated, they consisted of large wires which may increase fin effects experienced during diffusion studies. A 2635A Hydra Series II Data Bucket (Fluke Corporation, WA, USA) with T-type thermocouples was used to simulate three diffusion studies while monitoring the system temperatures with thinner thermocouples to reduce fin effects. Temperatures for two locations on the surface of the FTIR, the DMSO inside the chamber, and the contact point between the sensing window and the sample inside the DMSO were monitored for the parallel diffusion studies to better characterize the thermal profile of the system. The change in thermocouple placement from the original placement illustrated in Figure 39 is detailed in the diagram in Figure 57.

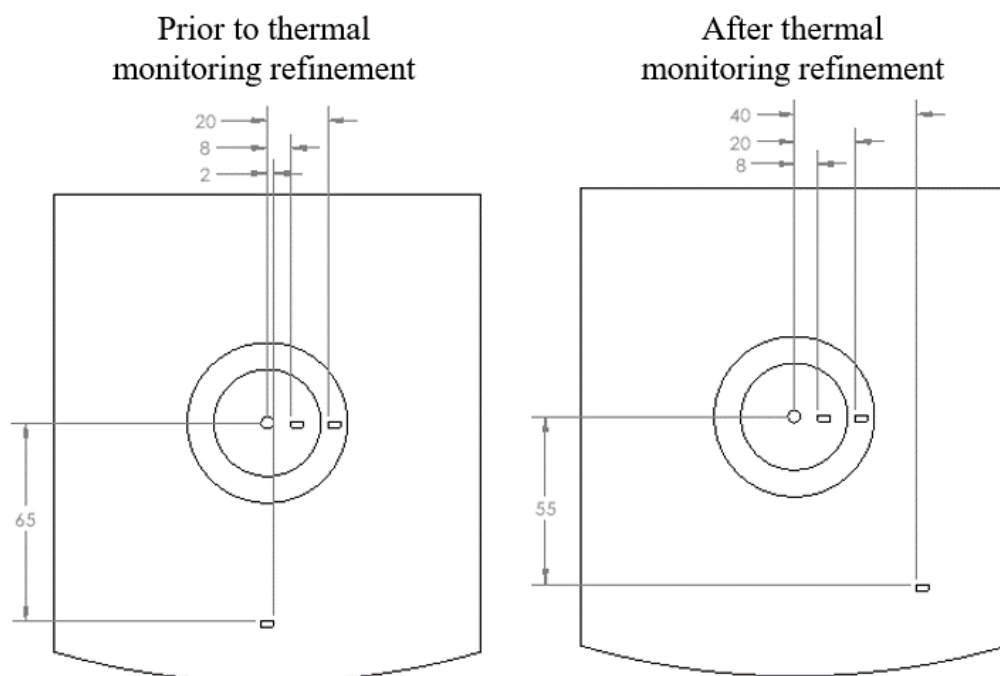


Figure 57 Thermal control design setup modification for diffusion studies with revised thermocouple placement. The original thermocouple placement (left) was modified for the refined monitoring system (right) to minimize the contribution of the PCM bags to the temperature registered by the thermocouple compared to the surface of the FTIR.

The three parallel diffusion studies to test the thermal monitoring system described in Section \_\_\_ were repeated using the modified thermocouple placement and T-type thermocouple. A fourth T-type thermocouple was placed in the DMSO just after it was added inside the sample holder to monitor the temperature of the DMSO throughout each test. The temperature of the DMSO and the three locations on the surface of the FTIR was again recorded every 5 minutes. The thermal profile for DMSO inside the sample holder and the contact point between the sample and the FTIR surface obtained using T-type thermocouples for the three parallel temperature-controlled diffusion studies is shown in Figure 58. The average profile for each measurement is indicated by purple triangle markers, and the target temperature is marked in green. The system remained within a temperature range of  $4^{\circ}\text{C} \pm 4^{\circ}\text{C}$ .

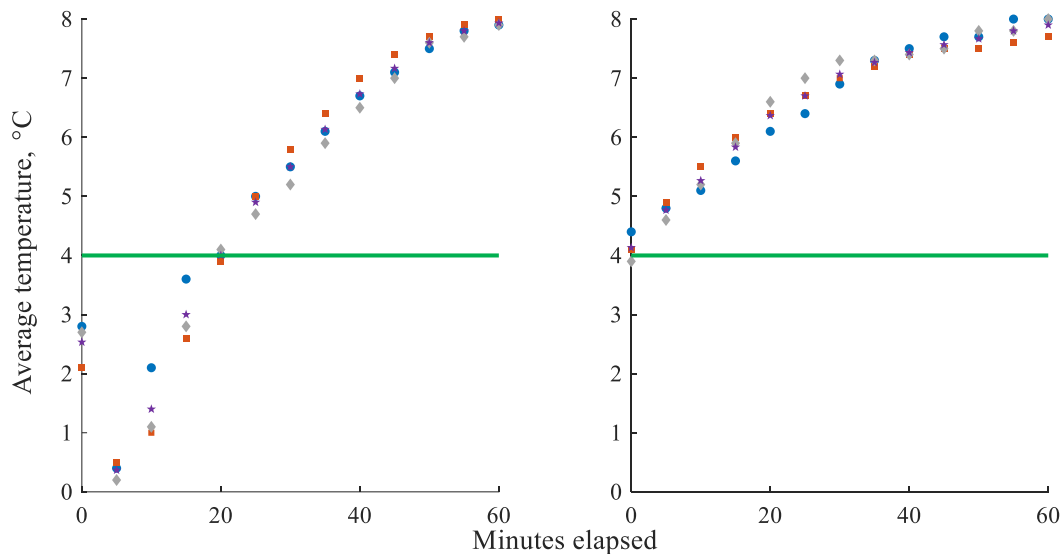


Figure 58 Thermal profile for DMSO inside the sample holder (left) and the contact point between the sample and the FTIR surface (right) obtained using T-type thermocouples for three parallel temperature-controlled diffusion studies and corresponding average profiles. The values for the first, second, and third studies are presented as blue circles, and orange squares, gray diamonds, respectively. The average values are represented by purple stars and the target temperatures for the sample and DMSO are represented by a green line.

While temperatures range around the desired temperature of 4°C for the sample, refinement of the thermal control system is necessary. The vacuum sealed bags did not facilitate wrapping of the bags around the sample holder while maintaining sufficient contact with the FTIR surface, thus, did not perform as expected. Revision of the packaging for the PCM could provide better resistance to warming from the air surrounding the system. Similarly, while the tubing from the circulation bath was also insulated, improvement of the insulation may reduce the effect of any heating from the air around the tubing as coolant travels to and from the sample holder to reduce any fluctuations in temperature which may be experienced during data collection.

## **CHAPTER 7 OVERALL ASSESSMENT OF RESEARCH OUTCOMES**

### **7.1 Choice of reference standard for diffusion studies**

Preservation of testicular tissue is desirable for prepubescent males undergoing treatments such as radiation therapy which can result in sterilization. While diffusion and toxicity models [6-8] can be used to determine recommended CPA concentrations for faster loading and unloading and improve preservation outcomes, these models rely on known diffusion coefficients as inputs. Determination of the diffusion coefficient for CPAs, such as DMSO, in testicular tissue is complicated by tissue geometry, cellular make-up of the tissue, density, and environmental temperature. A reference standard with properties similar to live tissue which can be fabricated efficiently and repeatedly would allow sources of error to be identified and accounted for during development of methodology to determine CPA diffusion coefficients in tissues and transfer of technology between investigators without introducing the complications inherent in tissue. Thus, alginate-gelatin and agarose were evaluated as candidate reference materials for diffusion studies utilizing FTIR as described by Fieldson and Barbari [10, 11].

Thickness of a sample is an essential input to determine the diffusion coefficient of DMSO in each candidate reference material. Thus, an ATOS Scanbox was used to estimate the thickness of an alginate-gelatin batch and an agarose batch before and after packing into a custom sample holder designed for use during diffusion studies. Subsequent batches were used to determine the diffusion coefficient of DMSO in each material, assuming thicknesses based on an equation obtained using the ATOS Scanbox thickness estimations. The thicknesses for sodium alginate-gelatin and agarose are summarized in Table 20. The effective diffusion coefficients and equilibrium absorbance values determined at room temperature and 4°C for each material are also included. As expected, the effective mass diffusion coefficients for agarose decrease with temperature.

Table 20 Thickness and effective diffusion coefficient and equilibrium absorbance values for sodium alginate-gelatin and agarose 22°C and 4°C

	Thickness, mm	$D_{\text{eff}} \times 10^{-6}$ [cm <sup>2</sup> /s]		$A_{\infty}$	
		22°C	4°C	22°C	4°C
SA-gel	1.7 ± 0.2	4.3 ± 0.3		0.07 ± 0.01	
Agarose	1.1 ± 0.1	9.2 ± 0.2	5.58 ± 0.15	1.38 ± 0.01	1.28 ± 0.13

While the variation in thickness was similar for the alginate-gelatin (12.9%) to that of agarose (12.8%), alginate-gelatin could not be prepared as thinly as samples of agarose. In addition, the use of the precision slicer for the agarose allows the thickness to be changed as desired, but the thickness of the alginate-gelatin samples is limited to the depth of the casting wells used. While there was more variation than expected in the estimated thicknesses after packing for both alginate-gelatin and agarose, the estimated effective diffusion coefficients showed low variability.

While diffusion coefficients for DMSO in alginate or agarose are not available in the literature for comparison, Scott, Woodward, and Thompson (1989) used modified sorption methods to determine the  $D_{\text{eff}}$  for glucose in alginate beads with nominal diameters of 2mm at 30°C [84]. Values of 6.6, 5.5 and 5.0 x 10<sup>-6</sup> cm<sup>2</sup>/s were determined for beads of 1%, 2%, and 3% weight/volume with reported standard deviation of 0.3 x 10<sup>-6</sup> cm<sup>2</sup>/s (4.5, 5.5, and 6.0% standard deviations, respectively). Scott, Woodward, and Thompson (1990) proposed that the increasing standard deviations were due to changes in the pore structure and composition of the alginate samples as the wt% of the alginate increased. Thus, the greater standard deviation for the alginate-gelatin obtained in this dissertation (7%) is to be expected as 20 wt% alginate was used in the formation of the alginate-gelatin samples for this work.

Similarly, Mignot and Junter (1990) studied diffusion of glucose through agar membranes at 37°C [85]. The membranes were fixed between a reservoir of glucose solution and a reservoir of distilled water. Small samples were removed at set time points from the distilled water reservoir to measure

the amount of glucose which had diffused through the membrane. The glucose concentration was plotted over time and a logarithmic solution to Fick's second law was fit to the data to determine the diffusion coefficient. The effective diffusion coefficient was reported as  $5.45 \times 10^{-6} \text{ cm}^2/\text{s}$  through an agar membrane without cells encapsulated. However, Mignot and Junter (1990) only reported the results from one free membrane, thus no indicators of variation were reported. Nevertheless, the values determined in this work for DMSO in alginate-gelatin and agarose are in the same range as the reported values listed above and displayed in Figure 59.

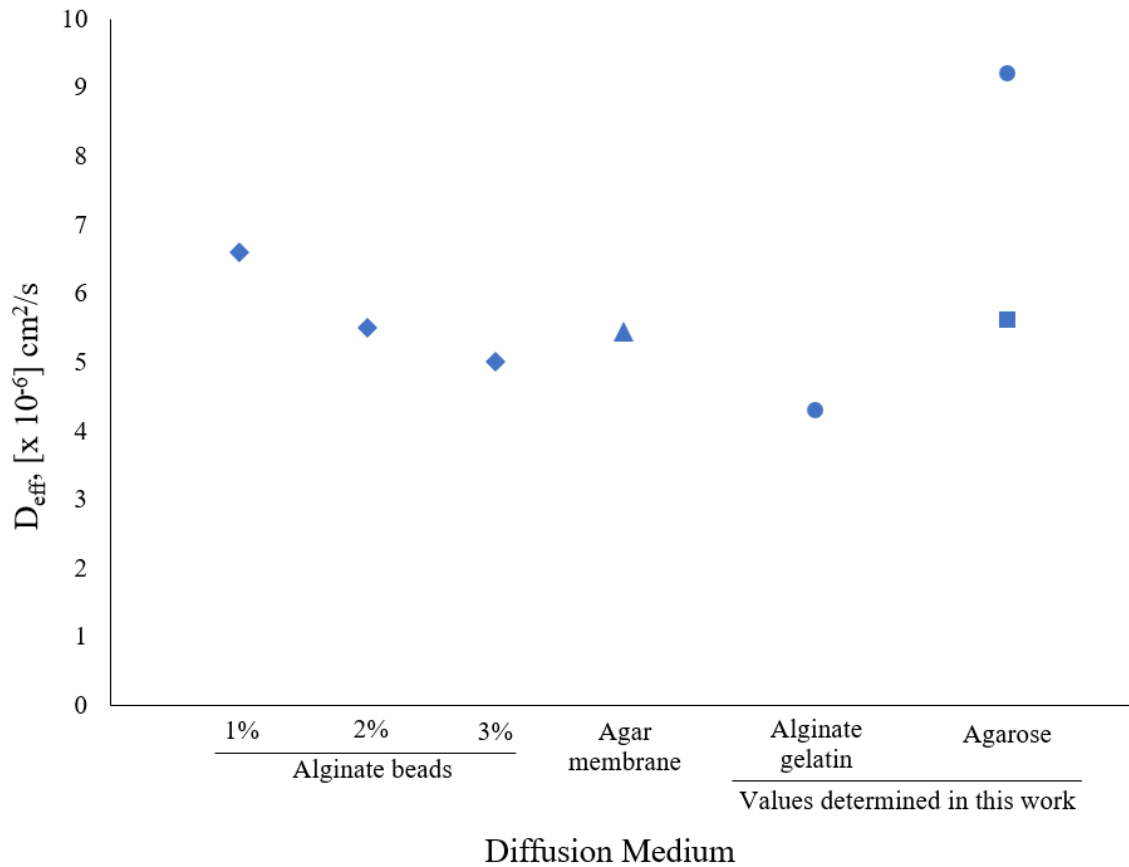


Figure 59 Effective diffusion coefficients for glucose or DMSO in different diffusion mediums. Values in alginate beads and agar membranes were determined for glucose at 30°C (diamond) and 37°C (triangle). Values in alginate-gelatin and agarose were determined for DMSO at 22°C (circle) and 4°C (square).

The small variabilities (< 5%) observed for the  $D_{\text{eff}}$  values of DMSO in agarose indicate that any sources of error from methodology and the material were minimized. In addition, no significant differences in average  $D_{\text{eff}}$  values were found when comparing between batches as well as between individual samples within the same batch using independent two-sample t-tests with one exception in the 4°C  $D_{\text{eff}}$  values. The only significant difference when using a significance value of  $\alpha = 0.05$  was determined to be between the average  $D_{\text{eff}}$  of the second and third replicates with a p-value just less than 0.05 ( $p = 0.045$ ). Furthermore, validation of the estimated effective diffusion coefficients for DMSO in agarose at 22°C and 4°C both indicated that any of the obtained  $D_{\text{eff}}$  values would result in a sufficient fit to the absorbance data series. As such, the pooled average effective diffusion coefficients of all nine samples at each temperature can be used as comparison values for diffusion studies when transferring technology between labs and between investigators. This is beneficial to ensure that any remaining variability that might be observed when studying diffusion in biological tissues is inherent to the tissue samples themselves. As such, agarose is the preferred reference material for ATR-FTIR diffusion studies using DMSO.

## **7.2 Development of temperature-controlled CPA delivery system**

While CPAs are often loaded at low temperatures, which decreases the rate of diffusion into tissues, the current holders for exposing tissues to CPAs using FTIR do not allow control of the loading temperature. Thus, development of a container which maintains a 1-dimensional diffusion environment while permitting temperature control throughout diffusion studies is necessary to study the relationship between CPA diffusion in tissues and sample temperature, which in turn will support CPA loading optimization efforts. A CPA delivery sample holder was machined out of acetal with an aluminum lid. The sample holder was designed to allow the introduction of a large amount of CPA to the top of samples during diffusion studies. The sample holder consisted of two

pieces, a ring and a ring cover. A series of rings were also machined from acetal with different inner diameters to accommodate samples of different sizes. Rings with inner diameters of 8mm, 7.4mm, and 6mm were used for alginate-gelatin, agarose, and testicular tissue samples, respectively. Compaction of samples into the sample chamber prevented leaking of CPA around the edges of samples and maintained a 1-D diffusion environment throughout diffusion studies. Images of the sample holder ring and the ring cover are shown in Figure 60.



Figure 60 Sample holder ring and cover and sample holder lid machined from acetal and aluminum, respectively.

A thermal system was designed using an existing “liquid-jacket” system manufactured by Pike Technologies connected to a cooling bath circulating 60% ethylene glycol beneath the FTIR surface and circling the sensing window. Bags of phase change materials were added around the sample holder to minimize heat transfer from the environment into the FTIR surface. Three parallel diffusion studies were performed without collecting absorbance data while using T-type thermocouples to minimize fin effects experienced by the thermocouples. The average thermal profile of the three diffusion studies utilizing the refined thermal monitoring system is shown on the left in Figure 61. The target temperature of 4°C is shown in green. The average temperature of

the DMSO inside the sample holder, shown in orange on the left, remains within a range of  $4^{\circ}\text{C} \pm 4^{\circ}\text{C}$ . However, the average temperature at the contact point between the sample and the sensing window, shown in purple on the left, remains within a range of  $6^{\circ}\text{C} \pm 2^{\circ}\text{C}$ . The temperatures of the front surface of the FTIR and the ringed surface around the sensing window plate remained at temperatures within  $10.6^{\circ}\text{C} \pm 0.3^{\circ}\text{C}$  and  $16.4^{\circ}\text{C} \pm 0.2^{\circ}\text{C}$ , respectively, for the entire hour. Both average temperature profiles are shown on the right of Figure 61.

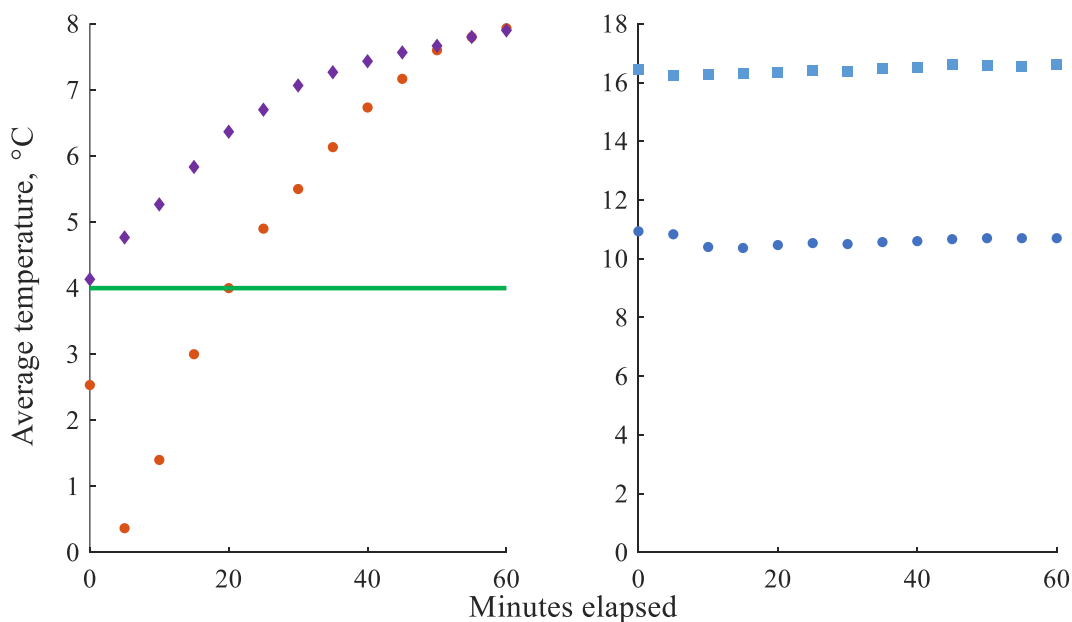


Figure 61 Average thermal profile of DMSO inside sample holder and contact point between sample and sensing window (left), and average thermal profile of the surface of FTIR (right) of three parallel thermal controlled diffusion studies. In the left figure, the experimental temperature values for the DMSO inside the sample holder and the contact point between the sample and the sensing window are presented as orange circles and purple diamonds, respectively. The target temperature for the DMSO and the sample is represented by a green line. In the right figure, the temperatures for the front surface of the FTIR and the surface of the ring around the sensing window plate are represented by dark blue circles and light blue squares, respectively.

While the DMSO remains within a small range of temperature centered around  $4^{\circ}\text{C}$ , the bags of phase change materials did not aid in maintaining the temperature at  $4^{\circ}\text{C}$  as well as expected.

The bags did not easily bend to wrap around the chamber while maintaining sufficient contact

with the FTIR surface. Thus, refinement of the container for the phase change materials is necessary to increase their effectiveness.

### **7.3 Determination of the temperature-dependent diffusion coefficient for testicular tissue**

Models which allow the prediction of viability outcomes of different loading conditions were developed to maximize the success of tissue cryopreservation procedures [6, 8]. However, reliable inputs, including mass diffusion coefficients, are required to allow application of these models to soft tissues, such as testicular tissue. While diffusion coefficients have been successfully identified for DMSO in reproductive tissues such as porcine and human ovarian tissue, the transport properties for DMSO in testicular tissue were unknown. To apply the models presented by Benson et al. (2018), methodology to measure diffusion of DMSO in testicular tissue at multiple temperatures was developed in this dissertation. In turn, this will expedite the identification of optimal loading conditions for DMSO in testicular tissue to minimize toxicity.

As with alginate-gelatin and agarose samples, the ATOS Scanbox was used to estimate the thickness of a batch of testicular tissues slices before and after packing in the sample holder. The thicknesses of samples from subsequent batches of testes, which were used in diffusion studies, were calculated based on these estimations and used as inputs during prediction of the diffusion coefficients. The thicknesses for testicular tissue are summarized in Table 21. The effective diffusion coefficients and equilibrium absorbance values determined at room temperature and 4°C are included as well.

Table 21 Thickness and effective diffusion coefficient and equilibrium absorbance values for testicular tissue at 22°C and 4°C

	Thickness, mm	$D_{\text{eff}} \times 10^{-6}$ [cm <sup>2</sup> /s]		$A_{\infty}$	
		22°C	4°C	22°C	4°C
TT	2.1 ± 0.7	11 ± 3	8 ± 6	1.96 ± 0.53	1.55 ± 0.

While testicular tissues could be sliced to approximate thicknesses of 1mm, only 1-3 slices per testis could be obtained with large enough diameters to be viable samples for diffusion studies. As such, it is very difficult to apply statistical analysis to diffusion coefficients generated from within a single testis. Analysis is largely based on pooled standard deviations compared between fresh batches of testes collected on different days. No significant differences were observed between the average effective diffusion coefficients of collection days at 22°C or 4°C when performing independent two-sided t-tests. Figure 62 summarizes the effective diffusion coefficients for alginate-gelatin, agarose, and testicular tissue found in this work along with the effective diffusion coefficients for DMSO in various tissue types mentioned in Section 1.3.1.

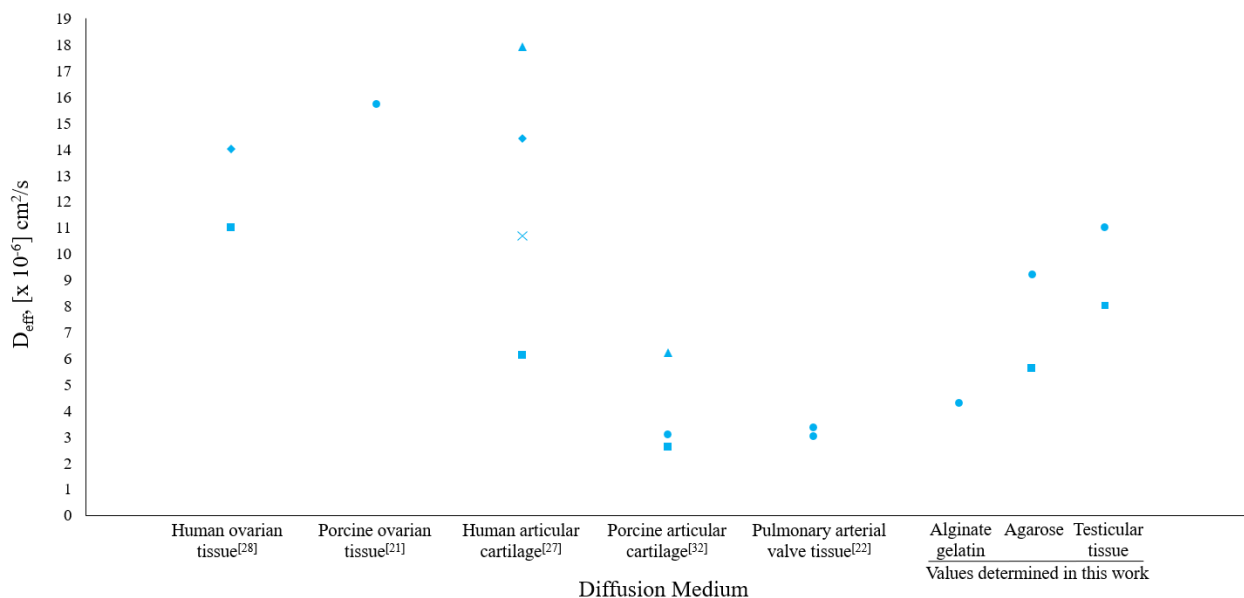


Figure 62 Effective diffusion coefficients reported for DMSO into various tissues together with diffusion coefficient for DMSO in alginate-gelatin, agarose, and testicular tissue, as established in this work. Values determined at 4°C, 17°C, 22°C, 27°C, and 37°C are represented by squares, X marks, circles, diamonds, and triangles, respectively.

Although, standard deviations observed for the  $D_{eff}$  values for DMSO in testicular tissue samples were large (27% at 22°C and 75% at 4°C), variation was comparable to that reported in the literature. The estimated standard deviations determined by Wang et al. (2014) ranged from 23 to 44% for glycerol in different tissue types from decellularized heart valves [38]. Similarly, the reported standard deviations were 9% at 22°C and 15% at 37°C for sucrose and 22% at 22°C for glucose in decellularized heart valves [39]. In fact, the variation observed in  $D_{eff}$  values for DMSO in testicular tissue was much lower than that observed for DMSO in porcine articular cartilage. Sharma et al. (2007) reported standard deviations of 57% at 22°C and 95% at 4°C [32]. Likewise, the reported variations in effective diffusion coefficients for propylene glycol in porcine articular cartilage were 60% at both temperatures. Furthermore, the standard deviation for DMSO in porcine ovarian tissue was 38% at room temperature when using the FTIR method. It should be noted that in most cases three samples were used to determine the average  $D_{eff}$  values and standard deviations

which will inherently result in larger variations. However, even increasing the number of samples to 6 for each temperature, Sharma et al. (2007) still reported higher standard deviations. Thus, the larger number of samples used for determining the overall average effective diffusion coefficients for DMSO in testicular tissue likely did not result in significantly lower variation. Furthermore, the variations in average  $D_{\text{eff}}$  of DMSO in testicular tissue for each collection day ( $n = 3$  for each day) were also comparable to those reported in the literature, ranging from 13-45% for 22°C experiments and 20-91% for 4°C experiments.

Though, some of the average  $D_{\text{eff}}$  values for individual collection days showed close fits to the remaining absorbance series during validation of the effective diffusion coefficients, the variation in the effective diffusion coefficient estimates is especially evident. As the same procedures were used to collect and process spectra, the low variations which were observed in the  $D_{\text{eff}}$  values for agarose indicates that the large variations ( $>30\%$ ) in  $D_{\text{eff}}$  values observed for testicular tissue are due to possible inhomogeneity in tissue composition. Thus, future efforts to optimize loading of DMSO in testicular tissue must take the inherent variation of the tissue into account during preservation planning.

### **7.3.1 Understanding the relationship between temperature and diffusion of DMSO in testicular tissue**

Calculating the diffusion energy can allow a deeper understanding of how diffusion of DMSO in testicular tissue relates to temperature. The activation energy can be determined using the Arrhenius Equation.

$$\ln(D_{\text{eff}}) = \ln(A) - \frac{E_a}{RT}$$

In this equation,  $A$  is the Arrhenius factor,  $R$  is the universal gas constant,  $T$  is the temperature in Kelvin, and  $E_a$  is the activation energy. As this equation exhibits a relationship similar to the

equation for a line, the activation energy can be estimated from the slope of a line generated by plotting the effective diffusion coefficients as a function of the temperatures at which they were obtained as shown using the diffusion coefficients in Figure 63.

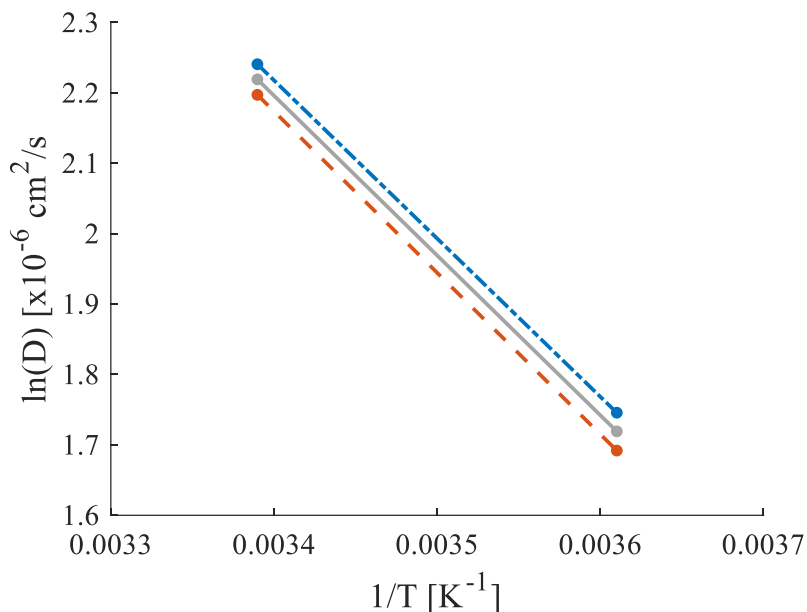


Figure 63 Arrhenius plot of the activation energy for diffusion of DMSO in agarose. The average values are indicated by a solid gray line. The values considering increasing by 1 standard deviation and decreasing by 1 standard deviation are represented by a dot-dashed blue line and a dashed orange line, respectively.

The activation energy can be estimated using only 2 effective diffusion coefficients at two temperatures. However, the accuracy of the activation energy estimation is limited by the standard deviations for the effective diffusion coefficients, even in the case of the lower variation observed in agarose (2.2% at 22°C and 2.7% at 4°C). For instance, if the average diffusion coefficients are used, the activation energy is 18.9 kJ/mol. However, if each diffusion coefficient is increased by one standard deviation, the activation energy becomes 18.7 kJ/mol. If each diffusion coefficient is decreased by one standard deviation, the activation energy is 19.1 kJ/mol. Both cases only introduce a 1.1% error in the activation energy estimation. While, increasing  $D_{\text{eff}}$  at one

temperature and decreasing the other results a larger error (9.5%) in the activation energy, this is still sufficiently low to better understand the temperature-dependence of diffusion in agarose. For example, if the diffusion coefficient at 22°C is increased by a standard deviation and the effective diffusion coefficient at 4°C is decreased by a standard deviation, the activation energy increases to 20.7 kJ/mol. Alternatively, if the diffusion coefficient at 22°C is decreased by a standard deviation and the effective diffusion coefficient at 4°C is increased by a standard deviation, the activation energy decreases to 17.1 kJ/mol.

A similar pattern is apparent, as can be seen in Figure 64, when estimating the activation energy for testicular tissue though larger errors are introduced with the greater standard deviations.

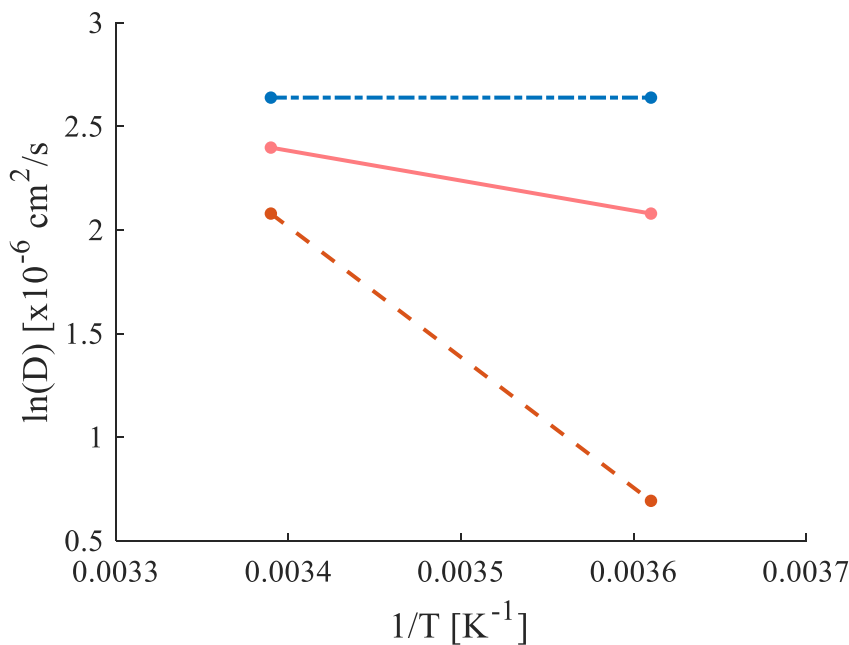


Figure 64 Arrhenius plot of the activation energy for diffusion of DMSO in testicular tissue. The average values are indicated by a solid pink line. The values considering increasing by 1 standard deviation and decreasing by 1 standard deviation are represented by a dot-dashed blue line and a dashed orange line, respectively.

Using the average effective diffusion coefficients, the activation energy is 12.0 kJ/mol. Increasing each diffusion coefficient by one standard deviation decreases the activation to 0 kJ/mol as the large standard deviation at 4°C increases  $D_{\text{eff}}$  to the same value as the maximum  $D_{\text{eff}}$  at 22°C, which is an unlikely outcome. On the other hand, decreasing each effective diffusion coefficient by one standard deviation increases the activation energy to 52.4 kJ/mol, a 336% change in the estimated value. If the diffusion coefficient at 22°C is increased by a standard deviation and the effective diffusion coefficient at 4°C is decreased by a standard deviation, the activation energy decreases to -21.1 kJ/mol, a 276% change. If the diffusion coefficient at 22°C is decreased by a standard deviation and the effective diffusion coefficient at 4°C is increased by a standard deviation, the activation energy increases greatly to 73.5 kJ/mol, a 513% change. Nevertheless, the activation energy calculated using the average effective diffusion coefficients for DMSO in testicular tissue is similar to that of DMSO in porcine articular cartilage which had a reported 44% standard deviation ( $18 \pm 7.9$  kJ/mol) [30] as well as that of sucrose in pulmonary artery matrices (15.9 kJ/mol) [39]. Thus, the activation energy calculated using the average  $D_{\text{eff}}$  values at each temperature can still be used to gain a better understanding of the temperature-dependence of DMSO diffusion in testicular tissue.

## **CHAPTER 8 FUTURE WORK**

### **8.1 Further development and application of reference material for diffusion studies**

In this dissertation, agarose was developed for use as a reference material for diffusion studies using ATR-FTIR technology. A diffusion coefficient was determined for 3.1M DMSO, which is a component of a common vitrification solution, VS55, also containing other common CPAs formamide and propylene glycol. Thus, determination of the diffusion coefficients for formamide and propylene glycol in agarose individually, as well as the effective diffusion coefficients of each component while in VS55 will allow application of optimization models, such as those developed by Benson et al (2018) for loading of these CPA mixtures [8].

In addition, while the variability in the estimated diffusion coefficients and heights is low enough to qualify agarose as a reference material, further characterization is necessary to qualify agarose as a reference standard. Only one batch of agarose was used to determine the thicknesses after packing into the sample holder. Increasing the number of batches measured using the ATOS Scanbox could improve thickness estimates. In turn, this would further improve the effective diffusion coefficient estimations as the uncertainty in the thickness input to the fitting algorithm would decrease. As agarose is compacted into the sample holder to prevent leaking, use of a pycnometer could allow comparison of the density before and after packing into the sample holder. Thus, the effect of changing density on the effective diffusion coefficient estimations could be investigated.

### **8.2 Refinement of sample holder and thermal control system**

Although a CPA delivery sample holder which maintains a 1-D diffusion environment by preventing leaking around the edges of contained samples was developed, refinement would be beneficial for the thermal control system. Machining a replacement lid which uses an insulating material such as acetal or another thermoplastic could reduce heat transfer through the top of the

sample holder system. Although, the thermal control system developed in this work maintains the temperature within an 8-degree range, redesign of the container for the phase change materials to facilitate better contact with the FTIR surface and the sample holder would reduce the heat transfer from the surrounding environment to the FTIR surface and decrease the range of temperatures experienced inside the sample holder.

### **8.3 Expansion of known temperature-dependent CPA properties of testicular tissue**

While nine samples were used to determine the effective diffusion coefficient for DMSO in testicular tissue, increasing the sample size is recommended to increase the understanding of the variation present in the tissue as well as facilitate more in-depth statistical analysis. A basic power analysis assuming a significance value,  $\alpha = 0.05$ , a minimum power of 0.8, that the same number of diffusion studies will be conducted on all collection days, and that the average  $D_{\text{eff}}$  and standard deviation for all nine samples at 22°C is typical for testicular tissue can be used to predict the required number of samples, as shown in Equation 5.

$$N = \frac{\sigma^2 \left( z_{1-\beta} + z_{1-\alpha/2} \right)^2}{(\mu_0 - \mu_1)^2} \quad (\text{Eqn 5})$$

When considering the average  $D_{\text{eff}}$  for collection days 1 or 3 at 22°C as  $\mu_1$ , the recommended number of samples is 18. However, the recommended number of samples increases to 71 when considering the average  $D_{\text{eff}}$  for collection day 2 at 22°C. To balance the necessity of understanding the variation in the tissue and the time required to collect absorbance values and determine the diffusion coefficient, averaging the recommended number of samples based on collection days 1 and 3 with the recommended number of samples based on collection day 2 results in a required 45 samples. If 3 diffusion studies are conducted each day as demonstrated in this dissertation, the

necessary absorbance time series could be collected and processed within 3 weeks. Repeating these estimations using the average effective diffusion coefficients and standard deviation determined at 4°C, 31 samples are recommended based on the average  $D_{\text{eff}}$  for collection day 1, and 71 samples are recommended based on the average  $D_{\text{eff}}$  for either of collection days 2 and 3. Averaging these numbers results in a 51 recommended diffusion studies which could be collected and processed within 4 weeks.

As mentioned in Section 7.3.1, the effective diffusion coefficient for DMSO in testicular tissue was estimated at room temperature and 4°C. While the activation energy of diffusion can be calculated using the average diffusion coefficient at each temperature, large errors in the activation energy calculation can be observed when taking into account the large standard deviations for the  $D_{\text{eff}}$  values. Thus, determination of the effective diffusion coefficient for DMSO in testicular tissue at a third temperature, such as 15°C, would allow an improved estimation of the activation energy by providing a third data point for fitting the estimation line.

Application of the toxicity cost function developed by Benson et al. (2018) using the diffusivity values determined in this work to testicular tissues could enable determination of the optimal DMSO loading conditions to ensure good outcomes [8]. However, DMSO is often used in mixture with other CPAs, such as formamide and propylene glycol, as is the case in a commonly used vitrification solution, VS55. Thus, the study of diffusion for the other components of VS55 individually as well as the VS55 solution itself into testicular tissue would be beneficial for future preservation procedure optimization and modeling work.

## REFERENCES

- [1] S. Unni, S. Kasiviswanathan, S. D'Souza, S. Khavale, S. Mukherjee, S. Patwardhan, and D. Bhartiya, "Efficient cryopreservation of testicular tissue: effect of age, sample state, and concentration of cryoprotectant," *Fertil Steril*, vol. 97, no. 1, pp. 200-8 e1, 2012.
- [2] J. Poels, A. Van Langendonckt, M. C. Many, F. X. Wese, and C. Wyns, "Vitrification preserves proliferation capacity in human spermatogonia," *Hum Reprod*, vol. 28, no. 3, pp. 578-89, 2013.
- [3] Y. Baert, A. Braye, R. B. Struijk, A. M. van Pelt, and E. Goossens, "Cryopreservation of testicular tissue before long-term testicular cell culture does not alter in vitro cell dynamics," no. 1556-5653 (Electronic), 2015.
- [4] J. Onofre, Y. Baert, K. Faes, and E. Goossens, "Cryopreservation of testicular tissue or testicular cell suspensions: a pivotal step in fertility preservation," *Hum Reprod Update*, vol. 22, no. 6, pp. 744-761, 2016.
- [5] B. P. Best, "Cryoprotectant Toxicity: Facts, Issues, and Questions," *Rejuvenation Res*, vol. 18, no. 5, pp. 422-36, 2015.
- [6] J. D. Benson, A. J. Kearsley, and A. Z. Higgins, "Mathematical optimization of procedures for cryoprotectant equilibration using a toxicity cost function," *Cryobiology*, vol. 64, no. 3, pp. 144-51, 2012.
- [7] A. F. Davidson, C. Glasscock, D. R. McClanahan, J. D. Benson, and A. Z. Higgins, "Toxicity Minimized Cryoprotectant Addition and Removal Procedures for Adherent Endothelial Cells," *PLoS One*, vol. 10, no. 11, pp. e0142828, 2015.
- [8] J. D. Benson, A. Z. Higgins, K. Desai, and A. Eroglu, "A toxicity cost function approach to optimal CPA equilibration in tissues," *Cryobiology*, vol. 80, pp. 144-155, 2018.
- [9] M. Fujisawa, "Regulation of testicular function by cell-to-cell interaction," *Reproductive Medicine and Biology*, vol. 5, no. 1, pp. 9-17, 2006.
- [10] G. T. Fieldson, and T. A. Barbari, "The use of FTi.r.-a.t.r. spectroscopy to characterize penetrant diffusion in polymers," *Polymer*, vol. 34, no. 6, pp. 1146-1153, 1993.
- [11] G. T. Fieldson, and T. A. Barbari, "Analysis of diffusion in polymers using evanescent field spectroscopy," *AIChE Journal*, vol. 41, no. 4, pp. 795-804, 1995.
- [12] A. Travers, J. P. Milazzo, A. Perdrix, C. Metton, A. Bironneau, B. Mace, and N. Rives, "Assessment of freezing procedures for rat immature testicular tissue," *Theriogenology*, vol. 76, no. 6, pp. 981-90, 2011.
- [13] H. Valli-Pulaski, K. A. Peters, K. Gassei, S. R. Steimer, M. Sukhwani, B. P. Hermann, L. Dwomor, S. David, A. P. Fayomi, S. K. Munyoki, T. Chu, R. Chaudhry, G. M. Cannon, P. J. Fox, T. M. Jaffe, J. S. Sanfilippo, M. N. Menke, E. Lunenfeld, M. Abofoul-Azab, L. S. Sender, J. Messina, L. M. Klimpel, Y. Gosiengfiao, E. E. Rowell, M. H. Hsieh, C. F. Granberg, P. P. Reddy, J. I. Sandlow, M. Huleihel, and K. E. Orwig, "Testicular tissue cryopreservation: 8 years of experience from a coordinated network of academic centers," *Hum Reprod*, vol. 34, no. 6, pp. 966-977, 2019.
- [14] S. Bojic, A. Murray, B. L. Bentley, R. Spindler, P. Pawlik, J. L. Cordeiro, R. Bauer, and J. P. de Magalhães, "Winter is coming: the future of cryopreservation," *BMC Biology*, vol. 19, no. 1, pp. 56, 2021.
- [15] T. H. Jang, S. C. Park, J. H. Yang, J. Y. Kim, J. H. Seok, U. S. Park, C. W. Choi, S. R. Lee, and J. Han, "Cryopreservation and its clinical applications," *Integr Med Res*, vol. 6, no. 1, pp. 12-18, 2017.

- [16] Y. A. Lee, Y. H. Kim, S. J. Ha, B. J. Kim, K. J. Kim, M. S. Jung, B. G. Kim, and B. Y. Ryu, "Effect of sugar molecules on the cryopreservation of mouse spermatogonial stem cells," *Fertil Steril*, vol. 101, no. 4, pp. 1165-75 e5, 2014.
- [17] J. O. Karlsson, and M. Toner, "Long-term storage of tissues by cryopreservation: critical issues," *Biomaterials*, vol. 17, no. 3, pp. 243-56, 1996.
- [18] K. G. Brockbank, Z. Z. Chen, and Y. C. Song, "Vitrification of porcine articular cartilage," *Cryobiology*, vol. 60, no. 2, pp. 217-21, 2010.
- [19] S. Phatak, H. Natesan, J. Choi, K. G. M. Brockbank, and J. C. Bischof, "Measurement of Specific Heat and Crystallization in VS55, DP6, and M22 Cryoprotectant Systems With and Without Sucrose," *Biopreserv Biobank*, vol. 16, no. 4, pp. 270-277, 2018.
- [20] B. Wowk, G. M. Fahy, S. Ahmadyar, M. J. Taylor, and Y. Rabin, "Vitrification tendency and stability of DP6-based vitrification solutions for complex tissue cryopreservation," *Cryobiology*, vol. 82, pp. 70-77, 2018.
- [21] J. Han, B. Sydykov, H. Yang, H. Sieme, H. Oldenhof, and W. F. Wolkers, "Spectroscopic monitoring of transport processes during loading of ovarian tissue with cryoprotective solutions," *Sci Rep*, vol. 9, no. 1, pp. 15577, 2019.
- [22] A. Vásquez-Rivera, K. K. Sommer, H. Oldenhof, A. Z. Higgins, K. G. M. Brockbank, A. Hilfiker, and W. F. Wolkers, "Simultaneous monitoring of different vitrification solution components permeating into tissues," *The Analyst*, vol. 143, no. 2, pp. 420-428, 2018.
- [23] Z. Han, A. Sharma, Z. Gao, T. W. Carlson, M. G. O'Sullivan, E. B. Finger, and J. C. Bischof, "Diffusion Limited Cryopreservation of Tissue with Radiofrequency Heated Metal Forms," *Adv Healthc Mater*, vol. 9, no. 19, pp. e2000796, 2020.
- [24] I. N. Mukherjee, Y. Li, Y. C. Song, R. C. Long, and A. Sambanis, "Cryoprotectant transport through articular cartilage for long-term storage: experimental and modeling studies," *Osteoarthritis and Cartilage*, vol. 16, no. 11, pp. 1379-1386, 2008.
- [25] D. M. Tartakovsky, and M. Dentz, "Diffusion in Porous Media: Phenomena and Mechanisms," *Transport in Porous Media*, vol. 130, no. 1, pp. 105-127, 2019.
- [26] Oxford. "Diffusivity," May 3, 2022; lexico.com dictionary.
- [27] B. Carsi, J. L. Lopez-Lacomba, J. Sanz, F. Marco, and L. Lopez-Duran, "Cryoprotectant permeation through human articular cartilage," *Osteoarthritis and Cartilage*, vol. 12, no. 10, pp. 787-792, 2004.
- [28] R. V. Devireddy, "Predicted permeability parameters of human ovarian tissue cells to various cryoprotectants and water," *Molecular Reproduction and Development*, vol. 70, no. 3, pp. 333-343, 2005.
- [29] S. A. Isbell, C. A. Fyfe, R. L. M. Ammons, and B. Pearson, "Measurement of Cryoprotective Solvent Penetration into Intact Organ Tissues Using High-Field NMR Microimaging," *Cryobiology*, vol. 35, no. 2, pp. 165-172, 1997.
- [30] N. M. Jomha, G. K. Law, A. Abazari, K. Rekieh, J. A. W. Elliott, and L. E. McGann, "Permeation of several cryoprotectant agents into porcine articular cartilage," *Cryobiology*, vol. 58, no. 1, pp. 110-114, 2009.
- [31] P. Liu, Y. Huang, Z. Guo, J. Wang, Z. Zhuang, and S. Liu, "Discrimination of dimethyl sulphoxide diffusion coefficient in the process of optical clearing by confocal micro-Raman spectroscopy," *J Biomed Opt*, vol. 18, no. 2, pp. 20507, 2013.
- [32] R. Sharma, G. K. Law, K. Rekieh, A. Abazari, J. A. W. Elliott, L. E. McGann, and N. M. Jomha, "A novel method to measure cryoprotectant permeation into intact articular cartilage," *Cryobiology*, vol. 54, no. 2, pp. 196-203, 2007.

- [33] J. Crank, *The mathematics of diffusion*, 2d ed., Oxford, Eng: Clarendon Press, 1975.
- [34] H. Newton, "The cryopreservation of ovarian tissue as a strategy for preserving the fertility of cancer patients," *Human Reproduction Update*, vol. 4, no. 3, pp. 237-247, 1998.
- [35] S. Bhowmick, C. A. Khamis, and J. C. Bischof, "Response Of A Liver Tissue Slab To An Hyperosmotic Sucrose Boundary Condition: Microscale Cellular And Vascular Level Effectsa," *Annals of the New York Academy of Sciences*, vol. 858, no. 1, pp. 147-162, 1998.
- [36] P. Tomlins, P. Grant, S. Mikhalovsky, S. James, and L. Mikhalovska, "Measurement of Pore Size and Porosity of Tissue Scaffolds," *Journal of ASTM International*, vol. 1, no. 1, pp. 1-8, 2004.
- [37] J. B. Charles R. Mace, Anna Laromaine Sague, George M. Whitesides, Rebecca Cademartiri, *Alginate hydrogel fibers and related materials*, US PCT/US2011/043718, I. C. P. Services, 2012.
- [38] S. Wang, H. Oldenhof, X. Dai, A. Haverich, A. Hilfiker, M. Harder, and W. F. Wolkers, "Protein stability in stored decellularized heart valve scaffolds and diffusion kinetics of protective molecules," *Biochimica et Biophysica Acta (BBA) - Proteins and Proteomics*, vol. 1844, no. 2, pp. 430-438, 2014.
- [39] S. Wang, H. Oldenhof, T. Goecke, R. Ramm, M. Harder, A. Haverich, A. Hilfiker, and W. F. Wolkers, "Sucrose Diffusion in Decellularized Heart Valves for Freeze-Drying," *Tissue Eng Part C Methods*, vol. 21, no. 9, pp. 922-31, 2015.
- [40] L. T. Bello, P. A. da Ana, D. Santos, Jr., F. J. Krug, D. M. Zezell, N. D. Vieira, Jr., and R. E. Samad, "Mercury Amalgam Diffusion in Human Teeth Probed Using Femtosecond LIBS," *Appl Spectrosc*, vol. 71, no. 4, pp. 659-669, 2017.
- [41] S. Mahnic-Kalamiza, D. Miklavcic, and E. Vorobiev, "Dual-porosity model of solute diffusion in biological tissue modified by electroporation," *Biochim Biophys Acta*, vol. 1838, no. 7, pp. 1950-66, 2014.
- [42] A. Zheng, L. Cao, Y. Liu, J. Wu, D. Zeng, L. Hu, X. Zhang, and X. Jiang, "Biocompatible silk/calcium silicate/sodium alginate composite scaffolds for bone tissue engineering," *Carbohydr Polym*, vol. 199, pp. 244-255, 2018.
- [43] D. P. Leme, E. Visacre, V. B. Castro, and M. D. Lopes, "Testicular cytology by fine needle aspiration in domestic cats," *Theriogenology*, vol. 106, pp. 46-52, 2018.
- [44] J. F. Sotos, and N. J. Tokar, "Testicular volumes revisited: A proposal for a simple clinical method that can closely match the volumes obtained by ultrasound and its clinical application," *International Journal of Pediatric Endocrinology*, vol. 2012, no. 1, pp. 17, 2012.
- [45] H. M. Abdelaal, H. O. Kim, R. Wagstaff, R. Sawahata, P. J. Southern, and P. J. Skinner, "Comparison of Vibratome and Compressatome sectioning of fresh primate lymphoid and genital tissues for in situ MHC-tetramer and immunofluorescence staining," *Biological Procedures Online*, vol. 17, no. 1, pp. 2, 2015.
- [46] N. I. o. S. a. Technology, "Reference Standards," *NIST/SEMATECH e-Handbook of Statistical Methods*, 2, N. I. o. S. a. Technology, ed., National Institute of Standards and Technology, 2022, p. 53.
- [47] R. M. I. Bercik, "Standard Reference Materials Catalog," N. I. o. S. a. Technology, ed., U.S. Department of Commerce, 2022, p. iii.
- [48] R. Blaine, *Understanding Precision Statements for Standard Reference Materials* n.d.

- [49] H. S. Nielsen, "What Is Traceability and Why Do We Calibrate?," in ASQ Midwest Conference, 1999.
- [50] P. Di Ninni, F. Martelli, and G. Zaccanti, *Toward a reference standard for tissue phantoms*, p. ^pp. PWB: SPIE, 2011.
- [51] B. W. Pogue, and M. S. Patterson, "Review of tissue simulating phantoms for optical spectroscopy, imaging and dosimetry," *Journal of biomedical optics*, vol. 11, no. 4, pp. 041102, 2006.
- [52] I. Bernemann, N. Manuchehrabadi, R. Spindler, J. Choi, W. F. Wolkers, J. C. Bischof, and B. Glasmacher, "Diffusion of dimethyl sulfoxide in tissue engineered collagen scaffolds visualized by computer tomography," *Cryo Letters*, vol. 31, no. 6, pp. 493-503, 2010.
- [53] D. J. McHugh, F.-L. Zhou, I. Wimpenny, G. Poologasundarampillai, J. H. Naish, P. L. Hubbard Cristinacce, and G. J. M. Parker, "A biomimetic tumor tissue phantom for validating diffusion-weighted MRI measurements," *Magnetic Resonance in Medicine*, vol. 80, no. 1, pp. 147-158, 2018.
- [54] E. Souza, E. Costa, and G. Castellano, "Phantoms for diffusion-weighted imaging and diffusion tensor imaging quality control: A review and new perspectives," *Research on Biomedical Engineering*, vol. 33, no. 2, pp. 156-165, 2017.
- [55] S. Kwiatkowska-Marks, and J. Miłek, "Diffusive Properties of Alginate Biosorbents," *Ecological Chemistry and Engineering*, vol. 26, no. 1, pp. 149-163, 2019.
- [56] D. J. Handelsman, and S. Staraj, "Testicular size: the effects of aging, malnutrition, and illness," *J Androl*, vol. 6, no. 3, pp. 144-51, 1985.
- [57] U. Mehmetoglu, "Effective diffusion coefficient of sucrose in calcium alginate gel," *Enzyme Microb Technol*, vol. 12, no. 2, pp. 124-6, 1990.
- [58] B. Balakrishnan, and A. Jayakrishnan, "Self-cross-linking biopolymers as injectable in situ forming biodegradable scaffolds," *Biomaterials*, vol. 26, no. 18, pp. 3941-3951, 2005.
- [59] D. Diekjürgen, and D. W. Grainger, "Polysaccharide matrices used in 3D in vitro cell culture systems," *Biomaterials*, vol. 141, pp. 96-115, 2017.
- [60] G. Handriková, V. Štefuca, M. Polakovič, and V. Bálež, "Determination of effective diffusion coefficient of substrate in gel particles with immobilized biocatalyst," *Enzyme and Microbial Technology*, vol. 18, no. 8, pp. 581-584, 1996.
- [61] H. T. Pu, and R. Y. K. Yang, "Diffusion of sucrose and yohimbine in calcium alginate gel beads with or without entrapped plant cells," *Biotechnology and Bioengineering*, vol. 32, no. 7, pp. 891-896, 1988.
- [62] J. A. Rowley, G. Madlambayan, and D. J. Mooney, "Alginate hydrogels as synthetic extracellular matrix materials," *Biomaterials*, vol. 20, no. 1, pp. 45-53, 1999.
- [63] M. A. Samp, "Sodium Alginate Toughening of Gelatin Hydrogels and Elucidation of Possible Mechanisms," M.S., Rose Hulman Institute of Technology, Ann Arbor, 2017.
- [64] C. G. van Hoogmoed, H. J. Busscher, and P. de Vos, "Fourier transform infrared spectroscopy studies of alginate-PLL capsules with varying compositions," *J Biomed Mater Res A*, vol. 67, no. 1, pp. 172-8, 2003.
- [65] E. Puschmann, "Liquidus tracking: a promising vitrification technique for large scale encapsulated 3-d cell culture preservation," ProQuest Dissertations Publishing, 2015.
- [66] K. Song, L. Li, R. Li, M. Lim, P. Liu, and T. Liu, "Preparation, Mass Diffusion, and Biocompatibility Analysis of Porous-Channel Controlled Calcium-Alginate-Gelatin

- Hybrid Microbeads for In Vitro Culture of NSCs,” *Applied Biochemistry and Biotechnology*, vol. 173, no. 3, pp. 838-850, 2014.
- [67] N. Fatin-Rouge, K. Starchev, and J. Buffle, “Size Effects on Diffusion Processes within Agarose Gels,” *Biophysical Journal*, vol. 86, no. 5, pp. 2710-2719, 2004.
- [68] L. Gasperini, J. F. Mano, and R. L. Reis, “Natural polymers for the microencapsulation of cells,” *Journal of the Royal Society, Interface*, vol. 11, no. 100, pp. 20140817-20140817, 2014.
- [69] D. Ivanusic, K. Madela, and J. Denner, “Easy and low-cost stable positioning of suspension cells during live-cell imaging,” *Journal of biological methods*, vol. 4, no. 4, pp. e80-e80, 2017.
- [70] P. Y. Lee, J. Costumbrado, C.-Y. Hsu, and Y. H. Kim, “Agarose gel electrophoresis for the separation of DNA fragments,” *Journal of visualized experiments : JoVE*, no. 62, pp. 3923, 2012.
- [71] A. Dutta, "Chapter 4 - Fourier Transform Infrared Spectroscopy," *Spectroscopic Methods for Nanomaterials Characterization*, S. Thomas, R. Thomas, A. K. Zachariah and R. K. Mishra, eds., pp. 73-93: Elsevier, 2017.
- [72] P. Larkin, *Infrared and Raman Spectroscopy : Principles and Spectral Interpretation*, Saint Louis, UNITED STATES: Elsevier, 2011.
- [73] F. Cheng, Q. Cao, Y. Guan, H. Cheng, X. Wang, and J. D. Miller, “FTIR analysis of water structure and its influence on the flotation of arcanite (K<sub>2</sub>SO<sub>4</sub>) and epsomite (MgSO<sub>4</sub>·7H<sub>2</sub>O),” *International Journal of Mineral Processing*, vol. 122, pp. 36-42, 2013.
- [74] A. Saarai, V. Kasarkova, T. Sedlacek, and P. Saha, “On the development and characterisation of crosslinked sodium alginate/gelatine hydrogels,” *J Mech Behav Biomed Mater*, vol. 18, pp. 152-66, 2013.
- [75] V. M. Wallace, N. R. Dhumal, F. M. Zehentbauer, H. J. Kim, and J. Kiefer, “Revisiting the Aqueous Solutions of Dimethyl Sulfoxide by Spectroscopy in the Mid- and Near-Infrared: Experiments and Car–Parrinello Simulations,” *The Journal of Physical Chemistry B*, vol. 119, no. 46, pp. 14780-14789, 2015.
- [76] F. Faghihzadeh, N. M. Anaya, L. A. Schifman, and V. Oyanedel-Craver, “Fourier transform infrared spectroscopy to assess molecular-level changes in microorganisms exposed to nanoparticles,” *Nanotechnology for Environmental Engineering*, vol. 1, no. 1, pp. 1, 2016.
- [77] K. L. A. Chan, and S. G. Kazarian, “New Opportunities in Micro- and Macro-Attenuated Total Reflection Infrared Spectroscopic Imaging: Spatial Resolution and Sampling Versatility,” *Applied spectroscopy*, vol. 57, no. 4, pp. 381-389, 2003.
- [78] S. G. Kazarian, and K. L. A. Chan, “Micro- and Macro-Attenuated Total Reflection Fourier Transform Infrared Spectroscopic Imaging,” *Applied spectroscopy*, vol. 64, no. 5, pp. 135A-152A, 2010.
- [79] PerkinElmer, "FT-IR Spectroscopy Attenuated Total Reflectance (ATR)," Perkin Elmer Life and Analytical Sciences, 2005, pp. 1-5.
- [80] K. L. C. Andrew, and G. K. Sergei, “Chemical imaging of the stratum corneum under controlled humidity with the attenuated total reflection Fourier transform infrared spectroscopy method,” *Journal of Biomedical Optics*, vol. 12, no. 4, pp. 044010, 2007.

- [81] A. Pluen, R. K. Netti Pa Fau - Jain, D. A. Jain Rk Fau - Berk, and D. A. Berk, "Diffusion of macromolecules in agarose gels: comparison of linear and globular configurations," no. 0006-3495 (Print), 1999.
- [82] G. Lawrie, I. Keen, B. Drew, A. Chandler-Temple, L. Rintoul, P. Fredericks, and L. Grøndahl, "Interactions between Alginate and Chitosan Biopolymers Characterized Using FTIR and XPS," *Biomacromolecules*, vol. 8, no. 8, pp. 2533-2541, 2007.
- [83] C. H. Pi, P. I. Dosa, and A. Hubel, "Differential Evolution for the Optimization of DMSO-Free Cryoprotectants: Influence of Control Parameters," *J Biomech Eng*, vol. 142, no. 7, 2020.
- [84] C. D. Scott, C. A. Woodward, and J. E. Thompson, "Solute diffusion in biocatalyst gel beads containing biocatalysis and other additives," *Enzyme and Microbial Technology*, vol. 11, no. 5, pp. 258-263, 1989.
- [85] L. Mignot, and G.-A. Junter, "Diffusion in immobilized-cell agar layers: influence of microbial burden and cell morphology on the diffusion coefficients of l-malic acid and glucose," *Applied Microbiology and Biotechnology*, vol. 32, no. 4, pp. 418-423, 1990.

**APPENDIX SUMMARY OF DIFFUSION COEFFICIENTS EQUILIBRIUM  
ABSORBANCE VALUES, SUM OF SQUARES ERROR, AND MEAN  
SQUARE ERROR FOR DIFFUSION STUDIES**

Table 22 Effective diffusion coefficient, equilibrium absorbance value, sum of squares error, and mean square error for agarose samples obtained at room temperature

<b>Batch #</b>	<b>Sample #</b>	<b>D<sub>eff</sub> x 10<sup>-6</sup> [cm<sup>2</sup>/s]</b>	<b>A<sub>∞</sub> Value</b>	<b>SS [x 10<sup>-2</sup>]</b>	<b>MSE [x 10<sup>-4</sup>]</b>
1	1	8.9	1.375	2.68	2.23
1	2	8.8	1.362	3.48	2.85
1	3	9.2	1.362	3.50	2.92
2	1	9.1	1.380	4.44	3.70
2	2	9.3	1.375	3.39	2.83
2	3	9.4	1.374	3.53	2.94
3	1	9.1	1.387	3.54	2.95
3	2	9.2	1.380	3.44	2.87
3	3	9.5	1.379	3.83	3.19

Table 23 Effective diffusion coefficient, equilibrium absorbance value, sum of squares error, and mean square error for agarose samples obtained at 4°C

<b>Batch #</b>	<b>Sample #</b>	<b>D<sub>eff</sub> x 10<sup>-6</sup> [cm<sup>2</sup>/s]</b>	<b>A<sub>∞</sub> Value</b>	<b>SS [x 10<sup>-2</sup>]</b>	<b>MSE [x 10<sup>-4</sup>]</b>
1	1	5.6	1.368	6.69	11.2
1	2	5.3	1.414	22.9	38.2
1	3	5.6	1.210	4.25	7.09
2	1	5.5	1.501	4.13	6.88
2	2	5.4	1.215	3.54	5.90
2	3	5.7	1.049	3.82	6.37
3	1	5.7	1.234	6.08	10.1
3	2	5.6	1.236	2.40	4.01
3	3	5.7	1.332	3.45	5.75

Table 24 Effective diffusion coefficient, equilibrium absorbance value, sum of squares error, and mean square error for testicular tissue samples obtained at room temperature

Day #	Sample #	$D_{\text{eff}} \times 10^{-6}$ [cm <sup>2</sup> /s]	$A_{\infty}$ Value	SS	MSE [ $\times 10^{-3}$ ]
1	1	15	1.488	0.218	1.82
1	2	12	2.070	2.21	18.4
1	3	11	2.049	2.43	20.2
2	1	4	2.103	0.863	7.19
2	2	13	2.249	0.713	6.77
2	3	13	1.485	1.09	9.07
3	1	6	1.653	0.242	2.01
3	2	10	1.440	1.48	12.3
3	3	8	3.115	2.06	17.1

Table 25 Effective diffusion coefficient, equilibrium absorbance value, sum of squares error, and mean square error for testicular tissue samples obtained at 4°C

Day #	Sample #	$D_{\text{eff}} \times 10^{-6}$ [cm <sup>2</sup> /s]	$A_{\infty}$ Value	SS	MSE [ $\times 10^{-3}$ ]
1	1	5	1.731	1.64	27.4
1	2	4	1.565	2.45	40.8
1	3	6	0.916	1.60	26.6
2	1	3	1.875	0.210	3.51
2	2	21	1.749	1.30	21.7
2	3	6	1.584	0.436	7.27
3	1	15	1.391	0.723	12.0
3	2	3	1.868	0.360	60.0
3	3	11	1.241	0.579	96.5